Spatial regulation of TBC-2, a *C. elegans* Rab5 GAP, during endosome maturation

By
Fiona Law

Faculty of Medicine
Department of Anatomy and Cell Biology
McGill University, Montréal, Canada
December 2016

A thesis submitted to McGill University in partial fulfillment of the requirements of the degree of Doctor of Philosophy

Table of Contents

Abstract

Clathrin-mediated endocytosis (CME) is a conserved cellular process that requires the concerted functions of many trafficking proteins. Among those are the Rab GTPases, which coordinate endosome trafficking. In the degradation of cargo, the Rab5 GTPase present on the early endosome (EE) is deactivated and removed from the membrane, while the Rab7 GTPase is recruited for function on the late endosome (LE). During this transition, Rab5 requires a GTPase Activating Protein (GAP) to catalyze the hydrolysis of its bound GTP.

How Rab5 GAPs localize specifically onto maturing endosomes for function is unclear. Using a previously identified Rab5 GAP called TBC-2 in *C. elegans,* we showed that TBC-2 localization requires both the Pleckstrin Homology (PH) domain and the region encompassing the coil-coiled (CC) domain. Removal of the PH domain still permitted TBC-2 binding for its GAP activity, but this resulted in an altered localization pattern that coincided strongly with LEs. Additional removal of the CC domain region, however, abolished TBC-2 binding. We found that binding by both PH domain and CC domain region is mediated by Class III phosphoinositide 3-kinase (PI3K) generated PI3P. Consistent to this, loss of Class III PI3K subunits resulted in a trafficking defect that was similar to loss-of-function *tbc-2*. This led us to propose that TBC-2 uses a PI3P dependent coincidence strategy for its localization and that the binding of the PH domain to PI3P is a regulatory step in this process.

To identify players involved in TBC-2 localization, a potential regulator named *vh45* was isolated from a genetic screen. These mutant worms display a *tbc-2*-like endocytic phenotype that is basolaterally restricted. The causative gene has been found to be located on Chromosome II, apart from the *tbc-2* locus.

This work contributes to the understanding of the mechanisms employed by Rab5 GAPs for their spatiotemporal localization. It can be applied towards etiology of disease states that arise from defects in Rab5 GAP function and/or in the endosome maturation program.

Résumé

L'endocytose clathrine-dépendante (CME) est un processus cellulaire conservé qui résulte du bon fonctionnement de plusieurs protéines de transport. Parmi elles figure les GTPases de la Rab5, qui jouent un rôle prépondérant pour coordonner le trafic vers les endosomes. Lors de la dégradation de cargos, Rab5 qui est présent au niveau des endosomes précoces (EE), est inhibée et retirée de la membrane, tandis que la GTPase Rab7, une protéine agissant au niveau des endosomes tardifs, est recrutée. Au cours de cette transition, Rab5 a besoin de la protéine d'activation des GTPases de la Rab5 (GAP) pour catalyser l'hydrolyse de sa GTP liée.

Comment les GAPs de Rab5 se localisent de manière spécifique aux endosomes matures est un processus qu'il reste encore à élucider. Dans ce travail de recherche, j'utilise la protéine GAP de Rab5 du nématode *Caenorhabditis elegans*, TBC-2 et je démontre que la localisation de TBC-2 requiert que cette protéine aie sont domaine Pleckstrin Homology (PH) intact, ainsi que sa région englobant le domaine CC. Une perte du domaine PH de TBC-2 n'affecte pas l'activité GTPase de la protéine; en revanche, sans ce domaine, le patron de localisation est affecté et corrèle fortement avec un phénotype d'endosome tardifs. Une perte additionnelle du domaine CC abolit la capacité de ciblage de TBC-2. J'ai découvert que la capacité de liaison de ces deux domaines à leur cible est médiée par l'intermédiaire de la phosphoinositide 3-kinase (PI3K) de classe III, qui est générée pas PI3P. De manière cohérente et similaire à ce qu'on peut observer avec un mutant entrainant une perte de fonction (*tbc-2*), une perte de la sous-unité de PI3K induit un défaut au niveau du trafic cellulaire. Ces fait observés nous ont amené à emmètre comme hypothèse que TBC-2 utilise une stratégie basée sur la présence de PI3P pour permettre sa bonne localisation intracellulaire et que la liaison du domaine PH à PI3P est une étape importante pour la régulation de ce processus.

De manière à identifier les protéines impliquées dans la localisation de TBC-2, un criblage génétique a été effectué et a permis d'isoler un régulateur potentiel de ce processus, *vh45*. Les nématodes ayant la mutation pour ce gène engendrent un phénotype endocytique similaire à *tcbc-2* et la protéine est restreinte au côté basolateral. Ce gène est localisé sur le chromosome II, séparé du locus de *tbc-2*.

Ce travail contribue à améliorer le niveau de connaissance relatif au(x) mécanisme(s) d'action employé par les GAPs de Rab5 pour la localiser de manière spatio-temporelle. Le contenu de ces recherches peut être appliqué de manière à mieux comprendre l'étiologie de certaines maladies qui découlent d'un défaut au niveau de la fonction des GAPs de la Rab5 et/ou du programme de maturation des endosomes.

Acknowledgements

First and foremost, I want to thank my supervisor Dr. Christian Rocheleau for the opportunity to work in his laboratory and to the funding agency Canadian Institutes of Health Research (CIHR). I want to thank my committee members Drs. Dieter Reinhardt, Nathalie Lamarche and Peter McPherson for their insightful comments on the progress of my project. Thanks to the lab technician, Jung Hwa Seo, for her assistance. The support from my fellow labmates past and present has been instrumental in getting through some very tough times. I wish to thank the collective PPL, the extensive ETM group and the Anatomy and Cell Biology Department for their welcoming and supportive environment. I have a lot of fun memories with everyone.

I thank Icten Meras and Kimberley Gauthier for their suggestions on this thesis, and Ljiljana Nikolajev for translating the English abstract into French. Finally, my family has been an incredible source of support in this journey of personal strength and persistence. To my mother for her tremendous generosity. To my late father, who encouraged me to pursue my curiosities.

Contribution of authors

This thesis was written in standard format according to guidelines from the Graduate and Postdoctoral Studies of McGill University. This thesis consists of a comprehensive review of the literature in the introduction, a material and methods section, three chapters of results, and finally, followed by a discussion.

A recently submitted article to the Journal of Cell Science included several figures from this thesis (Figures 8, 15, 16, 17, 18) and the work from our collaborators Ziqing Wang (from the laboratory of Guangwei Du at the University of Texas Health Scence Centre at Houston) and Jennifer L. DeLeon (from the laboratory of Wei-Xing Zong at Rutgers University, formerly of Stony Brook University). The authors of the article are Fiona Law*, Jung Hwa Seo*, Ziqing Wang, Jennifer L. DeLeon, Yousstina Bolis, Ashley Brown, Wei-Xing Zong, Guangwei Du and Christian E. Rocheleau. * denotes authors who have contributed equally to this work.

Chapter 3. Structural and functional analysis of TBC-2

Figure 8: Primer design, construction, purification of bacterially expressed recombinant TBC-2 constructs were jointly designed by F Law and JH Seo. Microinjection of the constructs into *tbc-2(tm2241)* worms was performed by F Law. Images (A-I) F Law, (J-O) JH Seo.

Figure 9-14: F Law

Table 2: F Law

Chapter 4. Class III PI3K generated PI3P negatively regulates RAB-5 during endosome maturation

Figure 15: (A) Primer design, construction, purification of bacterially expressed recombinant GST-PH, GST-CC and GST-PH-CC for the lipid overlay assay was done by JH Seo. (B-C) Liposome assay and analysis using purified GST-PH, GST-CC were done by Z Wang (University of Texas Health Science Centre at Houston, Houston, TX).

Figure 16: (A-D) RNAi of *gfp*, *vps-34*, *vps-15* and *bec-1* to worms were collectively

performed and imaged by JH Seo, Y Bolis and A Brown. (E-G) images of MTM-1 and MTM-1(C378S) were taken by F Law. (H-J) Double RNAi for *rab-7* and *vps-34* was performed by JH Seo.

Figure 17: (A-D) RNAi experiment and images were taken by JH Seo. (E-H) Transgenic strains were constructed and imaged by F Law.

Figure 18: JH Seo

Figure 19-21: F Law

Chapter 5. Characterization of *vh45*, a potential TBC-2 regulator

Figure 22-23: F Law

Figure 24: Modified figure from Doitsidou *et al*. (Doitsidou et al., 2010)

Figure 25: Genomic extraction and computational analysis for *vh45* was performed by F Law.

Figure 26: F Law

Table 3, 4: F Law

Chapter 6. Discussion

Figure 27: F Law

List of figures

List of tables

C. elegans nomenclature

According the *C. elegans* genetic nomenclature guidelines (Riddle, 1997), several points of particular importance to this thesis are as follows:

1) Genes are named with an italicized three or four letter prefix, a hyphen and an Arabic number. An italicized Roman numeral may follow to indicate on which chromosome the locus is located. Phenotypes of genes may be referred by its non-italicized gene name with the first letter capitalized. Protein products of genes are written non-italicized and in all capitals.
2) Names of alleles are italicized and may follow the gene name in parentheses. Two components make up the allele name: a letter portion and an Arabic number. The letter refers from which laboratory the allele was isolated. The allele designation for the Rocheleau laboratory is *vh*.
3) Extrachromosomal arrays are denoted with the laboratory's allele designation, followed by an italicized *Ex* and an Arabic number. Unlike that of integrated transgenes, extrachromosomal arrays are not inherited by all cells. Integrated transgenes are named similarly to extrachromosomal arrays but contain within its name *Is* rather than *Ex*.
4) Names of worm strains begin with two or three capitalized letters denoting the laboratory from where the strain was constructed, followed by an Arabic number. Strain names are not italicized. The Rocheleau lab designation for strains is QR.
5) Chromosome balancers suppress meiotic crossovers. They can exist as duplications (*Dp*) deficiencies (*Df*), inversions (*In*) or translocations (*T*). Their names are italicized, beginning with the allele designation, the nature of the aberration, and finally followed by an Arabic number. For example, *nDf2* is the second chromosome deficiency that

originated from the Horvitz lab (allele designation *n*) (Greenwald and Horvitz, 1980).

List of abbreviations

α: alpha

β: beta

δ: delta

γ: gamma

ADAMTS: a disintegrin and metalloproteinase with thrombospondin motifs

ADP: adenosine diphosphate

ATP: adenosine triphosphate

AlF_n: aluminum fluoride

AMPH-1: amphiphysin-1

Arf: ADP-ribosylation factor

Bcl2: B-cell lymphoma 2

BH3: Bcl2-homology-3

BioID: proximity-dependent biotin identification

BLASTp: protein BLAST (basic local alignment search tool)

BSA: bovine serum albumin

BRET: bioluminescence resonance energy transfer

C: carboxyl

CC: coiled-coil (refers to TBC-2 only)

CCP: clathrin-coated pit

CCV: clathrin-coated vesicle

CCZ1: calcium caffeine zinc sensitivity protein 1

CED-10: cell death abnormality-10

CIE: clathrin-independent endocytosis

CLIC-GEEC: clathrin-independent carrier-GPI-anchored protein-enriched endosomal compartment

CME: clathrin-mediated endocytosis

DIC: differential interference contrast

DNA: deoxyribonucleic acid

DENN: differentially expressed in normal and neoplastic cells

dsRNA: double stranded RNA

EE: early endosome

EEA1: early endosome antigen 1

EGFR: epidermal growth factor receptor

ER: endoplasmic reticulum

EMS: ethyl methanesulfonate

ESCRT: endosomal sorting complexes required for transport

ev: empty vector

F1: first generation

F2: second generation

Fab1/PIKfyve: formation of aploid and binucleate cells 1/phosphoinositide kinase for 5 position containing a FYVE finger

FYVE: Fab1, YOTB, Vac1, EEA1

GAP: GTPase-activating protein

GDF: GDI-displacement factor

GDI: GDP-dissociation inhibitor

GDP: guanosine diphosphate

GEF: guanine nucleotide-exchange factor

GON-1: abnormal gonad development

GPCRs: G protein-coupled receptors

GPI-AP: glycosylphosphatidylinositol-anchored protein

GRAM: glucosyltransferases, Rab-like GTPase activators and myotubularin

GST: glutathione S-transferase

GTP: guanosine triphosphate

Gyp: GAPs for Ypt/Rab proteins

HEAT: Huntingtin, Elongation factor 3, protein phosphatase 2A, yeast kinase TOR1

HOPS: homotypic fusion and vacuole protein sorting

HLH-6: helix loop helix-6

HRL3: Hlh-6 regulatory element 3

Hrs: hepatocyte growth factor-regulated tyrosine kinase substrate

ILVs: intraluminal vesicles

IPTG: isopropyl β-D-1-thiogalactopyranoside

KIF16B: kinesin family member 16B

L4: *C. elegans* larval 4th stage

LAMP1: lysosomal-associated membrane protein 1

LC3: microtubule-associated protein light chain 3

LE: late endosome

LGG-1: LC3, GABARAP, and GATE-16-1

LOESS: locally weighted smoothing

LPA: lysophosphatidic acid

LPC: lysophosphocholine

LRRK: leucine-rich repeat kinase

miRNA: micro RNA

Mon1: monensin sensitivity 1

Mb: megabase pairs

MMP: million mutation project

MTM: myotubularin

MTMR: myotubularin-related

MVB: multivesicular body

N: amino

ORP1L: oxysterol-binding protein-related protein 1L

PA: phosphatidic acid

PARIS-1: prostate antigen recognized and identified by SEREX (serological identification of antigens by recombinant expression cloning)

PC: phosphatidylcholine

PE: phosphatidylethanolamine

PH: pleckstrin homology

PHD: plant homeodomain

PS: phosphatidylserine

PX: Phox

PI: phosphoinositide

PI3P: phosphatidylinositol 3-phosphate

PI(3,4,5)P_3: phosphatidylinositol 3,4,5-triphosphate

PI(3,5)P_2: phosphatidylinositol 3,5-biphosphate

PI3K: phosphoinositide 3-kinase

PI(4,5)P_2: phosphatidylinositol 4,5-bisphosphate

PI4P: phosphatidylinositol 4-phosphate

PLCδ: phospholipase C δ

PPK-3: PI kinase

PROPPINs: β-propellers that bind polyphosphoinositides

PtdIns: phosphatidylinositol

PTEN: tumour suppressor phosphatase and tensin homologue deleted on chromosome 10

Rab: Ras-related proteins in brain

Ran: Ras-related nuclear protein

Ras: rat sarcoma

RabF: Rab family sequences

RabFS: Rab family sub-family conserved

RabGGT: Rab geranylgeranyltransferase

Rabex-5: Rabaptin-5 associated exchange factor for Rab5

RE: recycling endosome

REP: Rab escort protein

RILP: Rab7 interacting lysosomal protein

RME-1: receptor mediated endocytosis-1

RNA: ribonucleic acid

RNAi: RNA interference

S1P: sphingosine-1-phosphate

SAND-1: SAND endocytosis protein family protein 1

Sec1: staphylococcal enterotoxin C1

SMART: simple modular architecture research tool

SNAP: soluble *N*-ethylmaleimide-sensitive factor attachment protein

SNARE: soluble *N*-ethylmaleimide-sensitive factor attachment protein receptor

SORF: suppressor of organelle fusion

Sos: sons of sevenless

SXN: sorting nexin

TBC: Tre2/Bub2/Cdc16

TGN: trans-Golgi network

THR: TBC1D2 homology region

TRAPP: transport protein particle

TSP1: type 1 thrombospondin domain

VAC14: Vac14, pikFYVE complex component

VAP-A: VAMP-associated ER protein-A

VAMP: vesicle-associated membrane protein

Vav: Vav GEF is named after the 6th letter of the Hebrew alphabet to symbolize the 6th oncogene discovered by the Barbacid Laboratory (Squibb Institute for Medical Research, NJ).

V-ATPase: vacuolar ATPase

VPS: vacuole protein sorting

Vps9: vacuole protein sorting 9

WGS-SNP: whole genome sequencing-single-nucleotide polymorphism

Original contributions to knowledge

The major novel findings of this thesis are the following:

1. TBC-2 localizes onto membranes via its PH domain and the CC domain region. The CC domain region is critical for this role.

2. Rab5 uses its effector, Class III PI3K, to mediate its inactivation by recruiting TBC-2.

3. The potential TBC-2 regulator *vh45* is not an allele of *tbc-2*. The gene containing the *vh45* mutation is located on Chromosome II.

Chapter 1. Introduction and literature review

1.1 Intracellular trafficking

The ability for living organisms to respond to the dynamics of the outside environment and to internalize material for synthesis of cellular components in growth and development is necessary for survival. Macroautophagy (or autophagy), phagocytosis, and endocytosis are conserved intracellular trafficking routes that serve to internalize resources, recycle cellular contents for resource redistribution, and manage components for signal transduction into the cell interior.

Autophagy is the major intracellular pathway for long-lived protein and organelle degradation that occurs as a function of cellular homeostasis (Kaur and Debnath, 2015). This process can also occur under nutrient-starved conditions to salvage resources for cell survival (Kaur and Debnath, 2015).

Phagocytosis is the receptor-mediated engulfment of particles that are >0.5 μm in size (Flannagan et al., 2012). It is an important aspect of apoptotic corpse clearance and immunity that occurs only in professional phagocytes such as neutrophils, macrophages, and dendritic cells (Flannagan et al., 2012).

Endocytosis is the intake of materials such as fluids, molecules, lipids, or components of the plasma membrane. Internalized vesicles are typically ~100 nm in diameter, although they can reach up to 5 μm in diameter (Conner and Schmid, 2003; Lim and Gleeson, 2011). The mechanism by which molecules are internalized can be classified as either clathrin-dependent (McMahon and Boucrot, 2011) or clathrin-independent (Johannes et al., 2015; Mayor and

Pagano, 2007). Clathrin-mediated endocytosis (CME) is the most well-characterized pathway of endocytosis and occurs in all eukaryotic cells.

1.1.1 Clathrin-mediated endocytosis

The defining feature of the CME pathway is clathrin, a three-legged polymer composed of three heavy chains and three light chains (Royle, 2006). CME begins with the assembly of the clathrin coat on the cytoplasmic face of the plasma membrane (McMahon and Boucrot, 2011) (**Figure 1**). This coat provides curvature to the plasma membrane during the process of membrane budding (Avinoam et al., 2015). Continual deformation and budding to a clathrin-coated pit (CCP) eventually produces a structure that attaches to the plasma membrane by a short stalk (Avinoam et al., 2015; McMahon and Boucrot, 2011). Stalk scission by the mechanochemical enzyme dynamin releases the nascent clathrin-coated vesicle (CCV) into the cytoplasm (McMahon and Boucrot, 2011). Vesicles formed from CME are ~100 nm in diameter, although vesicles as large as 200 nm have been reported (Cureton et al., 2009; McMahon and Boucrot, 2011).

1.1.2 Clathrin-independent endocytosis

Clathrin-independent endocytosis (CIE) can be categorized into dynamin-dependent or dynamin-independent pathways (Mayor and Pagano, 2007; Mayor et al., 2014). CIE typically relies more on lipids than CME (Cheng et al., 2006) and has specificity for particular cargoes,

such as serum albumin (Schubert et al., 2001) or GPI-APs (glycosylphosphatidylinositol-anchored proteins) (Sabharanjak et al., 2002). It is possible for certain cargoes to use both CME and CIE for internalization, as is the case for EGFR (epidermal growth factor receptor) (Sigismund et al., 2013; Sigismund et al., 2008). How cargo is selected for CIE is not completely known; however, ubiquitination to the cytoplasmic tails is involved (Sigismund et al., 2013).

The most well-studied form of CIE is caveolin1-mediated endocytosis. Caveolins are integral membrane proteins that associate with cholesterol-rich lipid raft domains to form flask-shaped invaginations. These invaginations of ~60-80 nm in diameter are called caveolae (Parton and Simons, 2007). Scission of a caveola requires dynamin (Parton and Simons, 2007).

Another CIE pathway that requires integral proteins is flotillin-mediated endocytosis. Flotillins are homologous to caveolins and are associated with lipid rafts (Frick et al., 2007; Sandvig et al., 2011). This pathway can be either dynamin-dependent or independent (Mayor et al., 2014; Sandvig et al., 2011). It is used to internalize GPI-APs (Glebov et al., 2006) and proteoglycans (Payne et al., 2007).

The dynamin-independent CLIC–GEEC (clathrin-independent carrier-glycosylphosphatidylinositol [GPI]-anchored protein-enriched endosomal compartment) pathway is a polarized form of endocytosis that occurs at the leading edge of migrating cells (Howes et al., 2010). It internalizes fluid, bulk membrane (Howes et al., 2010) and GPI-APs (Johannes et al., 2015; Kirkham et al., 2005).

One final type of CIE is macropinocytosis, a cholesterol-dependent and dynamin-independent process that occurs at ruffled regions of the cell (Cao et al., 2007b; Doherty and

McMahon, 2009). It uptakes large volumes of material that is mainly fluid-based (Mayor and Pagano, 2007).

1.2 Compartments of the endocytic pathway

Upon entry into the cytoplasm, the CCV sheds its clathrin lattice and fuses to the early endosome (EE) (McMahon and Boucrot, 2011) (**Figure 2**). The EE possesses a slightly acidic lumen (pH ~6.5) with specialized regions of tubular networks; both features aid to sort cargo (Jovic et al., 2010). Recycled cargoes can be transported from tubular networks for their return to the plasma membrane via the recycling endosome (RE) (e.g. transferrin receptors or low density lipoprotein receptor), or to the trans-Golgi network (TGN) via the retromer complex (Jovic et al., 2010; Seaman, 2012; Waguri et al., 2003). On the other hand, cargoes destined for degradation are shuttled toward the perinuclear region of the cell to the lysosomes via the late endosomes (LEs) (e.g. epidermal growth factor receptor and its ligand) (Jovic et al., 2010).

The LE undergoes further acidification of its lumen by vacuolar-ATPases (V-ATPases) (Marshansky and Futai, 2008) to create an environment optimal for the function of lysosomal hydrolases ferried from the TGN (Mironov and Pavelka, 2008). LEs have heterogeneous morphologies (Huotari and Helenius, 2011). Most LEs contain intraluminal vesicles (ILVs) and are therefore sometimes referred to as multivesicular bodies (MVBs) (Huotari and Helenius, 2011).

ILVs sequester and inactivate transmembrane receptors that still signal through their cytoplasmic tails. The formation of ILVs involves the function of four complexes called ESCRT

(endosomal sorting complexes required for transport) -0, -I, -II, -III that are recruited in a sequential manner (Schmidt and Teis, 2012). A component of ESCRT-0 is Hrs (hepatocyte growth factor-regulated tyrosine kinase substrate), which recognizes and binds to monoubiquitinated lysine residues on the cytoplasmic tails of transmembrane cargo (Haglund et al., 2003; Raiborg et al., 2002).

The LE eventually fuses to the lysosome to form a hybrid endolysosome (Huotari and Helenius, 2011). The lysosome is an electron dense, perinuclear organelle that contains heavily glycosylated proteins such as LAMP1 (lysosomal-associated membrane protein 1) to protect itself from the degradative activity of acid hydrolases (Huotari and Helenius, 2011; Kundra and Kornfeld, 1999). The lysosome also functions as the terminal compartment for phagocytosis and autophagy (Huotari and Helenius, 2011; Luzio et al., 2007).

1.3 Molecular markers of endocytic components

Cargo transport from one compartment to another requires the coordinated function of trafficking proteins. Chief among them are the Rab GTPases and a class of secondary messenger lipids called phosphoinositides (PI) (**Figure 2**, **Figure 3**). Their intracellular distributions are so well restricted that they are often used as identity markers for endocytic compartments (Kutateladze, 2010; Wandinger-Ness and Zerial, 2014). These markers may also function in phagocytosis and autophagy (Eskelinen and Saftig, 2009; Flannagan et al., 2012).

1.3.1 Rab GTPases of the Ras superfamily

The Ras superfamily of small monomeric GTPases contains five major subfamilies—Ras, Rho, Ran, Arf/Sar, and Rab—which are classified based on their sequence and function (Mott and Owen, 2015): Ras GTPases are generally involved in cell growth and differentiation and are recognized as oncogenes (Karnoub and Weinberg, 2008); Rho GTPases regulate actin dynamics for processes such as polarity and cell cycle (Heasman and Ridley, 2008); Ran GTPase, the only member of its subfamily, functions in nuclear transport (Macara, 2001); finally, Arf/Sar and Rab GTPases are involved in vesicular trafficking (Donaldson and Jackson, 2011; Zerial and McBride, 2001).

Rab GTPases comprise the largest subfamily within the Ras superfamily (Stenmark, 2009), with more than 60 members in mammals (Klopper et al., 2012; Pereira-Leal and Seabra, 2001). Rab proteins are typically ubiquitously expressed; however, some members are tissue-specific. For example, while the A isoform of Rab6 is expressed in all cells (Echard et al., 2000), the B isoform is expressed specifically in microglia, pericytes and Purkinje cells of the central nervous system (Opdam et al., 2000).

The ability for a Rab GTPase to bind guanine nucleotides is essential to its function. With some exceptions (e.g. Rab11 (Shirane and Nakayama, 2006)), GTP (guanosine triphosphate)- and GDP (guanosine diphosphate)-bound forms respectively correspond to active and inactive states of Rab proteins (Stenmark, 2009). Activated Rab proteins bind to a number of functionally diverse effectors to induce a range of cellular responses. For this reason, Rab proteins are often referred to as “master regulators” for a particular group of actions in a specific pathway.

Two of the most well-studied Rab GTPases are Rab5 and Rab7. They recruit and coordinate effectors to carry out roles such as cargo sorting, vesicle tethering, fusion, and motility (Stenmark, 2009; Wandinger-Ness and Zerial, 2014) (**Figure 4**). Their functions are discussed later on in this introduction.

1.3.2 Structural features of Rab GTPases

Rab GTPases, like all members of the Ras superfamily, bind to guanine nucleotides through a conserved G domain composed of a six stranded β-sheet surrounded by five α-helices (Stenmark and Olkkonen, 2001). The G domain exists in two conformations (Stenmark and Olkkonen, 2001), with the greatest amount of shift occurring in regions called switch I and switch II (Cherfils and Zeghouf, 2013). Conformational change is mainly attributed to two residues—a conserved threonine in switch I and a conserved glycine in switch II—that both interact with the γ phosphate of GTP (Cherfils and Zeghouf, 2013). The interaction between Rab GTPases and guanine nucleotides is enhanced by a Mg^{2+} cofactor and a P-loop within the G domain (Burstein and Macara, 1992; Wittinghofer, 2014).

Rab GTPases are distinguished from other members of the Ras superfamily by five conserved regions called RabF regions (Rab family sequences, RabF1-5) that are located within and around switches I and II (Pereira-Leal and Seabra, 2000). Additional motifs found on the surface of Rab GTPases called RabSF (Rab family sub-family conserved) serve to categorize Rab members into their subfamilies. It is believed that Rab proteins bind to specific downstream effectors through their RabSF regions (Pereira-Leal and Seabra, 2000).

1.3.3 Regulators of Rab GTPases

The functional and spatiotemporal regulation of Rab GTPases is strictly controlled by a number of regulators (**Figure 5**). Upon its translation, a Rab GTPase is delivered to a RabGGT (Rab geranylgeranyltransferase) by REP (Rab escort protein) for prenylation of its hypervariable, C-terminal tail (Andres et al., 1993; Wu et al., 2009). This process involves attaching geranylgeranyl groups to two cysteine residues residing within CC or CXC motifs through thioether bonds (Farnsworth et al., 1994; Khosravi-Far et al., 1991).

GDI (GDP-dissociation inhibitor) functions similarly to REP but only recognizes prenylated, GDP-bound Rab proteins (Ullrich et al., 1993). As its name implies, GDI prevents GDP from dissociating from the Rab protein (Sasaki et al., 1990) and maintains Rab GTPases in the soluble, cytosolic fraction (An et al., 2003; Ullrich et al., 1993). The REP-GDI-Rab complex is disassembled by a membrane bound GDF (GDI-displacement factor) (Dirac-Svejstrup et al., 1997).

1.3.3.1 Rab guanine nucleotide-exchange factors

GEF (guanine nucleotide-exchange factor) functions by sterically hindering the Rab switch I region from the nucleotide binding site to displace the bound GDP (Cherfils and Zeghouf, 2013). It also binds to the switch II region, which likely stabilizes the Rab nucleotide-free transition state (Cherfils and Zeghouf, 2013). Rab GTPases have similar affinities towards

GDP and GTP; however, the higher cytoplasmic GTP concentration increases the likelihood for a GTP to occupy the Rab active site (Bos et al., 2007).

GEFs exist as monomeric or multimeric forms. The monomeric Rab5 subfamily of GEFs typically contain the Vps9 (vacuole protein sorting 9) catalytic domain (Barr and Lambright, 2010; Carney et al., 2006). A Rab7 bipartite GEF called Mon1-Ccz1 (monensin sensitivity 1-calcium caffeine zinc sensitivity protein 1) (Gerondopoulos et al., 2012; Lawrence et al., 2014) is described later in this introduction. The multimeric GEF complex TRAPP (transport protein particle) targets Rab1 for Golgi trafficking (Barrowman et al., 2010).

1.3.3.2 Rab GTPase-activating proteins

All Rab GTPases have an intrinsic ability to hydrolyze GTP (IRybin et al., 1996). The speed of this process, however, does not align with the rates of other cellular events. Rab GTPase-activating proteins (GAPs) are enzymes that can accelerate GTP hydrolysis by a factor of 10^5 (Albert et al., 1999).

Rab GAPs are categorized as either classical or non-classical. Classical Rab GAPs possess the conserved catalytic TBC (Tre2/Bub2/Cdc16) domain. In humans, there are 44 predicted TBC domain-containing Rab GAPs (Frasa et al., 2012; Gabernet-Castello et al., 2013). The non-classical Rab3GAP is composed of two subunits, neither of which have a TBC domain (Fukui et al., 1997; Nagano et al., 1998). Its catalytic strategy, however, is similar to the TBC domain and requires an arginine residue for function (Clabecq et al., 2000).

1.3.3.2.1 Sequence and structure of the TBC domain

The TBC domain is composed of 16 α-helices (Rak et al., 2000), which is structurally similar to the catalytic domains of Ras (Scheffzek et al., 1998; Scheffzek et al., 1996) and Rho (Nassar et al., 1998; Rittinger et al., 1997) GAPs. The TBC domain contains two signature motif sequences—IxxDxxR and YxQ—within each resides a conserved arginine (R, arginine finger) and glutamine (Q, glutamine finger) (Pan et al., 2006). Both residues cooperatively function in a dual-finger strategy: the positive side chain of arginine polarizes and prepares the γ phosphate of GTP (Rak et al., 2000) for a nucleophilic attack by a water molecule that is positioned by the glutamine (Bos et al., 2007) (**Figure 6**). Mutation of either arginine or glutamine to alanine reduces catalytic efficiency by 100-1000 fold (Pan et al., 2006).

Much of the information on the mechanics of TBC domain function comes from using aluminum fluoride (AlF_n, where n can be 3 or 4) in crystal structure analyses. AlF_n stabilizes the transition state between a GDP-bound Rab protein and its GAP by occupying the γ-phosphate position within the nucleotide-binding domain (Pan et al., 2006; Tempel et al., 2008).

1.3.3.3 Determinants for membrane localization of Rab GTPases

A number of factors have been found to target Rab proteins to their specific membranes. The hypervariable C-terminal region was once believed to be the sole determinant of this role, as demonstrated from early studies of Rab5 and Rab7 (Chavrier et al., 1991). However, it is now

known that other targeting cues exist: replacing RabF and RabSF regions of Rab5 for those of Rab27 causes Rab5 to mislocalize onto secretory vesicles (Ali et al., 2004), while Rab7 requires dephosphorylation at two conserved residues by the phosphatase PTEN (tumour suppressor phosphatase and tensin homologue deleted on chromosome 10) for GDI-assisted targeting onto LE membranes (Shinde and Maddika, 2016).

Rab GTPase regulators can function as targeting elements as well. For example, loss-of-function mutation to the yeast GEF Mon1-Ccz1 causes the Rab7 homolog to accumulate at the endoplasmic reticulum (ER) (Cabrera and Ungermann, 2013). Mislocalizing the Rab5 GEF Rabex-5 to mitochondria causes Rab5 to be targeted to the same organelle (Blumer et al., 2013). Loss of function to a REP affects the localization of intestinal RAB-5, RAB-7 and Rab27, without significantly affecting that of RAB-3, RAB-10, or RAB-11 (Tanaka et al., 2008). These findings suggest that Rab proteins utilize different strategies for membrane targeting.

1.3.4 Phosphoinositides

Phosphoinositides (PIs) are the phosphorylated derivatives of phosphatidylinositol (PtdIns)—a class of lipid composed of a diacylglycerol backbone attached to a polar inositol headgroup (Falasca and Maffucci, 2012). Seven species of PIs can be generated from phosphorylating position 3, 4, and/or 5 of the inositol ring (Lemmon, 2008) (**Figure 7**). Although PIs only comprise ~15% of the membrane phospholipid population in a cell (Viaud et al., 2016), they are potent secondary messenger molecules and function coordinately with Rab GTPases.

Distributions and cellular levels of PI species are spatially and temporally controlled through membrane-specific kinases and phosphatases (De Matteis and Godi, 2004; Lemmon, 2008) (**Table 1**). Predominant populations of PI species characterize particular compartments of the endocytic pathway: PI3P (phosphatidylinositol 3-phosphate) is primarily present on EEs (Gillooly et al., 2000), intraluminal vesicles of MVBs (Futter et al., 2001; Gillooly et al., 2000), pre-autophagosome components called omegasomes (Roberts and Ktistakis, 2013) and early phagosomes (Flannagan et al., 2012); PI(3,5)P_2 (phosphatidylinositol 3,5-biphosphate) is mainly found on LEs (Mayinger, 2012); and PI4P (phosphatidylinositol 4-phosphate) can be found at the Golgi apparatus (De Matteis et al., 2013; Mayinger, 2012).

Multiple PI species can reside on a given membrane. For example, PI(4,5)P_2 (phosphatidylinositol 4,5-bisphosphate) is commonly found on the plasma membrane of all eukaryotic cells for CCP formation (Posor et al., 2013), cytoskeletal integrity and ion channel activation (McLaughlin and Murray, 2005; Suh et al., 2006). On the other hand, PI(3,4,5)P_3 (phosphatidylinositol 3,4,5-triphosphate) and PI4P localize to certain regions of the plasma membrane for phagocytic engulfment, cell signalling (Hoeller et al., 2013; Masters et al., 2013) and protein docking (Hammond et al., 2012). PI4P has also been found on specialized tubules of EEs for cargo sorting (Henmi et al., 2016).

1.3.4.1 PI3P regulation by phosphoinositide 3-kinases

Phosphoinositide 3-kinases (PI3Ks) are lipid kinases capable of phosphorylating the inositol ring at the 3-hydroxyl position. They are categorized into three classes based on their

conserved sequence motifs and substrate preference: Class I phosphorylates PI(4,5)P_2 to generate PI(3,4,5)P_3; Class II phosphorylates both PtdIns and PI4P to generate PI3P and PI(3,4)P_2, respectively; and Class III phosphorylates PtdIns to generate PI3P (Marat and Haucke, 2016; Schink et al., 2013). Class I and III kinases can be inhibited by the fungal toxin Wortmannin or the pharmacological drug LY294002 (Jovic et al., 2010; Marat and Haucke, 2016).

1.3.4.2 PI3P generation on the EE

PI3P recruits downstream effectors possessing FYVE (Fab1, YOTB, Vac1, EEA1) or PX (Phox) domains. It can also bind to some effectors containing a PH (Pleckstrin Homology) domain (Lemmon, 2007; Lemmon, 2008; Maffucci and Falasca, 2001; Marat and Haucke, 2016) (**Figure 7**). On the EE, PI3P is generated through two strategies that both require activated Rab5 (Christoforidis et al., 1999b). In the first pathway, Class I PI3K and two phosphatases convert PI(3,4)P_2 and PI(3,4,5)P_3 originating from the plasma membrane into PI3P (Shin et al., 2005). In the second pathway, Class III PI3K generates PI3P directly from PtdIns (Christoforidis et al., 1999b).

1.3.4.2.1 VPS34, a component of the Class III PI3K

Class III PI3K is responsible for generating the bulk of the PI3P population on EEs (Gillooly et al., 2000; Schu et al., 1993). The Class III PI3K family has only one member: a conserved serine/threonine kinase called VPS34 (Herman and Emr, 1990; Volinia et al., 1995).

The VPS34 C-terminal portion binds to its regulatory partner, VPS15 (Budovskaya et al., 2002; Panaretou et al., 1997; Stack et al., 1995; Stack et al., 1993), which contains a prenylated tail to anchor the complex onto membranes (Herman et al., 1991; Panaretou et al., 1997).

1.3.4.2.2 Beclin 1 and Class III PI3K

The VPS15-VPS34 complex binds to Beclin 1 (Kihara et al., 2001a) that together form the core components of the Class III PI3K (Funderburk et al., 2010; Morris et al., 2015). This tripartite complex associates with other subunits for function in autophagy, endocytosis and protein sorting (Funderburk et al., 2010; Kang et al., 2011; Kihara et al., 2001b; McKnight et al., 2014).

Beclin 1 is a conserved tumour suppressor (Liang et al., 1999; Yue et al., 2003) that was first identified as a binding partner to the anti-apoptotic protein Bcl2 (B-cell lymphoma 2) through its BH3 (Bcl2-homology-3) domain (Liang et al., 1998; Sinha and Levine, 2008). BH3 domains are common in pro-apoptotic proteins, but Beclin 1 appears to have a more autophagic role: its interaction with Bcl2 has been found to function as a toggle switch between apoptotic and autophagic pathways (Boya et al., 2005; Marquez and Xu, 2012; Pattingre et al., 2005; Takacs-Vellai et al., 2005).

1.3.4.3 PI3P regulation by lipid phosphatases

PI3P turnover is associated with cargo degradation. For example, elevated Rab5 activity from either expression of a constitutively active, GTP-locked form or loss of Rab5 GAP leads to persistent PI3P levels on vesicles and inhibits cargo delivery to lysosomes (Chotard et al., 2010a; Li et al., 2009).

PI3P can be dephosphorylated at the 3-hydroxyl position of the inositol ring by members of the myotubularin (MTM) and myotubularin-related (MTMR) lipid phosphatase family (Clague and Lorenzo, 2005). The founding member of this family, MTM1, is ubiquitously expressed in mammals (Laporte et al., 1996; Laporte et al., 2002) and localizes to EE membranes through its GRAM (glucosyltransferases, Rab-like GTPase activators and myotubularin) domain (Cao et al., 2007a; Taylor et al., 2000; Tsujita et al., 2004).

Alternatively, PI3P may be phosphorylated at the 5-hydroxyl position to generate $PI(3,5)P_2$ by the 5-kinase Fab1/pikFYVE (formation of aploid and binucleate cells 1/phosphoinositide kinase for 5 position containing a FYVE finger) (Gary et al., 1998; Ikonomov et al., 2001). This kinase binds to PI3P via its FYVE domain (Sbrissa et al., 2002) and requires the activator VAC14 for function (Vac14, pikFYVE complex component) (Dove et al., 2002; Sbrissa et al., 2004). Phosphorylation by Fab1/pikFYVE is the only known pathway to produce $PI(3,5)P_2$ (Lemmon, 2008), while $PI(3,5)P_2$ is dephosphorylated by members of the MTM and MTMR family (Clague and Lorenzo, 2005).

1.4 Models of cargo transport

Currently, there are two models to explain how cargo is transported in the endocytic pathway. The pre-existing compartment model describes endocytic compartments as permanent, stable structures that require carrier vesicles to transport cargo between them (Griffiths and Gruenberg, 1991). On the other hand, the maturation model postulates that vesicles are formed *de novo* at the plasma membrane and fuse together into larger compartments. These endosomes undergo dynamic morphological and functional changes, and acquire different compartmental identities as they progress through the endocytic pathway (Huotari and Helenius, 2011; Murphy, 1991). In 2005, Rink and colleagues presented advanced live-cell imaging evidence showing that Rab5-positive vesicles gradually acquire strong Rab7 signal as the Rab5 signal is lost over time (Rink et al., 2005). This observation was further supported by data gathered by Vonderheit and Helenius of the same year (Vonderheit and Helenius, 2005). Altogether, this groundbreaking work led to a wide acceptance of the maturation model.

1.4.1 Rab function and endosome maturation

The Rab5 to Rab7 GTPase conversion is a conserved, multistep process that involves two interdependent cascades (Hutagalung and Novick, 2011). Essentially, an active Rab protein first recruits the GEF for the downstream Rab GTPase. When this downstream Rab protein is activated, it initiates a countercurrent GAP recruitment to inactivate the upstream Rab protein. A mathematical model called “cut-out switch” proposes that a sufficient level of activated Rab7 triggers a negative feedback for Rab5 inactivation (Del Conte-Zerial et al., 2008).

Rab5 to Rab7 conversion marks a series of transitions that are essential for an EE to mature into a LE (Huotari and Helenius, 2011). Several of these shifts—PI conversion from PI3P to PI(3,5)P_2, increase in lumen acidification and change in endosome fusion specificity—have already been described. Other features include a loss of tubular networks and an acquisition of lysosomal hydrolases from the TGN. Together, these developments close off access to the recycling pathway and promote cargo delivery to the lysosome.

1.4.2 Downstream effects of Rab5 activation

The EE master regulator Rab5 coordinates a number of events that are essential for vesicular fusion and cargo sorting. A key event is the recruitment of Class III PI3K for PI3P production (Murray et al., 2002). Several EE trafficking proteins require PI3P for their localization. For example, the ESCRT-0 component Hrs binds to PI3P through its FYVE domain (Raiborg et al., 2001), while subunits of the retromer called sorting nexins (SNXs) bind to PI3P through their PX domain (Carlton et al., 2004).

Some proteins require simultaneous binding to Rab5 and PI3P for localization. Two such examples are EEA1 (early endosome antigen 1), a tethering and docking factor for homotypic fusion between EEs (Christoforidis et al., 1999a; Mills et al., 1998; Simonsen et al., 1998), and Rabenosyn-5, a mediator of homotypic and heterotypic fusion between EEs with newly uncoated clathrin vesicles (de Renzis et al., 2002; Nielsen et al., 2000). Both proteins connect Rab5 positive vesicles to the SNARE (soluble N-ethylmaleimide-sensitive factor attachment protein receptor) fusion machinery: EEA1 interacts with SNARE subunits syntaxin6 and syntaxin13

(McBride et al., 1999; Simonsen et al., 1999), while Rabenosyn-5 binds to VPS45 (Nielsen et al., 2000) to regulate SNARE formation during endocytosis (Carr and Rizo, 2010). Fusion proceeds with the assembly of the trans-SNARE complex where four SNARE subunits entwine to bring apposing membranes close (Jahn and Scheller, 2006; Wickner and Schekman, 2008). Cis-SNARE complex disassembly involves the ATPase SNF (N-ethylmaleimide-sensitive factor) and cofactor SNAP (soluble N-ethylmaleimide-sensitive factor attachment protein) (Sollner et al., 1993).

Both Rab5 and PI3P appear to be required for plus- and minus-end movement of EEs on microtubules. The kinesin motor KIF16B (kinesin family member 16B) localizes onto an EE through its PX domain and maintains the compartment at the cell periphery for cargo sorting and recycling (Hoepfner et al., 2005). On the other hand, loss of function to either Rab5 or Class III PI3K reduces minus-end movement of EEs (Nielsen et al., 1999). The motor responsible for this process has not been identified.

1.4.3 Downstream effects of Rab7 activation

In mammals, the LE master regulator Rab7 is best known to bind to its homo-dimer effector RILP (Rab7-interacting lysosomal protein) through its C-terminal hypervariable region (Shinde and Maddika, 2016; Wu et al., 2005). RILP connects the endosome to the dynein-dynactin machinery for minus-end movement (Bucci et al., 2000; Cantalupo et al., 2001; Wu et al., 2005) by interacting with the projecting arm of dynactin called $p150^{Glued}$ (Johansson et al., 2007; Jordens et al., 2001; Schroer, 2004).

The interaction between RILP and the dynein-dynactin complex is modulated by another Rab7 effector: a cholesterol sensor called ORP1L (oxysterol-binding protein-related protein 1L) (Johansson et al., 2005; Johansson et al., 2007). At high levels of cholesterol, $p150^{Glued}$ binds to the Rab7-RILP complex (Phillips and Voeltz, 2016), and the LE is trafficked to the perinuclear region (Rocha et al., 2009). However, in conditions of low cholesterol, ORP1L undergoes a conformational change and binds instead to an ER protein called VAP-A (VAMP [vesicle-associated membrane protein]-associated ER protein-A) (Rocha et al., 2009). This action displaces the interaction between RILP and $p150^{Glued}$, thereby retaining the LE at the cell periphery (Rocha et al., 2009).

ORP1L is also involved in translocating a cytoskeletal protein called βIII spectrin onto the Rab7-RILP-dynein-dynactin complex (Holleran et al., 2001; Johansson et al., 2007; Muresan et al., 2001). βIII spectrin binds directly to acidic phospholipids of the LE membrane and bridges the endosome to the motor machinery (De Matteis and Morrow, 2000). Both ORP1L and βIII spectrin are essential for dynein-dynactin based minus-end movement (Johansson et al., 2007).

LE movement towards the perinuclear region is coupled to tethering and fusion between LEs, or LEs and lysosomes. Tethering is mediated by the HOPS (homotypic fusion and vacuole protein sorting) complex, which is recruited by RILP in an ORP1L-dependent manner (Luzio et al., 2007; Phillips and Voeltz, 2016; van der Kant et al., 2013). The HOPS complex is composed of six subunits: VPS11, 16, 18, 33, 39, and 41 (Balderhaar and Ungermann, 2013). VPS39 and VPS41 are located on opposite ends of the complex and bind to Rab7 (Balderhaar and Ungermann, 2013). VPS33 is a member of the Sec1 family and regulates the assembly of the

SNARE complex for fusion (Balderhaar and Ungermann, 2013; Seals et al., 2000; Wickner, 2010).

1.4.4 The Rab GTPase conversion during early to late endosome maturation

Activation of Rab5 is stabilized by a positive feedback loop that involves a complex composed of Rabaptin-5 and Rabex-5 (Horiuchi et al., 1997; Lippe et al., 2001; Zerial and McBride, 2001). This loop is interrupted when the PI3P-binding, bipartite Rab7 GEF Mon1/SAND-1-Ccz1 (Cabrera et al., 2014; Gerondopoulos et al., 2012; Lawrence et al., 2014; Nordmann et al., 2010; Poteryaev et al., 2007; Wang et al., 2003) displaces Rabex-5 (Poteryaev et al., 2010). The newly activated Rab7 (Poteryaev et al., 2010; Poteryaev et al., 2007) then employs a Rab5 GAP to catalyze Rab5 deactivation.

1.5 *Caenorhabditis elegans*, a model organism

Caenorhabditis elegans is a small (1.5 mm adult body length) soil nematode suitable for genetic manipulations in the laboratory (Riddle, 1997). Along with another model organism, the fruit fly *Drosophila melanogaster*, *C. elegans* is commonly used in genetic screens (Kutscher and Shaham, 2014; St Johnston, 2002). Two types of genetic screens exist: forward genetic screens provide an unbiased method by which mutated genes are identified based on a phenotype of interest, while reverse genetic screens target mutations to a particular gene to study phenotypic effects. When compared to the *Drosophila* genome, the *C. elegans* genome contains

more genes (Adams et al., 2000; Consortium, 1998), but fewer homologs that are linked to human diseases (O'Brien et al., 2004; Pandey and Nichols, 2011). Despite this drawback, *C. elegans* offers several strong features for laboratory use. First, it can be easily propagated by transferring several self-fertilizing hermaphrodites onto plates with a lawn of *Escherichia coli* as food source (Riddle, 1997; Stiernagle, 2006), and second, it has a shorter life cycle (three days at 20°C compared to more than 10 days for *Drosophila*) (Riddle, 1997).

C. elegans offers yet another advantage over *Drosophila*: its transparent body allows fluorescently-labelled markers to be easily imaged without special tissue preparations. This advantage is extremely useful for studying endocytosis, where imaging can be performed in live cells (Grant and Sato, 2006). Several endocytic model systems in the nematode have already been established. They are the intestine, oocytes, and macrophage-like coelomocytes (Sato et al., 2014; Wang and Audhya, 2014).

It is estimated that at least 83% of *C. elegans* genes have human homologues (Lai et al., 2000). The relative ease in generating mutations from *C. elegans* forward genetic screens (Jorgensen and Mango, 2002; Sin et al., 2014) has allowed researchers to establish large collections of genetic alleles. In one ambitious example, the Million Mutation Project (MMP) was developed to provide the *C. elegans* research community with mutant alleles for more than 20 000 genes. These alleles are carried in a library of ~2000 mutagenized *C. elegans* strains (Thompson et al., 2013). Inquiries on the nature and location of MMP mutations, as well as information on all annotated nematode genes and related publications can be found from a centralized, up-to-date online database called Wormbase (Howe et al., 2016).

1.5.1 TBC-2, a *C. elegans* Rab5 GAP

The *C. elegans* genome contains 21 predicted members of the TBC domain family. The RAB-5 GAP called TBC-2 (Chotard et al., 2010a) is the most well-characterized (Wormbase.org). Mutants carrying *tbc-2* strong loss-of-function deletion allele (*tm2241* or *sv41)* are viable but possess several trafficking defects. In the intestine and coelomocytes, cargo accumulates from defective degradative and recycling pathways (Chotard et al., 2010a; Sun et al., 2012). There is premature degradation of endocytosed yolk protein in the oocytes, which reduces larval survival under starvation conditions (Chotard et al., 2010b). Finally, phagocytosed cell corpses have delayed delivery to lysosomes (Li et al., 2009).

1.5.2 Human homologs of TBC-2

TBC-2 is homologous to human TBC1D2A and TBC1D2B (Chotard et al., 2010a; Fukuda, 2011). TBC1D2A produces six variants (a-f), but only two have been characterized. Variant a is a prostate antigen called PARIS-1 (prostate antigen recognized and identified by SEREX [serological identification of antigens by recombinant expression cloning]) (Frasa et al., 2012; Zhou et al., 2002). Variant c, also known as Armus, has been the most thoroughly studied and is characterized as a Rab7 GAP (Frasa et al., 2012; Frasa et al., 2010).

Armus regulates Rab7 nucleotide cycling for fusion to the lysosome. Its loss of function reduces E-cadherin disassembly from adherens junctions while simultaneously causing an accumulation of E-cadherin at the perinuclear region (Frasa et al., 2010). A similar observation

can be found in autophagy, where autophagosomes accumulate upon reduced Armus activity (Carroll et al., 2013; Toyofuku et al., 2015).

The function of TBC1D2B is less understood. It is implicated in autophagy, although its exact role is unclear (Behrends et al., 2010; Popovic et al., 2012). TBC1D2B binds to Rab22, a Rab protein associated with the recycling pathway (Stenmark, 2009; Weigert et al., 2004), regardless of its nucleotide-bound state (Kanno et al., 2010). A GAP target of TBC1D2B has not yet been identified.

TBC1D2A is associated with certain disease states; however, no animal model currently exists. TBC1D2A is identified as a biallelic marker to predict susceptibility for multiple sclerosis (Cavanillas et al., 2011). TBC1D2A GAP activity is regulated by LRRK1 (leucine-rich repeat kinase 1) (Toyofuku et al., 2015), the paralog of LRRK2 (Toyofuku et al., 2015), which is commonly mutated in inherited Parkinson's disease (Li et al., 2014). Finally, Armus mRNA levels have been found to be regulated by a known oncogenic miRNA cluster called miR-17-5p (He et al., 2005; Serva et al., 2012).

1.5.3 Molecular domains of TBC-2

TBC-2 and its human homologs share four conserved domains. The PH domain is located at the N-terminus, followed by the coiled-coil (CC) domain, the TBC1D2 homology region (THR) domain, and the catalytic TBC domain at the C-terminus (Chotard et al., 2010a; Kanno et al., 2010). For the purposes of this thesis, only the coiled-coil domain of TBC-2 will be specifically referred to as ‘CC domain’. All other coiled-coil domains will be not be abbreviated.

1.5.3.1 Features of the PH domain

The PH domain is a lipid (Chen et al., 1997; Harlan et al., 1994; Koshiba et al., 1997; Lemmon, 2007) and protein (Lodowski et al., 2003; Touhara et al., 1994; Yao et al., 1994; Yao et al., 1997) binding domain that was first identified in the platelet protein pleckstrin (Haslam et al., 1993). It is the 11th most common domain in the human genome (Lemmon, 2007) and has a poorly conserved sequence composed of approximately 100 amino acids (Haslam et al., 1993). The only invariant residue identified so far is a tryptophan at the C-terminus (Shaw, 1996).

Despite its poor sequence conservation, all PH domains fold into seven β-strands that are characteristically arranged into two orthogonal antiparallel β-sheets (Lemmon and Ferguson, 2000; Maffucci and Falasca, 2001; Soisson et al., 1998; Wen et al., 2006). Of the six loops connecting the β-strands, loops β1/β2, β3/β4, and β6/β7 are hypervariable and contain key residues that make up the positively charged surface for PI binding (Lemmon and Ferguson, 2000; Maffucci and Falasca, 2001). At the C-terminal of the PH domain, an amphiphatic α-helix is held to the β-sheets through the conserved tryptophan residue (Blomberg et al., 2000; Lemmon and Ferguson, 2000; Maffucci and Falasca, 2001; Shaw, 1996).

The PH domain is best known for its ability to bind to PIs; however, only a fraction of them have high affinity and specificity for lipid target(s). PH domains have the strongest binding affinity towards PIP_3, $PI(3,4)P_2$, and $PI(4,5)P_2$ (Hurley and Misra, 2000; Lemmon, 2007; Maffucci and Falasca, 2001) but typically weak binding towards all other PI species (Hurley and Misra, 2000; Lemmon, 2007; McMahon and Boucrot, 2011). High affinity interactions for PI3P,

PI4P, and PI(3,5)P_2 are achieved instead by the FYVE domain, PX domain, PHD (plant homeodomain) finger or the lipid-binding sites of PROPPINs (β-propellers that bind polyphosphoinositides) family proteins (Lemmon, 2007).

PH domains with weak PI affinity are hypothesized to function cooperatively with other interacting domains to restrict protein distribution (Carlton and Cullen, 2005; Jean and Kiger, 2012). For trafficking regulators, binding to two or more targets that are coincidently present on a membrane can regulate their subcellular localization in a spatiotemporal manner (Carlton and Cullen, 2005; Jean and Kiger, 2012; Lemmon and Ferguson, 2000).

1.5.3.2 Features of the coiled-coil domain

The coiled-coil domain is composed of two or more right-handed, amphiphatic α-helices that entwine to form a left-handed supercoil (Aluru, 2006; Berg et al., 2002). Quaternary structured coiled-coil domains can be composed of homomeric or heteromeric helices that orient in a parallel and/or antiparallel manner (Woolfson, 2005). A single α-helix is composed of 3.6 residues per turn and is stabilized by hydrogen bonds formed between C=O and N-H groups of the main chain (Berg et al., 2002).

Each α-helical subunit of a coiled-coil domain has a primary structure that follows a repeating amino acid pattern with certain chemical properties. This pattern is called the heptad repeat and is denoted as $(abcdefg)_n$. Hydrophobic (*a* and *d*) and oppositely charged (*e* and *g*) residues interact with apposing α-helices to establish interhelical stability within a coiled-coil domain (Mason and Arndt, 2004; Parry, 1982; Woolfson, 2005). Hydrophobic residues of one

interacting helix are packed into spaces created by the residues of the neighbouring helix in an arrangement coined as “knobs into holes” (Aluru, 2006).

Coiled-coil domains can be used by trafficking proteins for localization. For example, Rabex-5 of the Rab5 activation complex contains a coiled-coil domain for binding to a membrane-bound Rabaptin-5 (Zhu et al., 2007). Alternatively, coiled-coil domains may be used to achieve avidity-mediated binding (Carlton and Cullen, 2005; Klein et al., 1998; Salim et al., 1996). In rarer instances, coiled-coil domains may bind to lipids. CIN85, an adaptor protein for EGFR internalization, sorting, and degradation (Kowanetz et al., 2004; Schroeder et al., 2010), binds to phosphatidic acids via basic residues located within its CC domain (Zheng et al., 2014).

1.5.4 TBC-2 function in the *C. elegans* intestine

TBC-2 recruitment during endosome maturation is a critically timed event in RAB-5 and RAB-7 conversion. Loss of its function alters cargo degradation and molecular identities of endocytic compartments. *tbc-2* mutant worms display enlarged intestinal vesicles that are mostly RAB-7 positive. When viewed under differential interference contrast (DIC) microscopy, these vesicles are found to contain globular, refractile material, which is believed to be undegraded lipids and proteins (Chotard et al., 2010a). From an *in vitro* GAP assay, TBC-2 can act on both RAB-5 and RAB-7 (Chotard et al., 2010a). This is consistent with the elevated level of RAB-5 in the membrane containing fraction of *tbc-2(tm2241)* worms (Liu and Grant, 2015) and with the RAB-7 and HOPS requirement for the *tbc-2(tm2241)* phenotype (Chotard et al., 2010a).

So far, the *tbc-2* mutant phenotype can only be phenocopied by expressing constitutively active RAB-5 (Chotard et al., 2010a). enlarged endosomes have been found in worms expressing mutated genes involved in basolateral recycling (*rab-10*, *amph-1* and *rme-1*) or to the pikFYVE homolog *ppk-3* can produce enlarged endosomes; however, these endosomes do not contain globular material (Chen et al., 2006; Grant et al., 2001; Nicot et al., 2006). By identifying genes that, when mutated, give rise to *tbc-2(tm2241)*-like mutant phenotypes, we can enhance our understanding on the functional regulation of TBC-2 in endocytic trafficking of polarized epithelia.

1.5.5 TBC-2 regulation in the *C. elegans* intestine and thesis rationale

Consistent with the Rab conversion model for countercurrent GAP recruitment, localization of TBC-2 onto endosome membranes requires *rab-7* (Chotard et al., 2010a). However, little is known about the mechanisms behind this recruitment. TBC-2 can serve as a good model in understanding GAP regulation for two reasons. First, although TBC-2 is identified as a Rab5 GAP, it is able to catalyze RAB-7 GTP hydrolysis (Chotard et al., 2010a). The ability for TBC-2 to act on two Rab proteins is not unique; some GAPs also have multiple targets (Frasa et al., 2012). Assuming that RAB-7 is a true *in vivo* target, studying how TBC-2 is localized may unveil mechanisms for compartment selection. Second, TBC-2 catalyzes RAB-5 GTP hydrolysis in both endocytosis and phagocytosis. However, unlike its recruitment on endosomes, TBC-2 appears to be recruited onto phagosomes in a RAB-7 independent manner (Li et al., 2009). Thus, studying TBC-2 recruitment can provide valuable information on which cues and signalling that GAP proteins respond to in various endocytic pathways.

GAPs typically possess multiple protein and/or lipid binding domains (Bos et al., 2007), which suggest that they are regulated by multiple elements. TBC-2 conserved domains have not been fully characterized for their function. The PH and CC domains are good candidates to target TBC-2 onto endosomal membranes, but no studies have been done to support this hypothesis. The role of the THR domain is unknown. The TBC domain contains the arginine finger (R689), which when mutated into alanine or lysine, generates a catalytically inactive form of TBC-2. This mutant is able to associate onto membranes (Chotard et al., 2010a; Li et al., 2009).

A region encompassing the CC domain has been found to be important for recruiting TBC-2 and its homologs onto intracellular compartments. In endocytosis, this region binds to basolateral recycling proteins RAB-10 and AMPH-1 (amphiphysin-1). The two proteins complex with each other and bind separately to distinct regions of TBC-2: RAB-10 binds to the N-terminal portion within the TBC-2 CC domain, while AMPH-1 binds to the segment that lies between the PH and CC domains (Liu and Grant, 2015). The TBC-2 CC domain containing region is also required for associating onto phagosomes (Li et al., 2009), but no protein partner has been identified yet. Another basolateral recycling marker, CED-10 (cell death abnormality-10), likely binds to the CC domain containing region to recruit TBC-2 (Sun et al., 2012) in a manner that is homologous to the interaction between mammalian Rac1 and Armus (Frasa et al., 2010).

To summarize, how TBC-2 is spatiotemporally regulated during RAB-5 to RAB-7 conversion is unknown. The goal of this thesis is to investigate the mechanisms required for TBC-2 recruitment during early to late endosome maturation in the worm intestine. I identified TBC-2 domains and residues essential for its localization and activity. I also made initial characterizations of a potential TBC-2 regulator isolated from a forward genetic screen.

Information from this thesis can uncover regulation strategies of other GAP proteins and contribute to a greater understanding of how trafficking events are coordinated during Rab conversion.

Figure 1

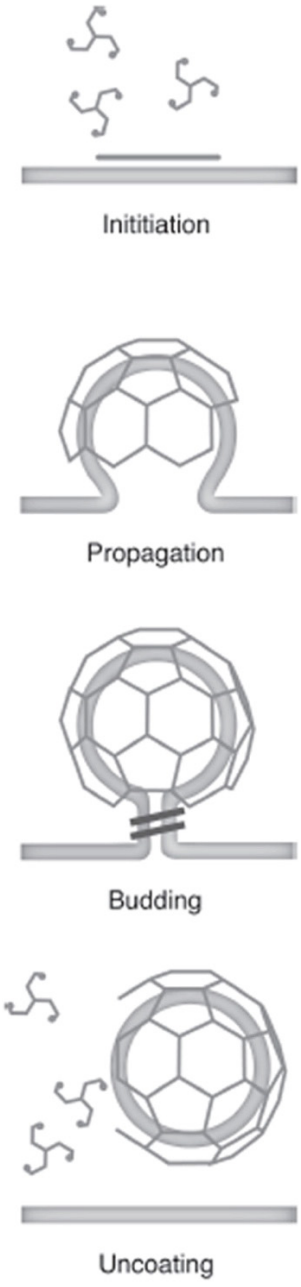

Figure 1. Four steps are involved in the formation of a vesicle from CME. They are initiation, budding, propagation and uncoating.

Figure 2

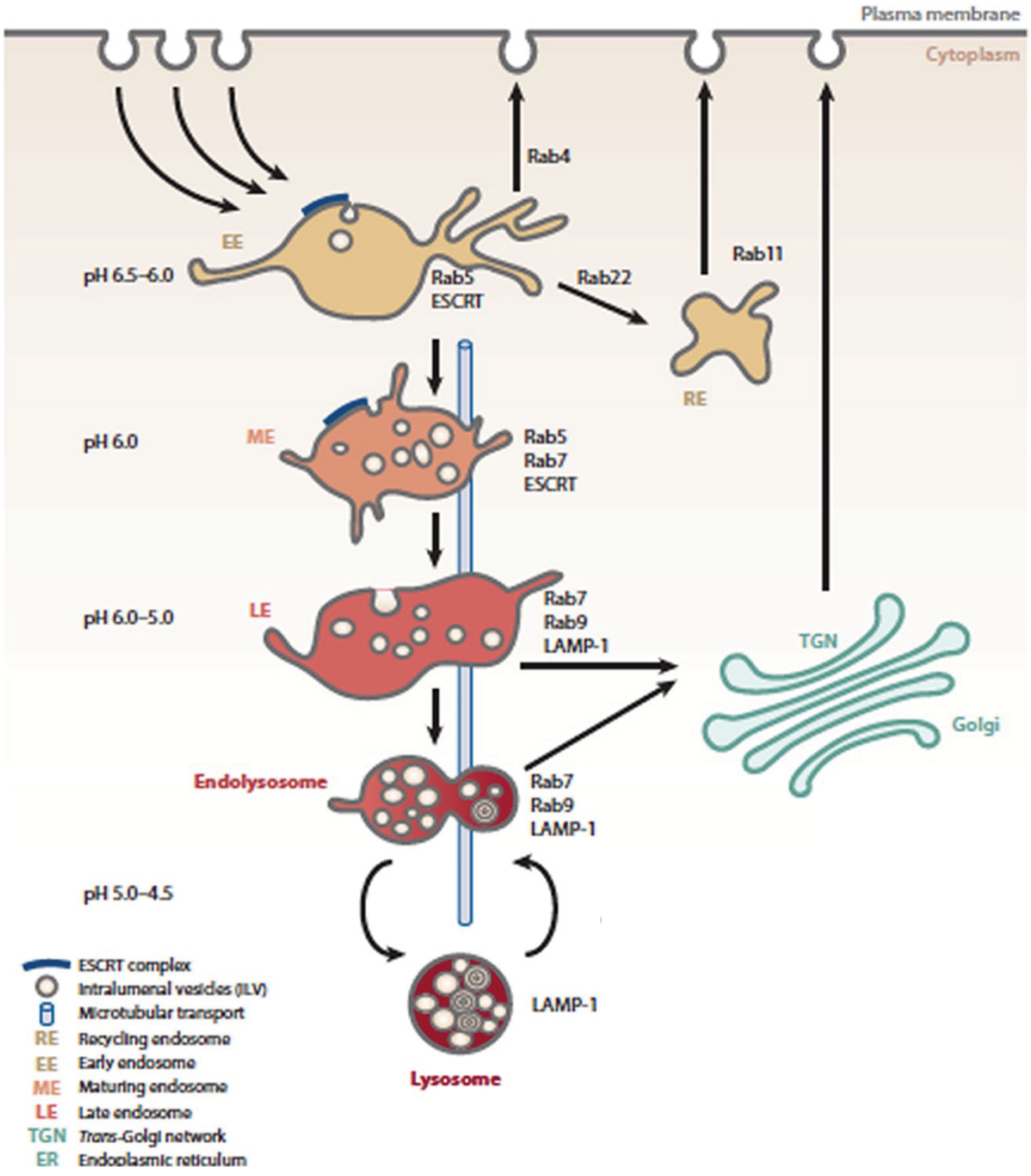
Plasma membrane
Cytoplasm
Rab4
EE
pH 6.5–6.0
Rab5
ESCRT
Rab22
Rab11
RE
pH 6.0
ME
Rab5
Rab7
ESCRT
pH 6.0–5.0
LE
Rab7
Rab9
LAMP-1
TGN
Golgi
Endolysosome
Rab7
Rab9
LAMP-1
pH 5.0–4.5
LAMP-1
Lysosome
ESCRT complex
Intraluminal vesicles (ILV)
Microtubular transport
RE Recycling endosome
EE Early endosome
ME Maturing endosome
LE Late endosome
TGN Trans-Golgi network
ER Endoplasmic reticulum

Figure 2. Localization of Rab GTPases and other trafficking components in endocytosis. Components of the endocytic pathway are associated with specific Rab GTPases. Rab5 associates with EEs, and Rab7 associates with LEs and lysosomes. The ESCRT complex is involved with the generation of ILVs. Retromer is required for retrograde trafficking from endosomes back to the TGN. LAMP1 is a glycosylated transmembrane protein that protects lysosomes from self-degradation by acid hydrolases.

Figure 3

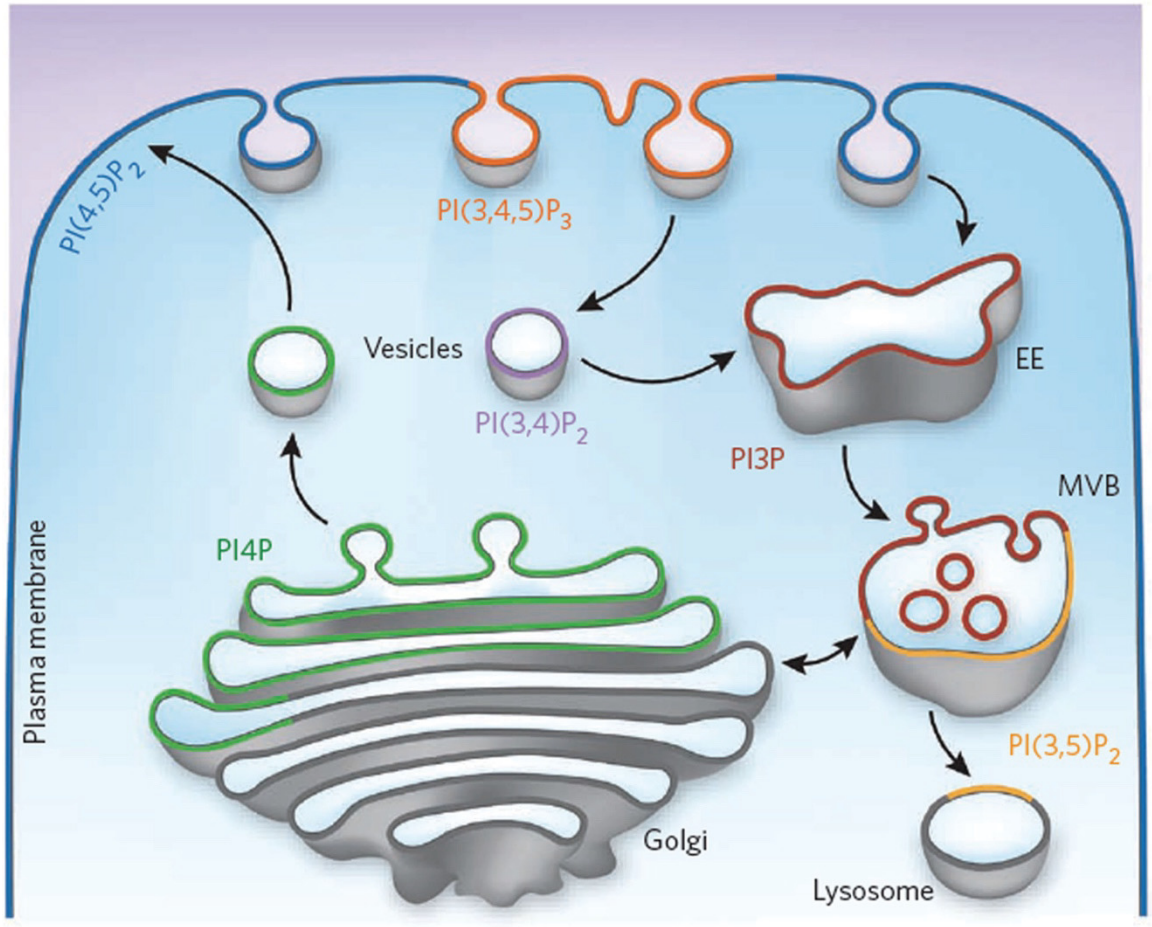
PI(4,5)P2
PI(3,4,5)P3
Vesicles
PI(3,4)P2
EE
PI3P
MVB
PI4P
Plasma membrane
Golgi
PI(3,5)P2
Lysosome

Figure 3. Localization of PIs on endocytic compartments. Predominant populations of PIs are spatially restricted. Lipids of importance for this thesis are PI3P, PI(3,5)P_2 and PI(4,5)P_2, which are respectively found on EEs, LEs, and the plasma membrane.

Figure 4

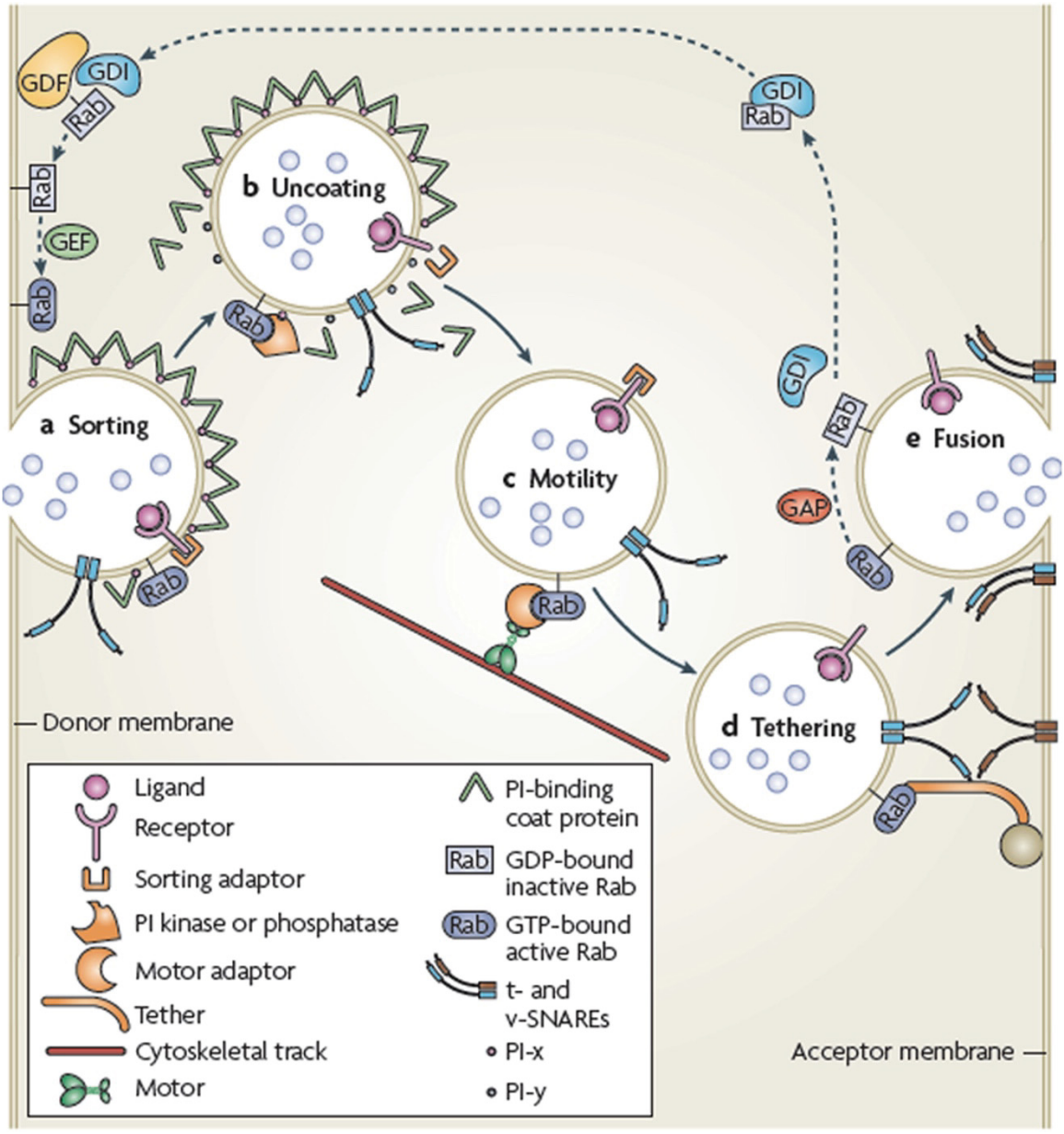
GDF
GDI
Rab
GEF
b Uncoating
a Sorting
c Motility
d Tethering
e Fusion
GAP
Donor membrane
Acceptor membrane
Ligand
Receptor
Sorting adaptor
PI kinase or phosphatase
Motor adaptor
Tether
Cytoskeletal track
Motor
PI-binding coat protein
GDP-bound inactive Rab
GTP-bound active Rab
t- and v-SNAREs
PI-x
PI-y

Figure 4. Roles of Rab GTPases. Multiple roles that Rab GTPases play are cargo sorting, vesicle tethering, vesicle fusion and fission, and vesicular motility.

Figure 5

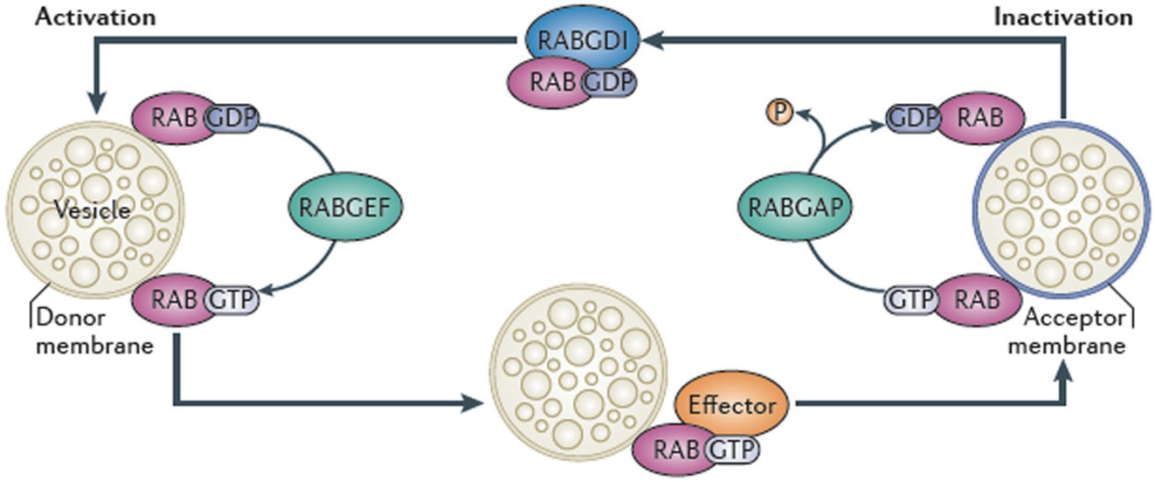
Activation
Inactivation
RABGDI
RAB GDP
RAB GDP
Vesicle
RABGEF
RAB GTP
Donor membrane
P
GDP RAB
RABGAP
GTP RAB
Acceptor membrane
Effector
RAB GTP

Figure 5. GTP/GDP cycles of Rab GTPases. Rab GTPases are described as molecular switches due to its GDP-bound (inactive) and GTP-bound (active) functional configurations. A GEF catalyzes the GDP to GTP switch on a GDP-bound Rab protein. Once activated, the Rab protein binds to effectors, which carry out diverse roles. To inactivate the Rab GTPase, a GAP accelerates the hydrolysis of its bound GTP. GDP-bound Rab is then removed from the membrane and kept in the cytoplasm by a GDI.

Figure 6

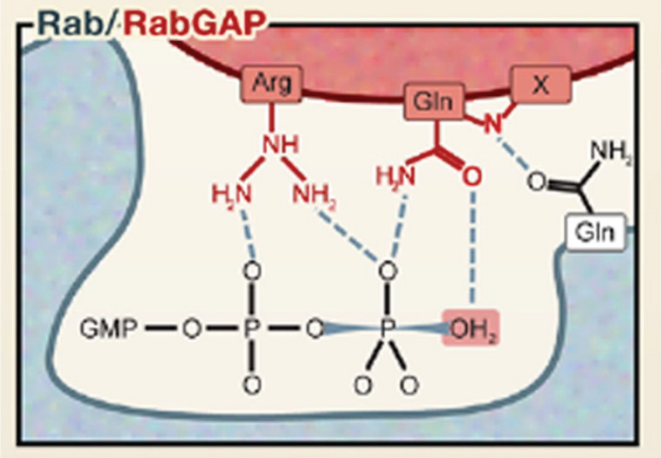
Rab/RabGAP
Arg
Gln
X
NH
H2N
NH2
H2N
O
N
NH2
O
Gln
O
O
GMP
O
P
O
P
OH2
O
O
O

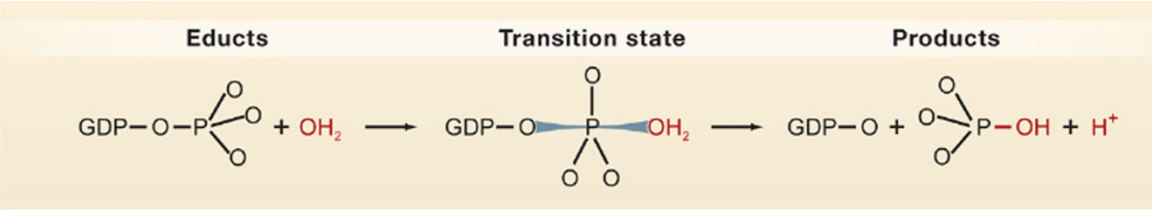
Educts
Transition state
Products
GDP
O
P
O
O
O
+ OH2
GDP
O
P
OH2
O
O
GDP
O +
O
O
P
OH
+ H+

Figure 6. GTP hydrolysis is catalyzed by arginine and glutamine fingers within the TBC domain. Schematic diagram depicting how arginine (Arg) and glutamine (Gln) fingers of the TBC domain position GTP for nucleophilic attack. Dashed lines denote H bonds. The diagram is based from crystal structure studies.

Figure 7

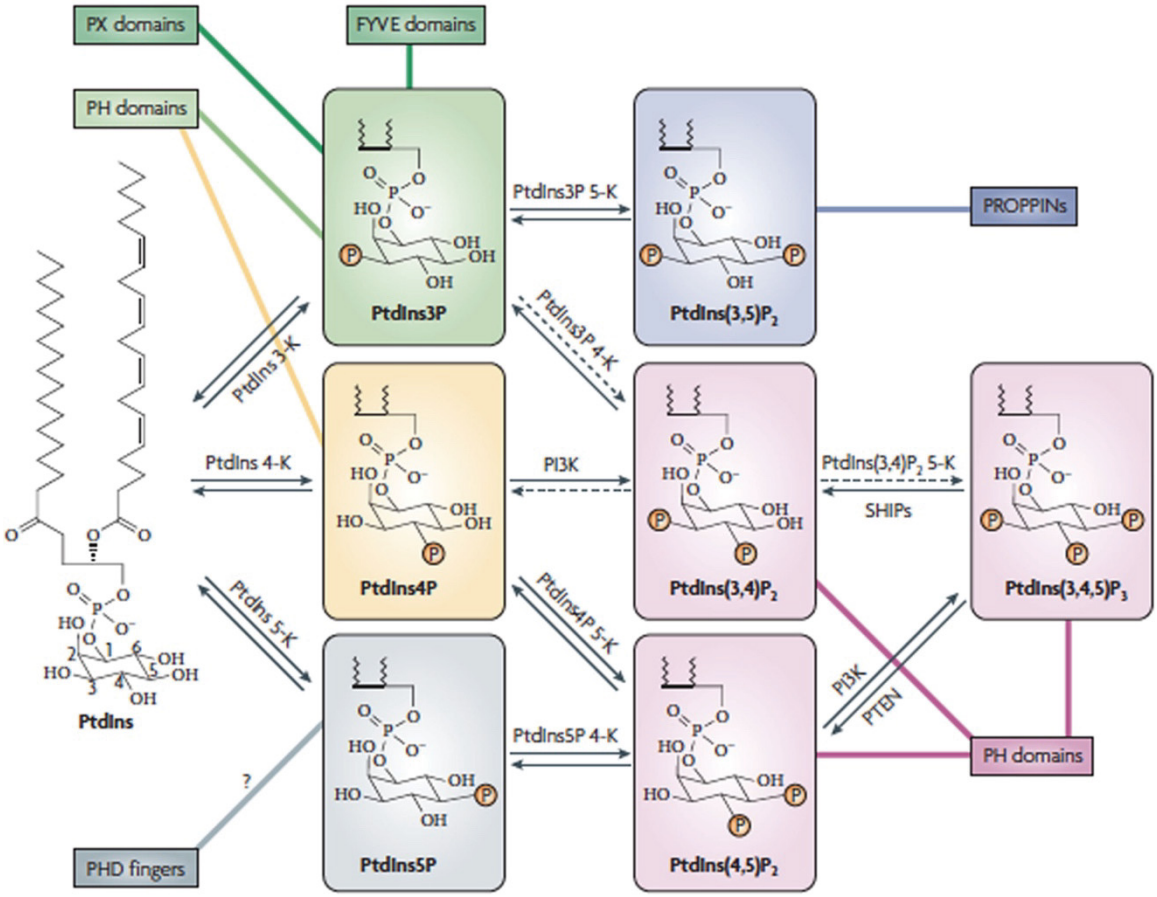
PX domains
FYVE domains
PH domains
PtdIns3P
PtdIns(3,5)P2
PROPPINs
PtdIns3P 5-K
PtdIns3P 4-K
PtdIns 3-K
PtdIns 4-K
PI3K
PtdIns(3,4)P2 5-K
SHIPs
PtdIns4P
PtdIns(3,4)P2
PtdIns(3,4,5)P3
PtdIns 5-K
PtdIns4P 5-K
PI3K
PTEN
PtdIns
PtdIns5P 4-K
PH domains
?
PHD fingers
PtdIns5P
PtdIns(4,5)P2

Figure 7. PI structures and the domains that bind to them. Seven different PIs are generated from phosphorylating position 3,4 and/or 5 of the inositol ring. Species of PIs can be interconverted through the actions of kinases and phosphatases. Different protein domains bind specifically to certain PIs.

Table 1. Localization of PI kinases, phosphatases and their substrates.

Table 1 | Phosphoinositide-metabolizing enzymes

Enzymatic activity	Isoform/gene	Predominant substrate	Localization	Disease
PI kinases				
PI(3)K	P110α–δ	PI(4,5)P_2	PM, N	Cancer (P110α)
	PI(3)K-C2α	PI (others?)	PM, TGN/E	–
	PI(3)K-C2β	PI (others?)	PM	–
	PI(3)K-C2γ	PI (others?)	GC	–
	Vps34	PI	GC, E	Bipolar disorder
PI(4)K	PI(4)K IIα	PI	GC, TGN/E; PM (some)	Bipolar disorder
	PI(4)K IIβ	PI	GC, TGN/E; PM (some)	–
	PI(4)K IIIα	PI	ER, GC	–
	PI(4)K IIIβ	PI	N, GC	–
PI(5)K	PIK-fyve	PI(3)P	LE	Francois–Neetens fleck cornea dystrophy
PIP(4)K	PIP(4)Kα,β,γ	PI(5)P	PM (α,β); ER (γ)	–
PIP(5)K	PIP(5)Kα,β,γ	PI(4)P	PM	–
PI phosphatases				
3-phosphatases	PTEN1,2	PI(3,4)P_2, PI(3,4,5)P_3	PM, GC, N	Cancer; Cowden disease
	MTM1	PI(3)P, PI(3,5)P_2	PM	Myopathy
	MTMR1–8	PI(3)P, PI(3,5)P_2	PM; some unknown	Charcot-Marie-Tooth type 4B1 (MTMR2)
4-phosphatases	Sac1-3	PI(4)P	ER, GC	–
	Synaptojanin1,2	PI(4)P?	–	–
	Type I, II	PI(3, 4)P_2	Unknown	–
5-phosphatases	Synaptojanin1,2	PI(4,5)P_2 and others	SV, PM, Mi	Bipolar disorder, Down syndrome
	OCRL	PI(4,5)P_2	TGN/E, Ly	Oculocerebrorenal syndrome of Lowe
	SKIP	PI(4,5)P_2	ER, PM	–
	PIPP	PI(4,5)P_2	PM	–
	SHIP1	PI(3,4,5)P_3	N, PM	Myeloid leukaemia; Paget's disease?
	SHIP2	PI(3,4,5)P_3	N, PM	Type II diabetes
	72kD-5-phosphatase	PI(3,4,5)P_3	GC	–
	5-phosphatase II	PI(3,4,5)P_3	Unknown	–
	5-phosphatase IV	PI(3,4,5)P	Unknown	–

E, endosome; ER, endoplasmic reticulum; GC, Golgi complex; hSac1-3, human homologues of yeast suppressor of actin 1 (Sac1); Vps34, human homologue of yeast Vps34p; LE, late endosome; Ly, lysosome; Mi, mitochondria; MTM1, myotubularin 1; MTMR1–8, MTM1-related proteins; N, nucleus; OCRL, oculocerebrorenal syndrome of Lowe; PI, phosphoinositide; PI(3)K, phosphatidylinositol 3-kinase; PI(4)K, phosphatidylinositol 4-kinase; PI(5)K, phosphatidylinositol 5-kinase; PIP(4)K, phosphatidylinositol phosphate 4-kinase; PIP(5)K, phosphatidylinositol phosphate 5-kinase; PIPP, proline-rich inositol polyphosphate 5-phosphatase; PM, plasma membrane; PTEN, phosphatase and tensin homologue; SHIP1-2, SH2-containing inositol phosphatases 1 and 2; SKIP, sphingosine kinase type 1-interacting protein; SV, secretory vesicle; TGN, trans-Golgi network.

Reprinted from EMBO Rep, 8(3), Phosphoinositide-metabolizing enzymes at the interface between membrane traffic and cell signalling, Krauß M, Haucke V, 241-246, 2007 with permission from John Wiley and Sons.

Chapter 2. Materials and methods

2.1 *C. elegans* strains

Handling and husbandry of *C. elegans* were performed as described elsewhere (Brenner, 1974). Wildtype N2 worms used in this thesis are from the Bristol strain. All worms were fed with the *Escherichia coli* strain HB101. Descriptions of genes and their alleles used in this thesis can be found on Wormbase. Unless otherwise stated, all worms were maintained at 20ºC and were ordered from the *Caenorhabditis* Genetics Center (University of Minnesota, Minneapolis, MN). Strains used in this thesis: wildtype (Bristol N2), QR15 *tbc-2(tm2241)II* (Chotard et al., 2010a), QR431 *tbc-2(tm2241)II*; *vhIs12*(P_{vha-6} GFP::TBC-2) (Chotard et al., 2010a), QR395 *vh45 II* (this study), QR449 *tbc-2(tm2241)II*; *vhEx12*(P_{vha-6}::GFP::TBC-2::Flag + P_{ttx-3}::GFP) (this study), QR457 *tbc-2(tm2241)II*; *vhEx20*(P_{vha-6}::GFP::TBC-2(ΔPH)::FLAG + P_{ttx-3}::GFP) (this study), QR459 *tbc-2(tm2241)II*; *vhEx22*(P_{vha-6}::GFP::TBC-2(ΔPH-CC):: FLAG + P_{ttx-3}::GFP) (this study), QR639 *tbc-2(tm2241)II*; *vhEx51*(P_{vha-6}::GFP:: RILPb::TBC-2(ΔPH-CC)::FLAG) (this study), QR459 *tbc-2(tm2241)II*; *vhEx22*(P_{vha-6}::GFP::TBC-2(ΔPH-CC)::FLAG + P_{ttx-3}::GFP) (this study), VC517 *bec-1(ok691)IV*, QR635 *bec-1(ok691)IV*; *vhEx12*(P_{vha-6}::GFP::TBC-2::FLAG + P_{ttx-3}::GFP) (this study), QR636 *bec-1(ok691)IV*; *vhEx20*(P_{vha-6}::GFP::TBC-2(ΔPH)::FLAG + P_{ttx-3}::GFP) (this study); from the MMP: QR494 *tbc-2(gk143714)II*, QR496 *tbc-2(gk331596)II*, VC20287, VC20509, VC20581, VC40005, VC40216, VC40512, VC40589; unknown linkage: QR247 *vhEx3*(P_{lin-31}::GFP::RAB-7; P_{vha-6}::GFP), QR581 *pwIs429* (P_{vha-6}::mCherry::RAB-7 + *Cb-unc-119*); *qxIs156* (*P*$_{hsp}$::MTM-1) (this study), QR599 *pwIs480* (*P*$_{vha-6}$::mCherry::RAB-5 + *Cb-unc-119*)/+; *qxIs156* (P_{hsp}::MTM-1)/+ (this study), XW2335 *qxIs156* (P_{hsp}::MTM-1 + P_{sur-5}::GFP) (Zou et al., 2009), XW2335 *qxIs156* (P_{hsp}::MTM-1 + P_{sur-5}::GFP) (Zou et al., 2009), XW3232 *qxIs210* (P_{hsp}::MTM-1 C378S + P_{sur-5}::GFP) (Zou et al., 2009), RT327 *unc-119(ed3) III*; *pwIs72* (P_{vha-6}::GFP::RAB-5 + *Cb- unc-119*) (Chen et al., 2006), RT476 *unc-119(ed3) III*; *pwIs170* (P_{vha-}

$_{6}$::GFP::RAB-7 + *Cb- unc-119*) (Chen et al., 2006), RT1103 *pwIs429* (P_{vha-6}::mCherry::RAB-7 + *Cb-unc-119*) (gift from Barth Grant), RT1239 *pwIs480* (P_{vha-6}::mCherry::RAB-5 + *Cb-unc-119*) (gift from Barth Grant), RT1239 *pwIs846*(P_{vha-6}::mCherry::RAB-5) (gift from Barth Grant). *vha-6* is an intestinal specific promoter.

The *tbc-2* allele called *tm2241* contains a 230 bp deletion with an 8 bp insertion mutation in the region within the 3rd and 4th exon (Wormbase.org). When expressed, the allele encodes for a product that is prematurely terminated. The truncated product is 177 amino acids in length and does not contain the TBC catalytic domain (Li et al., 2009).

2.2 Microscopy

For all differential interference contrast (DIC) and confocal images, live worms were mounted on 2% agarose pads on a glass slide, immersed in a drop of 100mM levamisol as described (Wormbook.com) and covered with a coverslip (18×18-1 for DIC, 18×18-1.5 for confocal, Fisherbrand). Images of the intestine were taken from worms at the 4th larval stage (L4) or from young adult worms. Images of the most proximal oocytes were taken from young adult worms. An Axio Zeiss A1 Imager compound microscope (Carl Zeiss, Oberkochen, Germany) with 100x/1.3 Plan-Neofluar oil immersion objective lens was used to view worms under DIC microscopy. DIC images were captured using an Axio Cam MRm camera and AxioVs40 V 4.5.0.0 AxioVision image software (Zeiss). For confocal microscopy, a LSM-780 laser scanning confocal microscopy with the Plan-Apochromat 63x/1.4 oil immersion objective lens (Zeiss) was used. Fluorescence signal was detected using the Argon multiline 488 nm excitation laser for

GFP or DPSS 561 nm laser for mCherry. Images were captured with a 32 channel GaAsP detector array and ZEN2010 image software. All images were taken at room temperature.

Raw data were analyzed using Fiji (Version 2015 December 22) or ImageJ (1.47v) (Schindelin et al., 2012; Schneider et al., 2012). For presentation purposes, images were modified using ImageJ or Adobe Photoshop CS6.

2.3 RNA interference

RNAi via feeding was conducted as described by Kamath et al. (Kamath et al., 2001). Feeding clones obtained from the Ahringer library (Kamath and Ahringer, 2003) were *rab-7* (II-8G13), *vps-15* (II-8E15), *vps-34* (I-2F20), *K12H6.9* (II-2G04) and *Y8A9A.2* (II-3B19). Homemade feeding clones for *Y27F2A.11* were made using FLo32 and FLo34 (3'- CAT TAA CCG GTA AGA CAG GCA AGT ACC, 5'-CAC TGC TAG CGT ATC CCT TGT TGG, respectively). The RNAi clone targeting *gfp* was used as negative control. All clones were verified by Sanger sequencing (Genome Quebec).

Bacteria containing the plasmid RNAi clones were selected using ampicillin. They were then induced to transcribe the clone using IPTG (isopropyl β-D-1-thiogalactopyranoside). In all RNAi treatments, L4 stage mothers were placed onto plates seeded with bacteria expressing double-stranded RNA (dsRNA) of interest. The offspring were observed for phenotypic changes at the L4 and/or young adult stage. In the double-RNAi epistasis experiments, two dsRNA-expressing bacterial cultures were mixed before spreading on RNAi plates.

2.4 Lipid binding assay

PIP Strips™ (Echelon Biosciences Inc.) were blocked with 3% BSA in Tris buffered saline with Tween 20 (1X TBST, 10 mM Tris, 150 mM NaCl pH 8.0 and 0.1% Tween 20) for one hour at room temperature. These strips were then incubated with 0.5 μg/ml of each GST (glutathione S-transferase)::TBC-2 fusion proteins or PIP2 GripTM as positive control and GST as negative control in blocking solution for one hour at room temperature. The strips were washed 3 times with 1X TBST for 10 minutes, before incubation in a 1:2000 dilution of α-GST polyclonal antibody (Sigma-Aldrich) in blocking solution for one hour at room temperature. After washing with TBST, the strips were incubated in a 1:10 000 dilution of goat α-rabbit horseradish peroxidase conjugate (Sigma- Aldrich) in blocking solution for one hour at room temperature. After 3 washes in 1X TBST, the lipid binding was detected with enhanced chemiluminescence substrate (Pierce).

2.5 Liposome binding assay

Liposomes for binding assays were prepared as described previously (Roach et al., 2012; Zhang et al., 2014). 1,2-dioleoyl-sn-glycero-3-phosphocholine (PC), 1,2-dioleoyl-sn-glycero-3-phosphoethanolamine (PE), 1,2-dioleoyl-sn-glycero-3-phosphate (PA), 1,2-dioleoyl-sn-glycero-3-phospho-(1'-myo-inositol-3'-phosphate) (PI3P) and 1,2-dioleoyl-sn-glycero-3-phospho-(1'-myo-inositol-4'-phosphate) (PI4P) were obtained from Avanti Polar Lipids (Alabaster, AL). Control liposomes were prepared by mixing PC and PE in a molar ratio of 67:33. Liposomes

containing acidic phospholipids were prepared by mixing PC and PE with one of PA, PI3P, or PI4P in a molar ratio of 65:32:3. After drying with a rotatory vacuum, the lipid mixtures were re-suspended with insider buffer (256 mM sucrose, 20 mM Tris HCl, pH 7.4), and subjected to 10 cycles of freezing in liquid nitrogen and thawing in 37°C water bath. The formed multilamellar lipids were then extruded through polycarbonate membranes (pore size 100 nm, Whatman) 10 times to generate small unilamellar liposomes. After washing with the binding buffer (150 mM NaCl, 20 mM Tris, pH 7.4) and centrifuging at 30,000 × g for one hour, the pelleted liposomes were resuspended with binding buffer and used within one week. 10 pmol purified GST-TBC-2-CC or GST-TBC-2-PH protein was mixed and incubated with the serially diluted liposomes at 4°C for 30 minutes. After centrifuge at 30,000 × g for 30 minutes, the supernatant was carefully removed. The pellets were resuspended with 1X SDS loading buffer and boiled for 5 minutes, and then separated by SDS-PAGE. GST-TBC-2-PH or GST-TBC-2-CC binding to liposomes was detected by an anti-GST antibody (Abcam) and followed by an IRDye 680-conjugated secondary antibody (Rockland Immunochemicals, Gilbertsville, PA), and visualized by a LI-COR odyssey imaging system. The intensity from western blot results was quantified using ImageJ.

2.6 Molecular cloning, construction and expression of fusion constructs

TBC-2 full-length (aa 2..908) and deletion constructs (ΔPH [aa 117-908] and ΔPH-CC [aa 391-908]) were fused to a GFP tag at their N-termini and a FLAG tag at their C-termini. They were then cloned into a BamHI and EcoRI digested vector derived from $P_{vha\text{-}6}$::GFP::TBC-2 (Chotard et al., 2010a). Forward primers JHo130 (5'-GTC GAC TGG ATC CGG TAC), FLo05

(5'-CAC TAT GGA TCC TGG AAG GCA ACG AAA TCA AAA TC) and FLo6 (5'-CAG TAA GGA TCC CTT CGA ATG TGT GAA GAA GAA AAT CG) were used for amplifying full-length TBC-2, TBC-2(ΔPH) and TBC-2(ΔPH-CC) respectively. The reverse primer for all deletion constructs was FLo7 (3'-CAT ATA GAA TTC TTA CTT ATC GTC GTC ATC CTT GTA ATC CAT ACA GTG GCC AGT ATC). FLo7 carries a FLAG tag.

GST fusion constructs of PH-CC (aa 18..390), PH (aa 18..116) and CC (aa 283..390) domains were amplified using vector P_{vha-6}::GFP::TBC-2 (Chotard et al., 2010a) as template. PH-CC domain was amplified using JHo160F (5'-CAT TAT GGA TCC AT TCT GCG GCG CCG GGG ACA ATC) and JHo154R (3'-GTG TTG GAA TTC TTA AAT AAG CTC TTC TTT TGT TCG TAA TG). PH domain was amplified using JHo160F and JHo153R (3'-GTG TTG GAA TTC TTA CTT CTT TTC CGT GTA CTT TGA AGA GCT TTC ATC C). CC domain was amplified using JHo161F (5'-CAC CAT GGA TCC GAA GAG AAA GTT ATT G) and JHo154R. PH-CC and PH domains were cloned into pGEX-5X-2, while CC domain was cloned into pGEX4T-3 using BamHI and EcoRI restriction sites. All clones were verified by Sanger sequencing (Genome Quebec).

The Rab7 binding domain of murine RILP (NP_001025109, aa 220-299, referred to simply as RILPb) was a kind gift from Aimee Edinger (UCI, Irvine, CA). The domain was originally fused to the C-terminus of a GST tag and cloned into a pGEX 4T-3 plasmid for expression in *Escherichia coli* strain, BL21. For our purposes, RILPb was first amplified with forward FLo35 (5'-GAC CCA ATG TGC CTG GAT GC) and reverse FLo36 (3'-GGA GCT GCA TGT GTC AGA GG) primers. Then, a BamHI restriction site was incorporated into either ends of the RILPb amplicon using forward FLo37 (5'-CAT AAG GAT CCT GTG GAT TCA

GCA GGG AAG AGC) and reverse FLo38 (3'-CAT ATA GGA TCC GCC ATC CTC ATC CTC ACT GC) primers. This fragment was then inserted into a P_{vha-6}::GFP::TBC-2(ΔPH-CC)::FLAG vector digested with BamHI. Orientation of the insert was confirmed through Sanger sequencing (Genome Quebec).

2.7 Generation of transgenic worms

Extrachromosomal arrays *vhEx12*, *vhEx20* and *vhEx21* were generated by injecting the plasmid of interest with the P_{ttx-3}::GFP coinjection marker (at a concentration of 50 ng/µl each) into the germ lines of young adults. This was done following protocols described by Berkowitz et al. (Berkowitz et al., 2008).

2.8 Complementation test

Complementation tests were performed for worms carrying *tbc-2* missense alleles from the MMP and for worms carrying the *vh45* mutation. To construct double heterozygous worms carrying a *tbc-2* missense allele and a *tbc-2(tm2241)* allele, *tbc-2(tm2241)* males were first crossed to *tbc-2* missense mothers. The F1 (first generation) hermaphrodites were observed for endocytic defects in the intestines. Severity of these phenotypes were compared to that of homozygous *tbc-2(tm2241)* worms.

To construct double heterozygous worms carrying a copy of the *vh45* mutation and a *tbc-2(tm2241)* allele, three crosses were performed. First, male worms carrying the Chromosome II

inversion balancer *mIn1* were crossed to *tbc-2(tm2241)* mothers. F1 *tbc-2(tm2241)/mIn1* progenies were then crossed to *vh45* hermaphrodites. Because *mIn1* carrying worms can be distinguished by a pharyngeal GFP reporter (Edgley and Riddle, 2001), non-balanced worms carrying a single copy of *tm2241* and *vh45* were easily selected. The intestinal phenotype of *tbc-2(tm2241)/vh45* worms were then compared to wildtype, homozygous *vh45* and *tbc-2(tm2241)* controls.

2.9 Protein domain analysis

Unless otherwise stated, all domain regions were determined by SMART (Simple Modular Architecture Research Tool, http://smart.embl-heidelberg.de/) (Letunic et al., 2015). Amino acid sequences were aligned using Clustal Omega (http://www.ebi.ac.uk/Tools/msa/clustalo/) (McWilliam et al., 2013).

2.10 Fluorescence intensity profiles from confocal images

Signals of fluorescent tags on membrane vesicles were measured using ImageJ: a line was drawn through a labelled vesicle to obtain arbitrary values of the fluorescent signal. These values were then graphed using GraphPad Prism version 6 (GraphPad Software, San Diego, CA) to construct intensity profiles.

2.11 Measurement of vesicular diameter and statistical analysis

Vesicular diameters were measured from three or more worms within the same treatment group using ImageJ (Schneider et al., 2012). On frequency graphs, all data were presented as means ± standard deviation. Statistical differences between genotypes were calculated using one-way ANOVA. Differences were considered statistically different at $P<0.001$. Graphical data were compiled using GraphPad Prism version 6 (GraphPad Software, San Diego, CA). Decimal places of all values were rounded to the nearest hundredth place.

2.12 Secondary structure predictions by PredictProtein and Coils

Secondary structure predictions were performed using RePROF (Rost and Liu, 2003; Yachdav et al., 2014). Prediction for residue solubility was performed by PROFacc (Rost and Liu, 2003). To predict for coiled-coil domains, amino acid sequences were fitted to the heptad repeat pattern using Coils (Lupas, 1996; Lupas et al., 1991; Toolkit, 2008-2016). In this program, heptad predictions were made using a sliding window of 28 residues. In such a window, the first residue was assigned the *a* position, the second residue was assigned the *b* position, the third residue was assigned the *c* position, and so on. Each residue within that window was then scored using a weighted matrix derived from myosins, paramyosins, tropomyosins, intermediate filaments type I - V, desmosomal proteins and kinesins. The weighted matrix was calculated based on the frequency for the evaluated amino acid to appear at a particular heptad position (Lupas, 1996; Lupas et al., 1991; Lupas). After scoring a set of resides, the window shifted down one position to the next residue of the sequence. In this new position, the residue at position *b*

from the previous assignment was reassigned as *a*, the residue at position *c* was reassigned as *b*, and so on. All residues within the window were scored again. This process was repeated until the window reached the end of the amino acid sequence. For each residue, its heptad position was predicted based on the highest score obtained. Probability values were then calculated from the scores. Residues with probability of >50% were considered to be part of a coiled-coil domain (Lupas, 1996).

2.13 Genomic DNA collection and Whole Genome Sequencing-Single Nucleotide Polymorphism strategy for *vh45* mapping

The forward genetic screen using EMS (ethyl methanesulfonate) to isolate *vh45* worms was conducted as previously described (Brenner, 1974). Overviews of the crossing scheme and Whole Genome Sequencing-Single Nucleotide Polymorphism are summarized in **Figure 24** and described by Doitsidou et al. and Minevich et al. (Doitsidou et al., 2010; Minevich et al., 2012). Briefly, the original isolated *vh45* line was outcrossed six times with wildtype N2 Bristol worms to reduce extraneous mutation in its background. The newly outcrossed *vh45* strain does not carry the LE marker GFP::RAB-7, which was originally used to identify mutagenized worms with enlarged LEs during screening. *vh45* worms from the final outcross were then crossed to the polymorphic Hawaiian strain, which is a source of ~112 000 unique SNPs (Minevich et al., 2012). F1 worms heterozygous for Hawaiian and Bristol SNPs were allowed to self-cross. In F2 (second generation), 30 worms displaying *vh45* homozygous phenotypes were chosen to establish clonal populations on worm plates.

Genomic DNA was prepared from two 15 cm plates containing confluent populations of worms. Live worms were washed off plates using M9 buffer and collected into 15 ml conical tubes. To remove *E. coli* collected from the plates, worms were washed 3 times by centrifuging at 2000 rpm for 2 minutes in M9 buffer. Afterwards, 5 ml of NTE buffer was added to each worm pellet and centrifuged again at 2000 rpm for 2 minutes.

Each worm pellet was resuspended in 7X volume of 1X working lysis buffer and transferred to a new 1.5 ml eppendorf tube. The solution was incubated at 65°C for one hour and was gently inverted twice at every 10 minutes. If the volume of the solution was >350 µl, it was evenly divided into two or three new eppindorf tubes. DNA from each tube was purified via phenol:chloroform extraction by adding an equal volume of phenol:chloroform:isoamyl alcohol (25:24:1, BioShop, Canada). Tubes were rotated on a nutator for 5 minutes and then spun down at 4000 rpm for another 5 minutes. The resulting top aqueous phase was transferred to a new tube. If the solution was previously split prior to the DNA purification step, the fractions were combined into a single new tube. Phenol:chloroform extraction was performed 2 more times.

To each tube, 1/7X volume of 3M sodium acetate and 2.5X volume of 100% ethanol were added. The tubes were gently mixed several times and allowed to sit at room temperature for 5 minutes for DNA precipitation. DNA pellet was obtained by centrifugation at 4000 rpm for 5 minutes. Remaining salts were washed off by adding one ml of 70% ethanol to each pellet. The pellet was spun down again at 4000 rpm for five minutes. Afterwards, the pellet was air-dried for five minutes. 200 µl (or 300 µl if the volume was previously split) of autoclaved ddH_2O was added to dissolve the pellet.

Four µl (or 6 µl if the volume was previously split) of RNase (New England Biolabs, ON, CA) were added to each tube RNA, which was then incubated at 37°C for 20 minutes. The DNA was purified again 3 times via phenol:chloroform extraction. Once the DNA was purified, 1/7X volume of 3M sodium acetate and 3X volume of -20°C 95% ethanol were added. The DNA solution was centrifuged at maximum speed for 15 minutes and the supernatant was removed. One ml of 70% ethanol was added to the DNA pellet and the solution was centrifuged again at maximum speed for 5 minutes. Remaining supernatant was removed via pipette.

The DNA pellet was dissolved in 50 µl of elution buffer (with Tris at pH 8.5) and tested for quality using a spectrophotometer at optical density of 260 nm and 280 nm. Only preparations with a 260 nm/280 nm ratio of 1.8 or above were sent to Genome Quebec (Montreal, QC, Canada) for sequencing.

Runs were performed on a HiSeq 2000 PE100 platform (Illumina) with paired-end sequencing for 300X coverage. The raw sequenced data was analyzed using CloudMap, a cloud-based, publicly available pipeline (Minevich et al., 2012). This software annotates the nature of genetic variants and calculates the frequencies of their detection from total reads along regions of the genome.

2.14 Cloudmap analysis

Sequenced raw data were analyzed using CloudMap's automated workflow without changing default function parameters. Data were entered in FASTQ format, as provided in the raw file from Genome Quebec.

Chapter 3. Structural and functional analysis of TBC-2

Preface

Membrane localization of TBC-2 brings the GAP in close proximity to its target RAB-5. How TBC-2 achieves its membrane targeting is not well known. TBC-2 contains four conserved domains, but very little is known of their purpose. To investigate the roles played by the domains and to understand their importance in TBC-2 function, colleagues and I performed a structure-function analysis. We found that the CC domain region is essential for TBC-2 localization. To investigate residues that are critical for TBC-2 function, I also analyzed the phenotypes of available missense *tbc-2* strains from the MMP. Two mutations affecting positions 466 of the THR domain and 784 of the TBC domain were found to cause a weak, *tbc-2*-like phenotype. The R466C missense may affect the interhelical stability of a predicted coiled-coil domain within the THR domain, while the P784L missense may affect GTP-bound RAB-5 recognition by the TBC domain. Future work is required to confirm if the two missense mutations cause a defect in TBC-2 localization or its GAP activity. Overall, this chapter presents evidence on the structural domains and residues required for TBC-2 localization in endocytosis.

3.1 The PH domain is not essential for TBC-2 endosome localization and function

To determine the importance of the PH and CC domains in TBC-2 localization, the N-terminus was truncated to produce two deletion constructs: GFP::TBC-2(ΔPH)::FLAG and GFP::TBC-2(ΔPH-CC)::FLAG. These constructs, as well as a control full-length protein construct (GFP::TBC-2::FLAG), were expressed in worms carrying the strong *tbc-2* loss-of-function allele *tm2241* to generate transgenic strains. The expressed fusion proteins were observed in these worms for membrane localization and *tbc-2(tm2241)* rescue.

The TBC-2 transgenes were expressed as extrachromosomal arrays, which were inherited in a non-Mendelian fashion. For this reason, the transgenes had mosaic expression in the intestine; cells that either did not have sufficient transgenic expression or did not inherit the extrachromosomal array were not rescued for the mutant phenotype (**Figure 8**). Expression of GFP::TBC-2(ΔPH)::FLAG, like that of the full-length GFP::TBC-2::FLAG, was able to restore *tbc-2(tm2241)* large endosomes back to wildtype sizes (**Figure 8 B, H**). The pattern of its membrane localization, however, was different than full-length TBC-2 and appeared to have stronger membrane association (**Figure 8 D, E, J, L**). This suggests that the PH domain is not necessary for TBC-2 function but may provide an inhibitory effect for TBC-2 endosome localization.

3.2 The CC domain region is critical for TBC-2 endosome localization and function

Further truncation of the region following the PH domain to the C-terminal end of the CC domain (a region referred to as CC domain region) of GFP::TBC-2(ΔPH)::FLAG generated GFP::TBC-2(ΔPH-CC)::FLAG. This fusion protein did not localize onto endosomes and was not

able to rescue the *tbc-2(tm2241)* intestinal phenotype (**Figure 8 D, F, J, N**). This indicates that while the PH domain and the CC domain region are both necessary for normal TBC-2 endosome localization and function, the CC domain region is critical for these roles.

3.3 Strains VC20287 and VC20509 give rise to a less severe *tbc-2(tm2241)*-like phenotype in the intestine

To find critical residues for TBC-2 localization and function, seven worm strains carrying *tbc-2* missense mutations were ordered from the MMP (Thompson et al., 2013) and observed for *tbc-2(tm2241)*-like phenotypes in the intestine and oocytes (**Figure 9, Table 2**). Two strains, VC20287 and VC20509 carrying *tbc-2* alleles *gk143714* and *gk331596* respectively, display enlarged vesicles in the intestine, within which globular, refractile material is found (**Figure 9 C, D**). However, unlike *tbc-2(tm2241)* mutants, neither strain has yolk platelet trafficking defects in the oocyte (**Figure 9 C', D'**). The mean vesicular diameters of enlarged vesicles from VC20287 (4.88 μm) and VC20509 (4.50 μm) worms were both significantly smaller than those of *tbc-2(tm2241)* (6.86 μm) (**Figure 9 J**, $P<0.001$), but they were larger than that of wildtype (1.91 μm). This suggests that *tbc-2* alleles carried by VC20287 and VC20509 worms produce a less severe phenotype than *tm2241*. The lack of yolk trafficking defect from either strain also suggests that TBC-2 regulation and/or activity differs between the intestine and oocytes.

3.4 The *gk143714* and *gk331596* alleles fail to complement *tbc-2(tm2241)*

gk143714, *gk331596* and *tm2241* are recessive alleles (undocumented observation). To find whether the *tbc-2(tm2241)*-like phenotypes were specifically caused by the effect of *gk143714* or *gk331596*, VC20287 and VC20509 worms were outcrossed four to five times to wildtype N2 worms. The crossed strains were then used in a complementation test with *tm2241*.

Worms carrying *gk143714*/*tm2241* or *gk331596*/*tm2241* still retained enlarged vesicles (**Figure 9 K, L**). This lack of phenotypic complementation back to wildtype suggests that the intestinal phenotypes indeed arise from the effect of *gk143714* and *gk331596* (Griffiths, 2000; Yook, 2005).

3.5 The *tbc-2(tm2241)*-like phenotype observed in *tbc-2(gk331596)* worms may arise from misfolding of a coiled-coil structure within the THR domain

tbc-2(gk331596) carries a R466C mutation that occurs within the THR domain (**Figure 10, Table 2**). The secondary structures of this domain were predicted by an online tool called RePROF, which is available from a protein sequence analysis website called PredictProtein (Yachdav et al., 2014). RePROF is reported to be a highly accurate secondary structure prediction tool that uses information from homologous alignments (Rost, 1996; Rost and Sander, 1993). The THR domain was predicted to fold into four helices (H), with a β-strand (β) situated between H2 and H3 (**Figure 11 A**). RePROF does not specify the type of helices (α, 3_{10}, or π) predicted; however, for the purpose of this thesis, all helices were presumed to be right-handed α-helices. α-helices are the most common kind of secondary structures (Cole and Bystroff, 2009; Pace and Scholtz, 1998), and they supercoil into left-handed coiled-coil domains (Mason and Arndt, 2004). The THR aa 518..530 segment was not found to fold into any secondary structure

(**Figure 11 A**). Instead, it is predicted to be exposed to the cytoplasm (**Figure 11 B**) and may exist as a soluble loop.

The R466C mutation occurs at a semi-conserved position (**Figure 10**) located within an exposed segment of the first helical structure (H1) (**Figure 11 A, B**). The substituted cysteine residue may form disulfide bonds and alter TBC-2 conformation; however, this scenario is unlikely because of the reducing environment in the cytoplasm (Cooper and Hausman, 2004).

To investigate whether H1 may be part of a coiled-coil domain, an online tool called Coils was used to evaluate whether the H1 primary structure matches the pattern of a heptad repeat. This program uses a weighted matrix derived from known coiled-coil structures to score the probability of queried residues to occur at given heptad positions (Lupas et al., 1991; Lupas). If a residue's probability is >50%, it is predicted to be part of a coiled-coil domain (Lupas, 1996). This is signified by a "C" located beneath the heptad assignment (**Figure 11 C**). A single coiled-coil forming helix was found within H1, in the aa 284..497 segment. Position 466 was predicted to occupy the *e* assignment (**Figure 11 C**), which is normally occupied by a polar, charged residue to establish interhelical electrostatic interactions (Mason and Arndt, 2004). The replacement of arginine by cysteine (a polar but uncharged amino acid) may therefore destabilize the coiled-coil structure and consequently reduce the function of the THR domain.

VC40589 worms carrying *tbc-2(gk708072)* have a A481T missense mutation that also occurs within the H1 helix of the THR domain (**Table 2, Figure 11 C**). Position 481 falls in the *f* assignment of the heptad repeat where the nonpolar alanine was replaced with a polar and uncharged threonine (**Figure 11 C**). However, unlike the strong heptad preference for nonpolar residues at positions *a* and *d*, or for charged and polar residues at positions *e* and *g*, the chemical properties required at other assignments are much less restricted (Mason and Arndt, 2004; Parry,

1982). Therefore, as supported by a wildtype intestinal phenotype (**Figure 9 I**), it suggests that the A481T mutation has no overt effects on coiled-coil domain formation and THR domain function.

3.6 The *tbc-2(tm2241)*-like phenotype observed from *tbc-2(gk143714)* worms may be caused by disrupted recognition by the TBC domain for its Rab target

The P784L missense mutation of *tbc-2(gk143714)* is located within the TBC domain (**Figure 10, Table 2**). The proline at this position is strongly conserved (**Figure 10**) and occurs at the start of the tenth helix (α10) (**Figure 12**). Prolines are usually found at the start of helices due to the features of their pyrrolidine ring (Kim and Kang, 1999; Richardson and Richardson, 1988): a structure that sterically contributes a rotatable angle to initiate helical formations (Chakrabarti and Chakrabarti, 1998). Additionally, the pyrrolidine ring does not contain a free NH group and bypasses the requirement to form an intrahelical NH···O=C bond with an upstream residue (Berg et al., 2002; Chakrabarti and Chakrabarti, 1998). According to ribbon representations of prototypical TBC domains from human TBC1D1 and yeast Gyp1p (Park et al., 2011; Rak et al., 2000), α10 is located adjacent to α11, a helix that composes part of the interaction surface for Rab GTPase binding (Pan et al., 2006; Park et al., 2011). The loss of proline at the start of α10 likely leads to poor helix formation, and may therefore affect the positioning of α11 for cognate Rab recognition.

A *tbc-2(tm2241)*-like phenotype was not found in VC40216 worms (**Figure 9 G, G'**). This strain carries *tbc-2(gk518013)*, which contains a G759E missense mutation (**Table 2, Figure 10**). From alignments, the glycine at position 759 was not found to be conserved (**Figure**

12). Additionally, it lies in loop 8 (L8), which is known to vary in terms of length and sequence between TBC domains (Rak et al., 2000) Moreover, ribbon representations of TBC domains show that L8 is not situated close to the TBC catalytic site (Pan et al., 2006), suggesting that the loop does not contribute to GAP activity. These results support that the G759E mutation likely does not affect TBC domain function.

3.7 The missense mutation in the PH domain and the CC domain region at G273 or V286 likely does not affect secondary structure folding of TBC-2

Earlier, we demonstrated that both the PH domain and CC domain region participate in TBC-2 localization and function (**Figure 8**). However, strains carrying missense mutations in either protein segment (VC40005, VC40512, and VC20581) do not exhibit *tbc-2(tm2241)*-like phenotypes in the intestine or oocytes (**Figure 9 E, E', F, F', H, H', Table 2**).

Strain VC40005 carries *tbc-2(gk143719)*. The R30C missense mutation of this allele occurs within the seven β-strands of the TBC-2 PH domain (**Figure 13 A**), specifically in the loop (L1) connecting β1 and β2 (**Figure 13 A, B**). This loop is known to be hypervariable and contains basic lysine and arginine residues to establish a positively charged surface for phospholipid interaction (Lemmon, 2008; Lemmon and Ferguson, 2000). The L1 of the TBC-2 PH domain indeed contains several arginine residues (R37, R38, R39), including the affected arginine at position 30 (**Figure 13 C, Table 2**). Despite this, the lack of *tbc-2*-like trafficking phenotypes detected in the intestine and oocytes (**Figure 9 F, F'**) suggests that R30 is neither responsible nor essential for PI interaction (Hyvonen et al., 1995; Russo et al., 2001). As a result, the R30C mutation likely does not affect PH domain function.

The *tbc-2(gk672402)* allele carried by strain VC40512 has a G273S mutation located within the intervening segment between the PH and CC domains. The wildtype intestinal phenotype observed from this strain (**Figure 9 H, H'**) suggests that the affected residue is not involved in binding to the endosome membrane.

The *tbc-2(gk347266)* allele from strain VC20581 contains a V286I mutation that occurs in the CC domain (**Figure 10**). Position 286 was assigned the heptad position *a* (**Figure 14**), which is normally occupied by a hydrophobic residue (Mason and Arndt, 2004; Parry, 1982). Because both valine and isoleucine have high hydrophobicities and are equally likely to reside at this heptad assignment (McLachlan and Karn, 1983; Parry, 1982), it is unlikely for the V286I mutation to affect function of the CC domain. Instead, the higher hydrophobicity of isoleucine (Kovacs et al., 2006) may actually provide greater stability to the helical bundle structure (Mason and Arndt, 2004; Zhu et al., 1993).

Summary

In summary, both the PH domain and CC domain region of TBC-2 were found to be important for normal localization of TBC-2 onto endosomes. The CC domain region, however, appears to serve a critical role in this process. Two missense mutation within *tbc-2* were each found to produce a weak *tbc-2(tm2241)*-like effect: R466C of the THR domain may affect the formation of a predicted coiled-coil structure, while P784L may affect binding to RAB-5 for GAP function. It is not known if these changes affect TBC-2 localization or function.

Figure 8

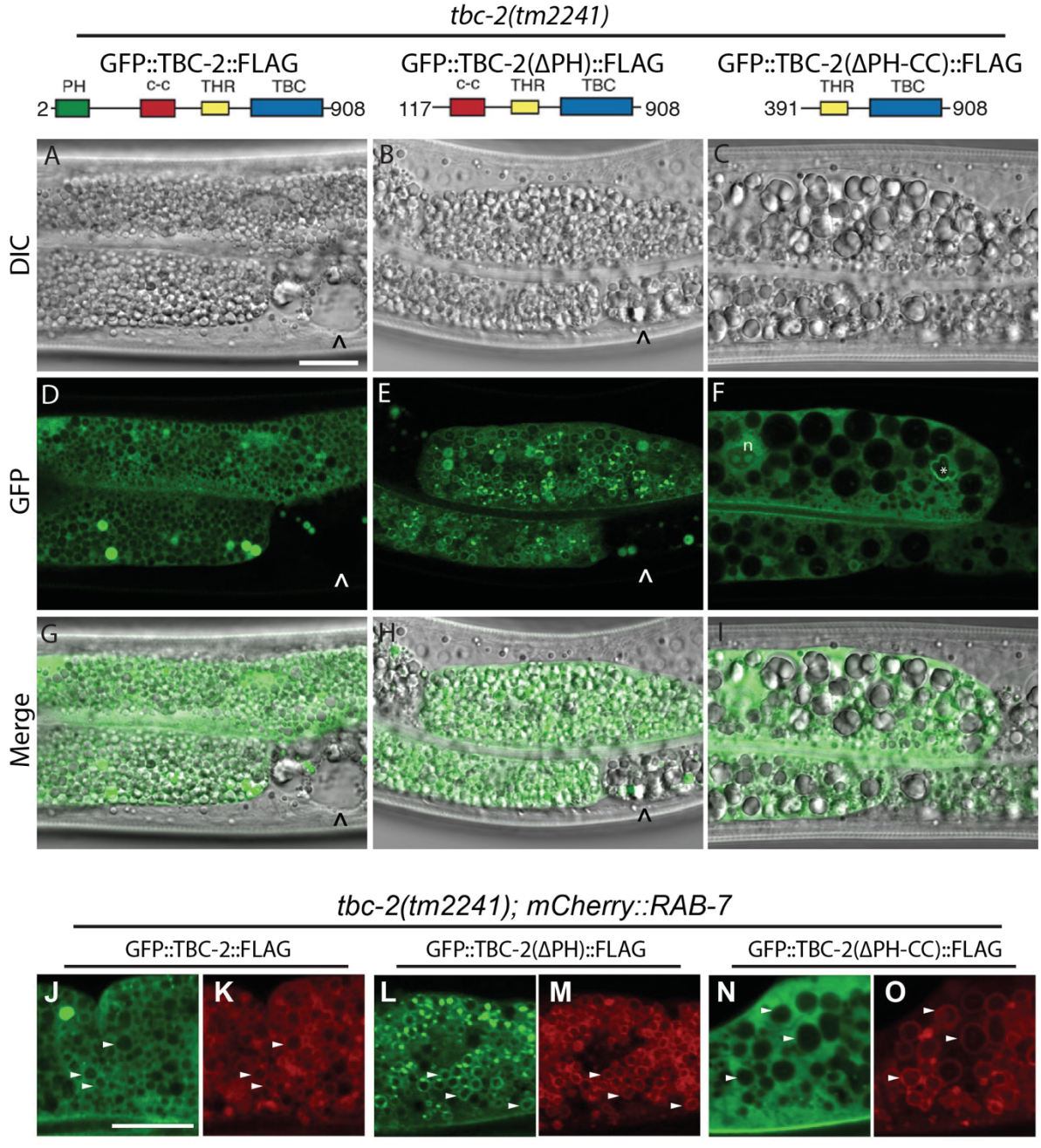
tbc-2(tm2241)
GFP::TBC-2::FLAG
PH
c-c
THR
TBC
2
908
GFP::TBC-2(ΔPH)::FLAG
117
GFP::TBC-2(ΔPH-CC)::FLAG
391
DIC
GFP
Merge
A
B
C
D
E
F
G
H
I
n
*
tbc-2(tm2241); mCherry::RAB-7
J
K
L
M
N
O

Figure 8. The PH domain of TBC-2 is not essential for *tbc-2(tm2241)* rescue or endosome localization. (A-I) Representative DIC (A-C), confocal (D-F) or merged (G-I) images of *tbc-2(tm2241)* L4 animals expressing *vhEx12* GFP::TBC-2::FLAG (A, D and G), *vhEx20* GFP::TBC-2(ΔPH)::FLAG (B, E and H), and *vhEx21* GFP::TBC-2(ΔPH-CC)::FLAG (C, F and I). All constructs were expressed as extrachromosomal arrays and exhibit mosaic expression. "^" marks cells that lack transgenic expression and are therefore not rescued for the *tbc-2(tm2241)* large vesicle phenotype (A-F). "n" denotes the nucleus, while "*" denotes a GFP-positive, irregularly shaped vesicle that was occasionally found (F). (J-O) Representative confocal images of *tbc-2(tm2241)* L4 larvae expressing *pwIs429* mCherry::RAB-7 and one of *vhEx12* (J and K), *vhEx20* (L and M), or *vhEx21* (N and O). GFP and mCherry signals are represented as green and red respectively. White arrowheads denote examples of vesicles displaying signals from both channels. Bar: (A and J) 10 μm.

Figure 9

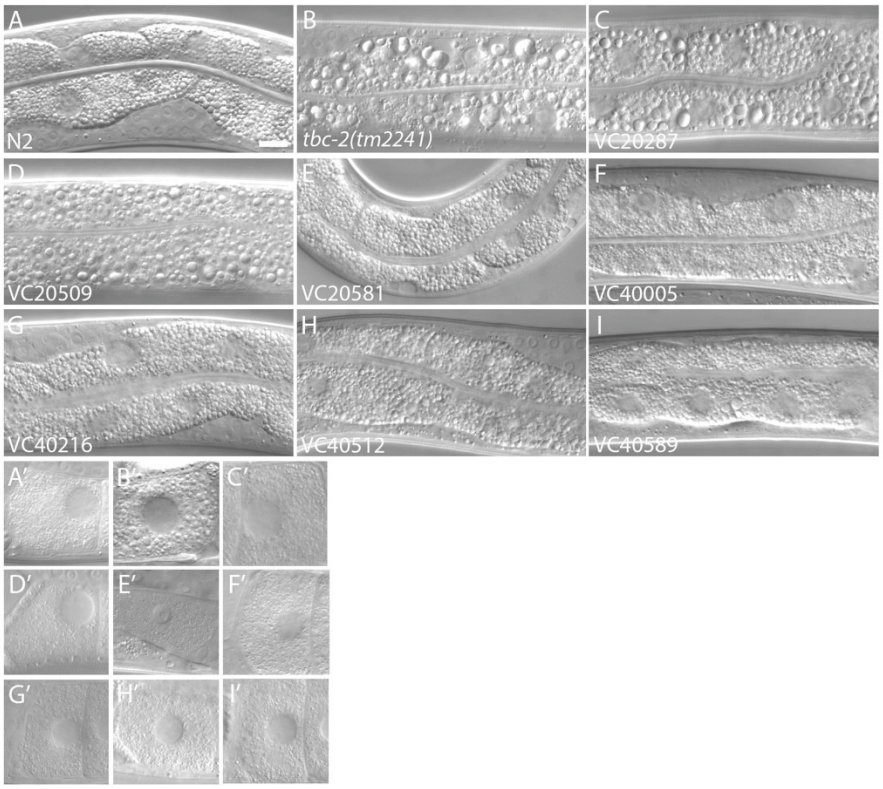

J

Genotype	Mean vesicular diameter (µm)	Std deviation (µm)	Mode (µm)	Min value (µm)	Max value (µm)
Wildtype (N2) (n=50)	1.91	0.29	1.71	1.35	2.96
tbc-2(tm2241) (n=62)	6.86	1.93	6.69	3.33	11.21
tbc-2(gk143714) **[VC20287]** (n=57)	4.88	0.95	5.22	2.96	7.41
tbc-2(gk331596) **[VC20509]** (n=58)	4.50	1.10	3.96	2.17	7.25

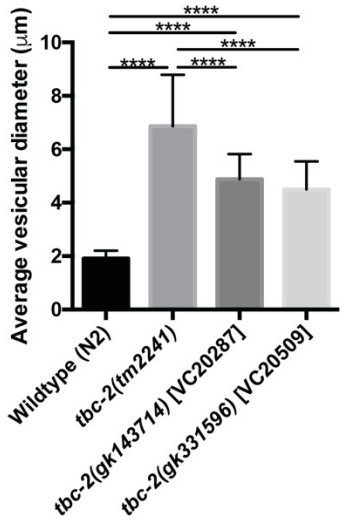

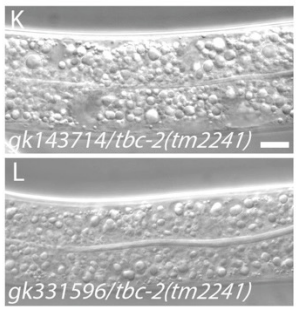

Figure 9. Strains VC20287 and VC20509 exhibit a *tbc-2(tm2241)*-like intestinal phenotype. (A-I') Representative DIC images of L4 stage intestine (A-I) and the most proximal oocyte from young adults (A'-I') from wildtype worm (A, A'), *tbc-2(tm2241)* mutant (B, B') and seven *tbc-2* missense allele carrying strains (C-I, C'-I'). Oocyte images are labelled in order that correspond to the intestinal images of given worm strains. (J) Quantitative summary of vesicular diameters measured from imaged worms. "n" denotes the number of vesicles measured per group. Decimal places of all values were rounded to the nearest hundredth place. Median vesicular diameters are represented in a frequency graph. Error bars represent standard deviations. ****, $P < 0.001$ (differences between treatments). (K, L) Representative DIC images of intestines from a complementation test for the *tbc-2(tm2241)* phenotype. VC20287 and VC20509 carry *tbc-2* alleles *gk143714* and *gk331596* respectively. *tbc-2(tm2241)* mutants were crossed to *gk143714* and *gk331596* worms to produce *trans*-heterozygous progenies. Bar (A), (K): 10 μm.

Figure 10

CLUSTAL O(1.2.1) multiple sequence alignment

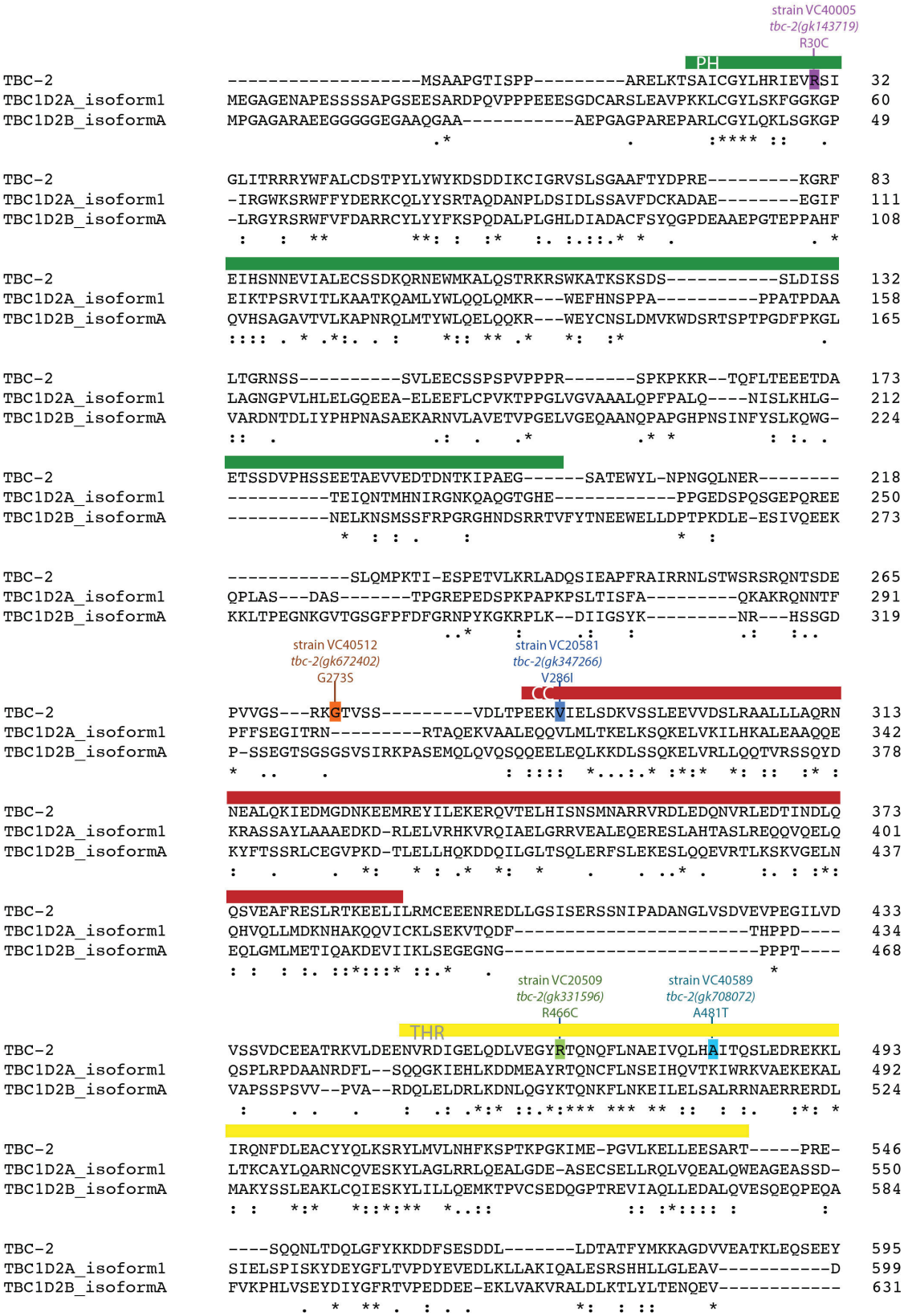

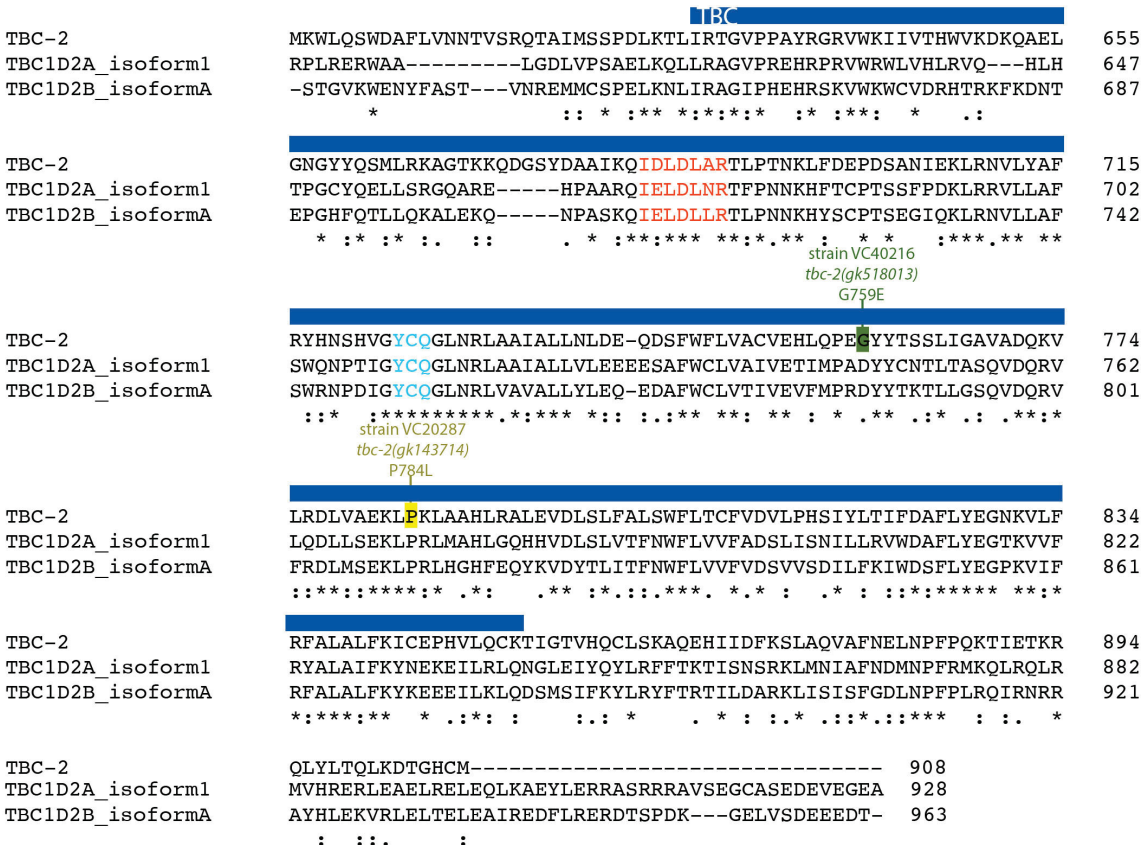


```
TBC-2                MKWLQSWDAFLVNNTVSRQTAIMSSPDLKTLIRTGVPPAYRGRVWKIIVTHWVKDKQAEL   655
TBC1D2A_isoform1     RPLRERWAA---------LGDLVPSAELKQLLRAGVPREHRPRVWRWLVHLRVQ---HLH   647
TBC1D2B_isoformA     -STGVKWENYFAST---VNREMMCSPELKNLIRAGIPHEHRSKVWKWCVDRHTRKFKDNT   687

TBC-2                GNGYYQSMLRKAGTKKQDGSYDAAIKQIDLDLARTLPTNKLFDEPDSANIEKLRNVLYAF   715
TBC1D2A_isoform1     TPGCYQELLSRGQARE-----HPAARQIELDLNRTFPNNKHFTCPTSSFPDKLRRVLLAF   702
TBC1D2B_isoformA     EPGHFQTLLQKALEKQ-----NPASKQIELDLLRTLPNNKHYSCPTSEGIQKLRNVLLAF   742

TBC-2                RYHNSHVGYCQGLNRLAAIALLNLDE-QDSFWFLVACVEHLQPEGYYTSSLIGAVADQKV   774
TBC1D2A_isoform1     SWQNPTIGYCQGLNRLAAIALLVLEEEESAFWCLVAIVETIMPADYYCNTLTASQVDQRV   762
TBC1D2B_isoformA     SWRNPDIGYCQGLNRLVAVALLYLEQ-EDAFWCLVTIVEVFMPRDYYTKTLLGSQVDQRV   801

TBC-2                LRDLVAEKLPKLAAHLRALEVDLSLFALSWFLTCFVDVLPHSIYLTIFDAFLYEGNKVLF   834
TBC1D2A_isoform1     LQDLLSEKLPRLMAHLGQHHVDLSLVTFNWFLVVFADSLISNILLRVWDAFLYEGTKVVF   822
TBC1D2B_isoformA     FRDLMSEKLPRLHGHFEQYKVDYTLITFNWFLVVFVDSVVSDILFKIWDSFLYEGPKVIF   861

TBC-2                RFALALFKICEPHVLQCKTIGTVHQCLSKAQEHIIDFKSLAQVAFNELNPFPQKTIETKR   894
TBC1D2A_isoform1     RYALAIFKYNEKEILRLQNGLEIYQYLRFFTKTISNSRKLMNIAFNDMNPFRMKQLRQLR   882
TBC1D2B_isoformA     RFALALFKYKEEEILKLQDSMSIFKYLRYFTRTILDARKLISISFGDLNPFPLRQIRNRR   921

TBC-2                QLYLTQLKDTGHCM--------------------------------  908
TBC1D2A_isoform1     MVHRERLEAELRELEQLKAEYLERRASRRRAVSEGCASEDEVEGEA  928
TBC1D2B_isoformA     AYHLEKVRLELTELEAIREDFLRERDTSPDK---GELVSDEEEDT-  963
```

Figure 10. Protein alignments of TBC-2 and TBC-2 human homologs. Wildtype *C. elegans* TBC-2 (NP_495156) and two TBC-2 human homologs (TBC1D2A: NP_001254500 and TBC1D2B: NP_653173) were aligned using Clustal Omega (McWilliam et al., 2013). Regions of TBC-2 PH (green bar, aa 18..116), CC (red bar, aa 283..390) and catalytic TBC (blue bar, aa 627..852) domains were based on output from SMART. The exact amino acid range of the THR domain (yellow bar, aa 451..543) was determined by aligning *C. elegans* TBC-2, human TBC1D2B isoform A and TBC1D2A isoform 1 using Clustal Omega and identifying an extended stretch of residues with identical or similar chemical properties. Locations of missense mutations from the seven MMP *tbc-2* alleles are labelled. Red and blue fonts denote regions of two conserved TBC catalytic signature motifs, which contain the conserved arginine (R) and glutamine (Q) residues (Chotard et al., 2010a). At the bottom of each alignment, conserved residues shared between sequences are labelled by an asterisk (*), while residues that share strong or weak chemical properties are respectively marked by a colon (:) or period (.).

Figure 11

A

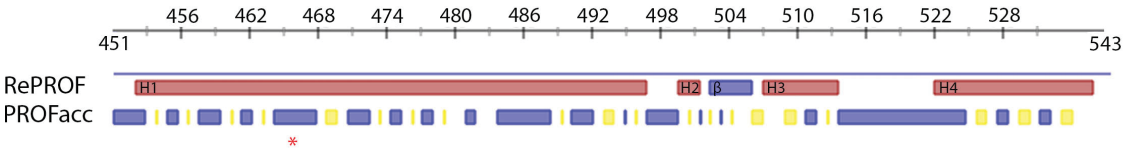

B

Exposed residues	Intermediate residues	Buried residues
451..453	482	454
455..456	485	457
458..460	509	461
462..463	512	464
465..469		470..471
472..474		475
476..477		478
479..480		481
483..484		492
486..491		496..497
493..495		499
498		504
500..503		506
505		508
507		513..514
510..511		517
515..516		531..532
518..530		535..536
533..534		539..540
537..538		

C

```
TBC-2 THR domain        451 NVRDIGELQDLVEGYRTQNQFLNAEIVQLHAITQSLEDREKKLIRQNFDLEACYYQLKSR    510
VC20509 THR domain      451 NVRDIGELQDLVEGYCTQNQFLNAEIVQLHAITQSLEDREKKLIRQNFDLEACYYQLKSR    510
heptad assignment           defgabcdefgabcdefgabcdefgabcdefgabcdefgabcdefgabcdefgabcdefg
CC segment                  -CCCCCCCCCCCCCCCCCCCCCCCCCCCCCCCCCCCCCCCCCCCCCC-------------

TBC-2 THR domain        511 YLMVLNHFKSPTKPGKIMEPGVLKELLEESART      543
VC20509 THR domain      511 YLMVLNHFKSPTKPGKIMEPGVLKELLEESART      543
heptad assignment           abcdefgabcdefgabfgabcdefgabcdefgg
CC segment                  --------------------------------
```

Figure 11. The missense mutation of *tbc-2(gk331596)* likely affects the helical structure for coiled-coil domain formation within the THR domain. (A-B) Secondary structures of the THR domain were predicted by an online tool called RePROF. Red boxes represent helices (H), while blue boxes represent β-strands (β). Location of R466C is denoted by a red asterisk (*). Solvent accessibility of residues was predicted by PROFacc. Blue boxes symbolize regions of exposed residues, while yellow boxes symbolize regions of buried residues. Intermediate residues are not colour-indicated. (B) A table providing further details on the positions of exposed, intermediate, or buried residues. (C) A heptad repeat was assigned to the THR sequence using Coils. The amino acids at position 466 is in red font. Residues believed to be part of a coiled-coil structure are labelled with the letter "C" at the bottom of each alignment. This prediction was based on a probability score of >50%.

Figure 12

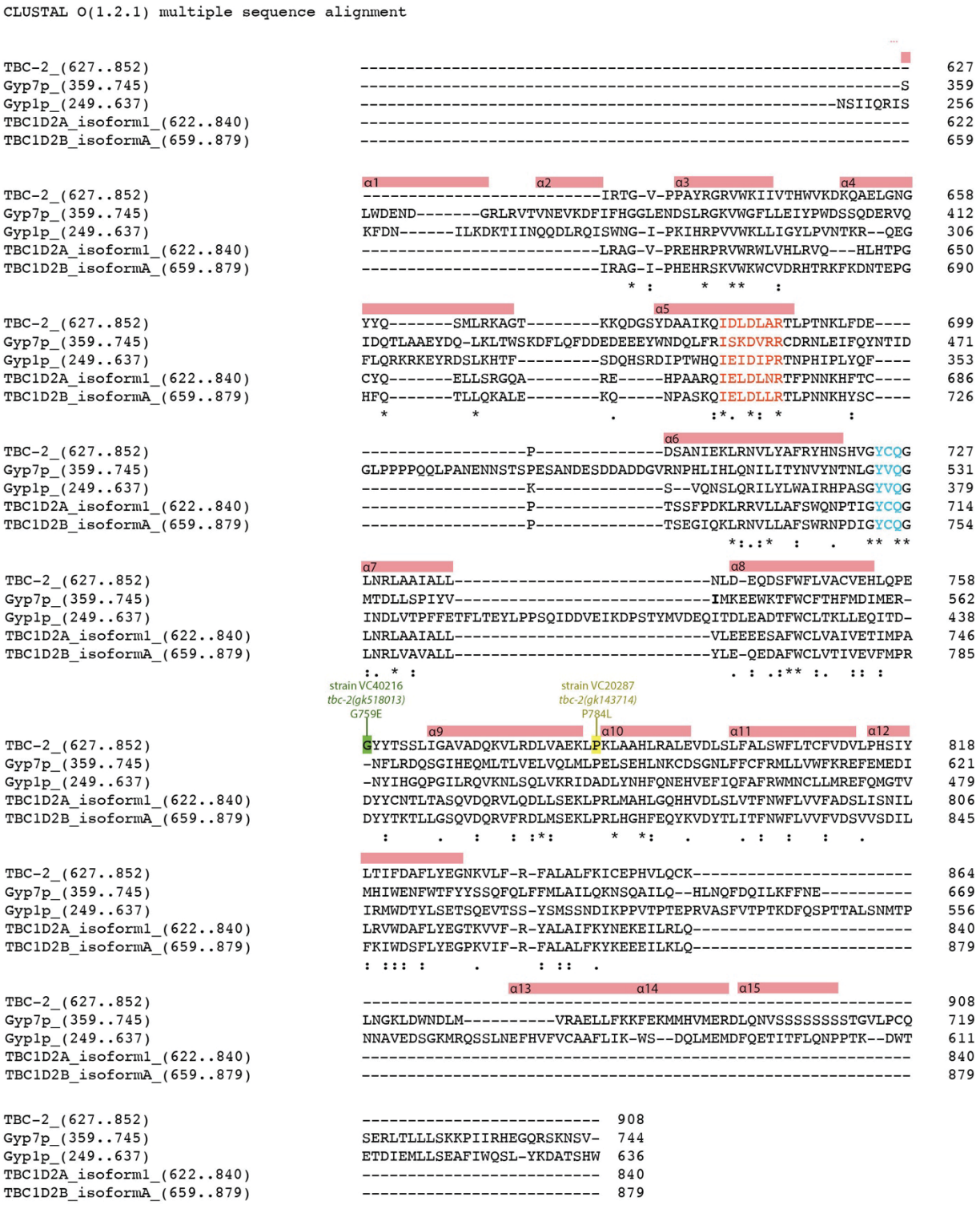
CLUSTAL O(1.2.1) multiple sequence alignment
TBC-2_(627..852)
Gyp7p_(359..745)
Gyp1p_(249..637)
TBC1D2A_isoform1_(622..840)
TBC1D2B_isoformA_(659..879)
α1
α2
α3
α4
α5
α6
α7
α8
α9
α10
α11
α12
α13
α14
α15
strain VC40216
tbc-2(gk518013)
G759E
strain VC20287
tbc-2(gk143714)
P784L

Figure 12. The missense mutation of *tbc-2(gk143714)* likely affects the Rab GTPase interaction interface of the TBC domain. TBC domain protein sequences from *C. elegans* TBC-2 (NP_495156), yeast Gyp1p (NP_014713), yeast Gyp7p (NP_010047), human TBC1D2A (NP_001254500) and TBC1D2B (NP_653173) were aligned using Clustal Omega. TBC regions of TBC-2 (aa 627..852), TBC1D2A (aa 622..840) and TBC1D2B (aa 659..879) were determined by SMART, while those of Gyp1p (aa 249..637) and Gyp7p (aa 359..745) were obtained elsewhere. (Albert et al., 1999). Position of TBC domain amino acid substitutions from *tbc-2(gk518013)* (strain VC40216) and *tbc-2(gk143714)* (strain VC20287) are highlighted in green and yellow respectively. Red and blue fonts indicate the location of TBC catalytic signature motifs IxxDxxR and YxQ. α-helical spanning regions were predicted based on alignment from TBC domains of yeast Gyp1p, and human TBC1D1 and TBC1D4 (Park et al., 2011). Due to differences in the boundaries of TBC domains determined by SMART and from published data (Park et al., 2011), α1 is only partially represented, while α16 lies outside of the alignment. At the bottom of each alignment, conserved residues shared between sequences are labelled by an asterisk (*), while residues that share strong or weak chemical properties are respectively marked by a colon (:) or period (.).

Figure 13

A

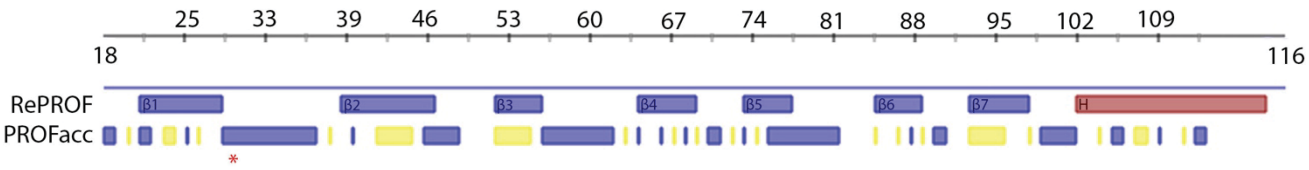

B

Exposed residues	Intermediate residues	Buried residues
18..19	27	20
21..22	38	23..24
25	40	26
28..36	49..50	37
39	64	41..44
45..48	81..82	51..54
55..61	84	62
63	90	66
65	95	68
67	101	71
69..70	108	73
72	112	83
74..80		85
86		87
88..89		91..94
97..100		96
103..104		102
107		105..106
110..111		109

C

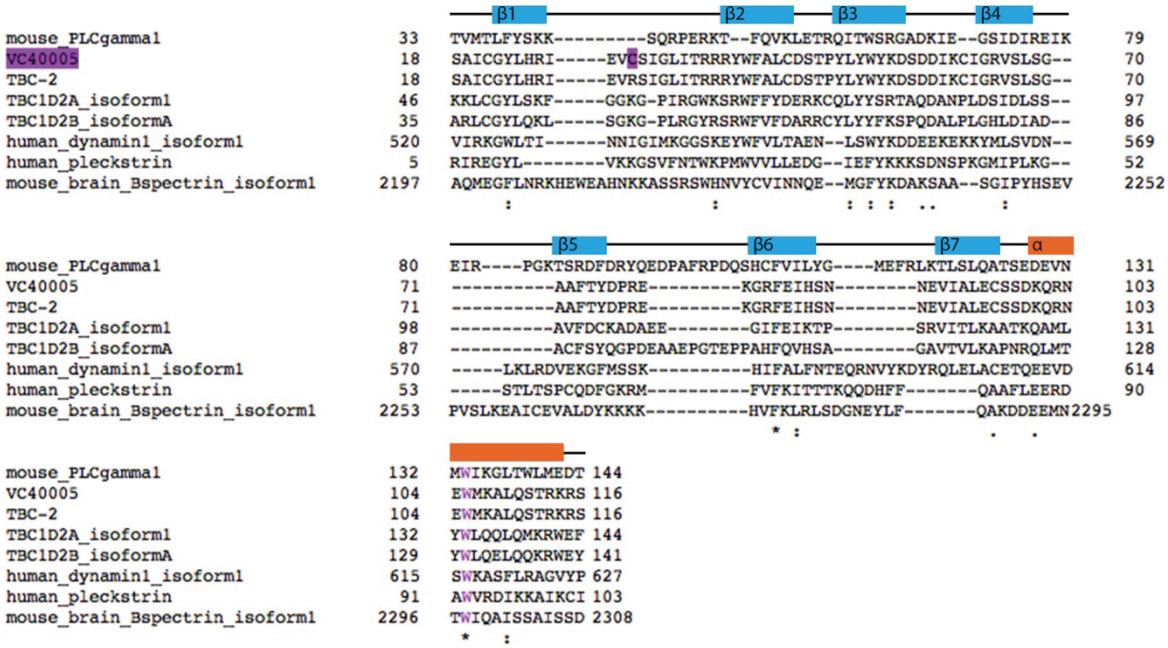

Figure 13. The R30C mutation of *tbc-2(gk143719)* occurring in the loop connecting β1 and β2 likely does not affect PH domain function. (A-B) Secondary structures of the PH domain were predicted using RePROF. Red boxes represent helices (H), while blue boxes represent β-strands (β). Location of R30C is denoted by a red asterisk (*). Solvent accessibility of residues was predicted by PROFacc. Blue boxes symbolize regions of exposed residues, while yellow boxes symbolize regions of buried residues. Intermediate residues are not colour-indicated. (B) A table providing further details on the positions of exposed, intermediate, or buried residues. (C) Sequences of PH domains from wildtype *C. elegans* TBC-2 (NP_495156, aa 18..116), missense *tbc-2(gk143719)* product from strain VC40005, human TBC1D2A (NP_001254500, aa 46..144) and TBC1D2B (NP_653173, aa 31..141), human pleckstrin (NP_002655, aa 5..103), human dynamin1 (NP_004399, aa 520..627), mouse β-spectrin (NP_787030, aa 2197..2308) and mouse PLCδ (EDL06292, aa 33..144) were aligned using Clustal Omega. Sequences of all PH domains were determined by SMART. The missense mutation of *gk143719* is highlighted in purple. Regions of β-strands (blue) and α-helices (orange) were based on RePROF data for TBC-2 PH domain. The conserved tryptophan (W) residue is purple font. At the bottom of each alignment, conserved residues shared between sequences are labelled by an asterisk (*), while residues that share strong or weak chemical properties are respectively marked by a colon (:) or period (.).

Figure 14

CC domain

```
TBC-2 CC domain          283 EEKVIELSDKVSSLEEVVDSLRAALLLAQRNNEALQKIEDMGDNKEEMREYILEKERQVT    342
VC20581 CC domain        283 EEKIIELSDKVSSLEEVVDSLRAALLLAQRNNEALQKIEDMGDNKEEMREYILEKERQVT    342
heptad assignment            efgabcdefgabcdefgabcdefgabcdefgabcdefabcdefgabcdefgabcdefgab
CC segment                   CCCCCCCCCCCCCCCCCCCCCCCCCCCCCCCCCCCCCCCCCCCCCCCCCCCCCCCCCCCC

TBC-2 CC domain          343 ELHISNSMNARRVRDLEDQNVRLEDTINDLQQSVEAFRESLRTKEELI              390
VC20581 CC domain        343 ELHISNSMNARRVRDLEDQNVRLEDTINDLQQSVEAFRESLRTKEELI              390
heptad assignment            cdefgabcdefgabcdefgabcdefgabcdefgabcdefgabcdefga
CC segment                   CCCCCCCCCCCCCCCCCCCCCCCCCCCCCCCCCCCCCCCCCCCCCCCCCCCC
```

Figure 14. The V286I mutation of *tbc-2(gk347266)* may further stabilize the CC domain without affecting its function. Sequences of TBC-2 CC domain (NP_495156, aa 283..390) from wildtype TBC-2 and missense product of *tbc-2(gk347266)* were aligned using Clustal Omega. A heptad repeat was assigned to the alignment using Coils. Isoleucine replaces valine at position 286 (red). Residues believed to be part of a coiled-coil structure are labelled with the letter "C" at the bottom of each alignment. This prediction was based on a probability score of >50%.

Table 2. *tbc-2* missense alleles used in this thesis.

Strain name	*tbc-2* allele	Mutated residue	Position of the mutation
VC20287	*gk143714*	P784L	Exon 9, within TBC domain
VC20509	*gk331596*	R466C	Exon 7, within THR region
VC20581	*gk347266*	V286I	Exon 5, within CC domain
VC40005	*gk143719*	R30C	Exon 2, within PH domain
VC40216	*gk518013*	G759E	Exon 9, within TBC domain
VC40512	*gk672402*	G273S	Exon 5
VC40589	*gk708072*	A481T	Exon 7, within THR region

*Strains are ordered according to the number of its name

Chapter 4. PI3P generated by the Class III PI3K negatively regulates RAB-5 during endosome maturation

Preface

From the previous chapter, a TBC-2 structure-function analysis revealed that both the PH domain and the CC domain region localize TBC-2 onto membranes. This chapter presents work on the relationship between TBC-2 localization, the Class III PI3K and its lipid product, PI3P. My colleagues and I collaborated with a group of researchers and showed that the TBC-2 PH domain, but not the CC domain, binds to PI3P. We further showed that loss to one of the Class III PI3K core components (*vps-34*, *vps-15* and *bec-1*) or overexpression of the MTM-1 myotubularin PI3 phosphatase resulted in *tbc-2(tm2241)*-like enlarged vesicles in the intestine that were mainly RAB-7 positive. Additionally, we observed that the full-length TBC-2 and, surprisingly, even the PH domain truncated form required VPS-34 for endosome localization. From these results, we identified dual roles played by the Class III PI3K in regulating TBC-2 localization and demonstrated that PI3P dependence for TBC-2 localization is not restricted to the PH domain alone.

4.1 The PH domain of TBC-2 binds to PI3P and PI4P *in vitro*

To investigate whether the TBC-2 PH domain or the CC domain binds to lipids, GST fused to the PH domain, CC domain or the segment encompassing both PH and CC domains (referred as PH-CC) were tested for binding using lipid overlay assays. We found that the PH domain and the PH-CC segment bound to both PI3P and PI4P (**Figure 15 A**). From two of the three experiments performed, PH-CC bound more robustly to PI3P than PI4P (**Figure 15 A'**). In contrast, the CC domain did not bind to any lipids.

These findings were validated through liposome binding assays. The PH domain bound onto liposomes composed of PC/PE/PI3P (phosphatidylcholine/phosphatidylethanolamine/ phosphatidylinositol 3-phosphate) and PC/PE/PI4P (phosphatidylcholine/ phosphatidylethanolamine/phosphatidylinositol 4-phosphate) with relatively equal affinity (**Figure 15 B, C**). The CC domain did not bind to any of the liposomes tested.

Together, these results from *in vitro* assays suggest that the PH domain targets TBC-2 to maturing endosomes by binding to PIs. We found that the CC domain does not bind to lipids. If the CC domain is responsible for membrane binding by the CC domain region, it may associate with a membrane protein via intermolecular interactions between coiled-coil structures (Burkhard et al., 2001).

4.2 Loss of the Class III PI3K subunits or overexpression of MTM-1 phenocopies the *tbc-2* mutant effect in the intestine

Because TBC-2 is a Rab5 GAP, we focused on the Class III PI3K, which produces the majority of PI3P on EEs (Gillooly et al., 2000; Schu et al., 1993). To determine if this kinase

complex regulates vesicular size in the intestine, wildtype worms were treated with *vps-34(RNAi)* (Roggo et al., 2002; Xue et al., 2003). Affected animals accumulated large vesicles in the intestine when compared to controls. These vesicles contained globular material that was morphologically similar to those found from *tbc-2(tm2241)* (**Figure 16 A, B**). When other subunits of the Class III PI3K were targeted by RNAi knockdown or strong loss-of-function mutation (Takacs-Vellai et al., 2005) (**Figure 16 C, D**), enlarged vesicles containing globular material were also observed. These data indicate that loss of the Class III PI3K VPS-34/VPS-15/BEC-1 complex produces vesicles that resemble enlarged, *tbc-2* mutant endosomes.

When PI3P levels were alternatively reduced in wildtype worms by overexpressing the lipid phosphatase MTM-1 using a heat shock promoter. At 23-24 °C, an intestinal phenotype similar to *vps-34(RNAi)*, *vps-15(RNAi)*, or *bec-1(ok691)* was observed (**Figure 16 E**). In contrast, overexpression of the catalytically inactive MTM-1(C378S) failed to induce a large vesicle effect. This indicates that the intestinal phenotype arose from the phosphatase activity of MTM-1 (**Figure 16 F**).

Previously, it was shown that *tbc-2(tm2241)* worms with RNAi knockdown to *rab-7* results in a small vesicle phenotype in the intestine (Chotard et al., 2010a). To provide greater support that the enlarged vesicles observed from loss of PI3P is linked to the *tbc-2(tm2241)* effect, *vps-34(RNAi)* worms were additionally treated with *rab-7(RNAi)*. Animals affected with *rab-7(RNAi)* alone had vesicles and granular material that were smaller than those of *gfp(RNAi)* controls (**Figure 16 A, H**). Double *vps-34(RNAi); rab-7(RNAi)* worms had vesicles that also reverted back to small sizes (**Figure 16 I, J**). From these findings, it shows that, like the *tbc-2(tm2241)* phenotype, the *vps-34(RNAi)* phenotype is *rab-7* dependent.

4.3 *vps-34(RNAi)* or overexpression of MTM-1 results in the formation of enlarged LEs

Enlarged vesicles observed from *tbc-2(tm2241)* mutants, or wildtype worms expressing constitutively active RAB-5(Q78L) are predominantly RAB-7 positive (Chotard et al., 2010a). To investigate if enlarged vesicles from loss of PI3P were similarly RAB-7 labelled, wildtype worms expressing fluorescently tagged RAB-5 or RAB-7 were imaged upon *vps-34* knockdown or MTM-1 overexpression. In both cases, the resulting enlarged vesicles were mostly RAB-7 positive, although some were labelled with RAB-5 (**Figure 17**). This data is consistent with the enlarged RAB-7 vesicles observed from loss-of-function *bec-1(ok691)* mutants (Ruck et al., 2011). Together, these results suggest that reduced PI3P or its derivatives (e.g. $PI(3,5)P_2$) produces a large LE phenotype that is similar to loss of *tbc-2* function or expression of constitutively active RAB-5(Q78L).

4.4 VPS-34 and BEC-1 are required for GFP::TBC-2::FLAG membrane localization

To show that the enlarged endosomes from reduced PI3P have a loss of TBC-2 function at their membrane, *tbc-2(tm2241)* mutants rescued with GFP::TBC-2::FLAG expression were treated to *vps-34(RNAi)*. These treated worms possessed a mostly cytoplasmic GFP::TBC-2::FLAG localization with enlarged vesicles when compared to *ev(RNAi)* negative controls (**Figure 18 A-F**). A similar cytoplasmic distribution was observed in homozygous *bec-1(ok691)* mutants when compared to heterozygous *bec-1(ok691)*/+ controls (**Figure 19 A-F**). This finding indicates that TBC-2 membrane localization is mediated by the Class III PI3K and further

supports PI3P binding by the PH domain. When these results are combined with the observations from **Figure 8**— where GFP::TBC-2(ΔPH)::FLAG had a stronger membrane localization than full-length TBC-2— it suggests that PI3P binding by the PH domain relieves an inhibitory mechanism for TBC-2 localization.

4.5 VPS-34 is required for GFP::TBC-2(ΔPH)::FLAG endosome localization

If VPS-34 promotes TBC-2 endosome localization via the PH domain, then localization of GFP::TBC-2(ΔPH)::FLAG should not be affected upon loss of PI3P. Contrary to this hypothesis, enlarged vesicles re-emerged when GFP::TBC-2(ΔPH)::FLAG expressing, *tbc-2(tm2241)* rescued worms were treated with *vps-34(RNAi)* (**Figure 18 G-L**). An identical effect was observed from loss-of-function *bec-1(ok691)* worms expressing GFP::TBC-2(ΔPH)::FLAG (**Figure 19 H, K**). In both instances, an enlarged vesicular phenotype was accompanied by reduced membrane localization of GFP::TBC-2(ΔPH)::FLAG. This suggests that the Class III PI3K promotes TBC-2 membrane localization not only though the PH domain, but also through the CC domain region.

4.6 Mammalian Rab7 binding domain does not effectively target GFP::TBC-2(ΔPH-CC) to LEs for TBC-2 catalytic activity

Strong colocalization observed between GFP::TBC-2(ΔPH)::FLAG and RAB-7 (**Figure 8 L, M, Figure 20**) suggests that the CC domain region binds to a LE-associated protein. I hypothesized that targeting GFP::TBC-2(ΔPH-CC)::FLAG to LEs may be able to rescue the *tbc-*

2(tm2241) phenotype. Because no *C. elegans* RAB-7 effector has yet been identified, the mammalian Rab7 effector RILP (Romero Rosales et al., 2009) was used for this experiment. Its Rab7 binding domain (referred to as RILPb) was fused to the N-terminus of TBC-2(ΔPH-CC) and expressed in *tbc-2(tm2241)* worms (**Figure 21 A**).

The localization of GFP::RILPb::TBC-2(ΔPH-CC)::FLAG was largely cytoplasmic and did not match the defined, membrane-bound pattern of mCherry::RAB-7 (**Figure 21 E, G**). In this sense, its localization was very similar to that of GFP::TBC-2(ΔPH-CC)::FLAG (**Figure 21 F, G**). GFP::RILPb::TBC-2(ΔPH-CC)::FLAG expressing worms still exhibited enlarged endosomes (**Figure 21 D, J**), although the vesicles were smaller when compared to those from GFP::TBC-2(ΔPH-CC) expressing worms (**Figure 21 K**, from 5.93um to 3.78um, $P<0.001$). This suggests that expression of GFP::RILPb::TBC-2(ΔPH-CC)::FLAG was able to reduce *tbc-2(tm2241)* endosome sizes to some degree. However, it is uncertain at this point whether endosome sizes were reduced from RILPb targeting and/or GFP::RILPb::TBC-2(ΔPH-CC)::FLAG overexpression.

Summary

To summarize, the work presented in this chapter provides evidence that the Class III PI3K generated PI3P is an important component for TBC-2 recruitment on endosomal membranes. It is required by both TBC-2 PH domain and CC domain region for this process. Enlarged vesicles produced from loss of PI3P levels have strong RAB-7 labelling and contained granular material, similar to the characteristics found in *tbc-2(tm2241)* vesicles.

Figure 15

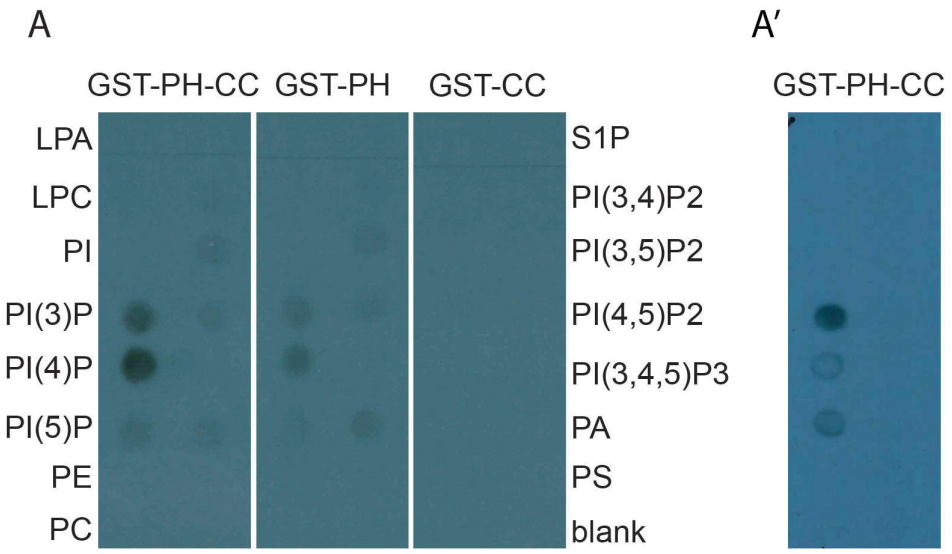
A
A′
GST-PH-CC
GST-PH
GST-CC
GST-PH-CC
LPA
LPC
PI
PI(3)P
PI(4)P
PI(5)P
PE
PC
S1P
PI(3,4)P2
PI(3,5)P2
PI(4,5)P2
PI(3,4,5)P3
PA
PS
blank

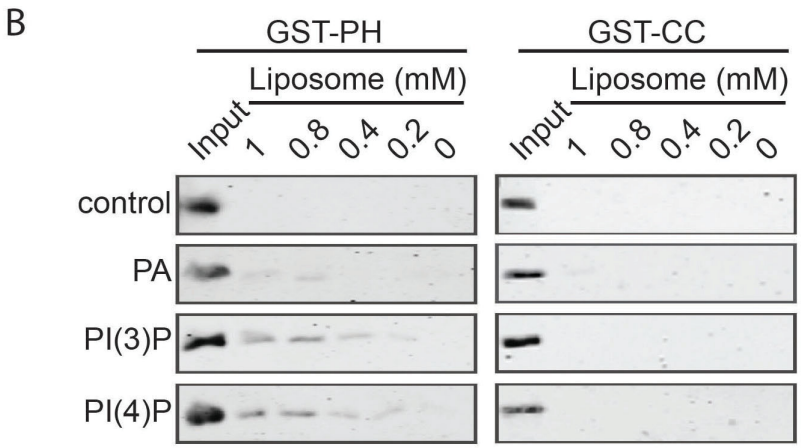
B
GST-PH
GST-CC
Liposome (mM)
Liposome (mM)
Input
1
0.8
0.4
0.2
0
control
PA
PI(3)P
PI(4)P

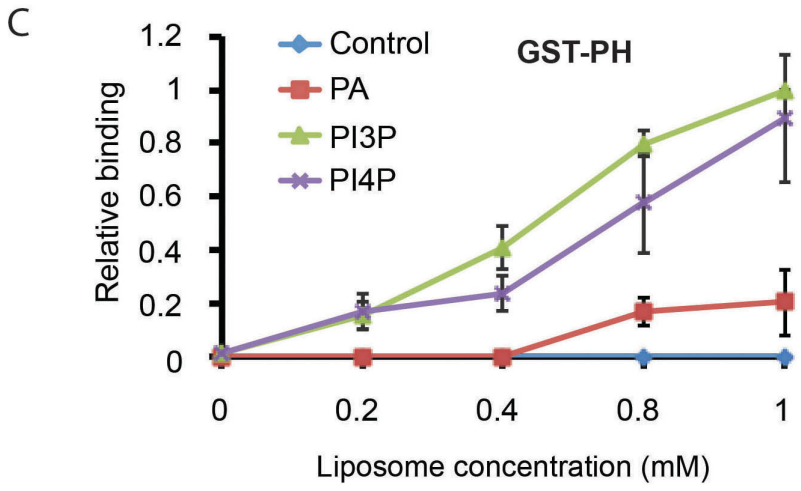
C
GST-PH
Control
PA
PI3P
PI4P
Relative binding
1.2
1
0.8
0.6
0.4
0.2
0
0
0.2
0.4
0.8
1
Liposome concentration (mM)

Figure 15. The PH domain of TBC-2 binds to PI3P and PI4P *in vitro*. (A) Representative image of a lipid overlay assay demonstrating that the PH-CC segment and PH domain bind to PI3P and PI4P. In two of three experiments, the PH-CC segment had stronger binding to PI3P than PI4P: (A') represents one such blot. In all three experiments, the CC domain did not bind to any lipids. (B) Binding between purified recombinant GST-PH and GST-CC proteins to liposomes were detected by Western blot using an anti-GST antibody. Control liposomes were composed of PC and PE. Treatment liposomes additionally contained PA (phosphatidic acid), PI3P, or PI4P. (C) Quantifications of GST-PH lipid binding onto liposomes were normalized to the inputs from (B). Results shown are from three independent experiments. Other lipids on the lipid assay membrane: LPA (lysophosphatidic acid), LPC (lysophosphocholine), PE (phosphatidylethanolamine), PC (phosphatidylcholine), S1P (sphingosine-1-phosphate) and PS (phosphatidylserine).

Figure 16

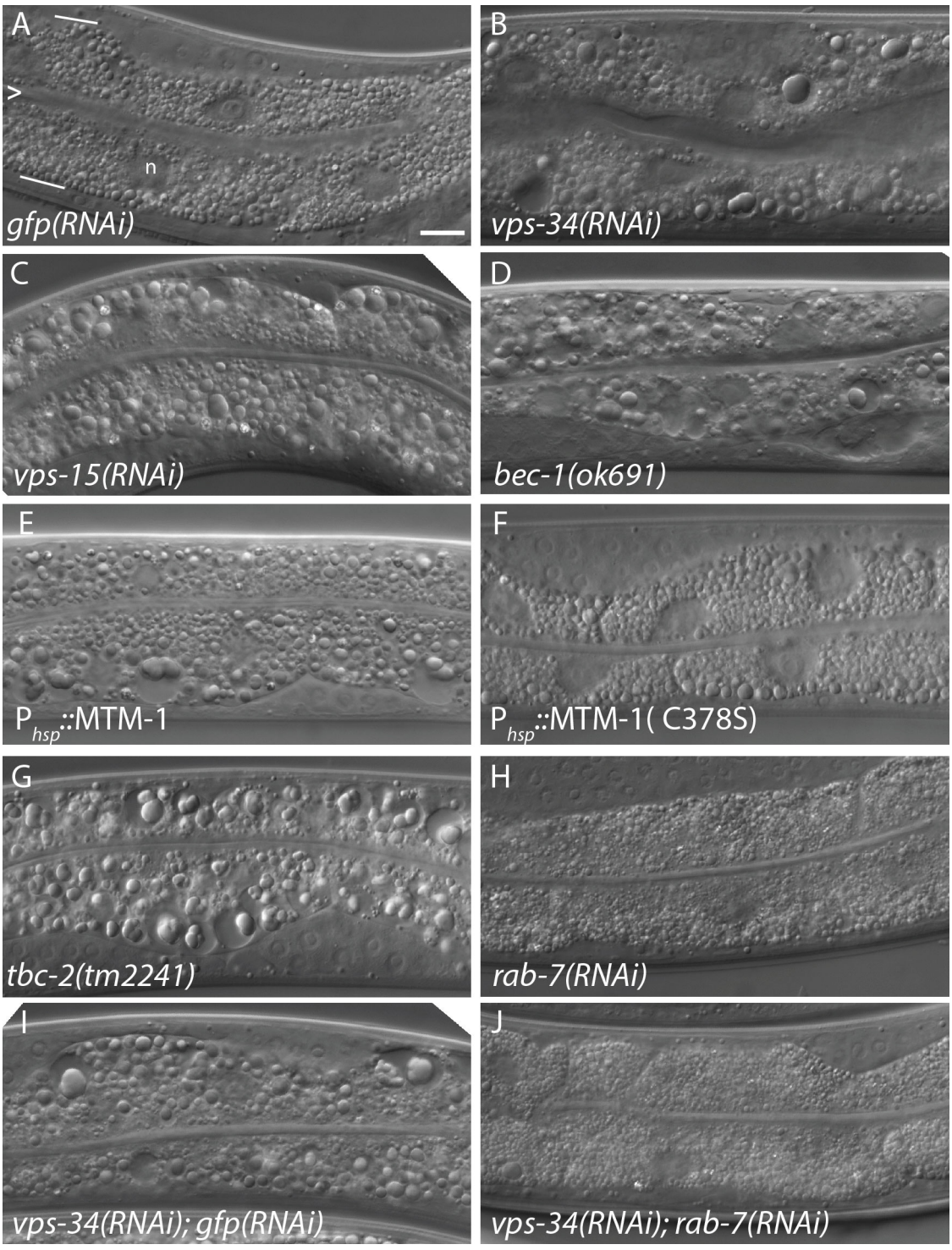
A
v
n
gfp(RNAi)
B
vps-34(RNAi)
C
vps-15(RNAi)
D
bec-1(ok691)
E
P hsp ::MTM-1
F
P hsp ::MTM-1(C378S)
G
tbc-2(tm2241)
H
rab-7(RNAi)
I
vps-34(RNAi); gfp(RNAi)
J
vps-34(RNAi); rab-7(RNAi)

Figure 16. Loss of function to the Class III PI3K or overexpression of the PI3P phosphatase MTM-1 causes a large vesicle phenotype in the intestine. (A-J) Representative DIC images of L4 stage larvae treated with *gfp(RNAi)* (A), *vps-34(RNAi)* (B), *vps-15(RNAi)* (C), or *bec-1(ok691)* (D); L4 stage larvae overexpressing *qxIs156* (P_{hsp}::MTM-1) (E), or *qxIs210* (P_{hsp}::MTM-1 C378S) (F); L4 stage *tbc-2(tm2241)* mutant larvae (G); wildtype L4 stage larvae treated with *rab-7(RNAi)* (H), *vps-34(RNAi); gfp(RNAi)* (I), or *vps-34(RNAi); rab-7(RNAi)* (J) are shown. *bec-1(ok691)* homozygous progenies were obtained from heterozygous mothers. For reference, the intestine is composed primarily of a single layer of binucleated cells. ">" marks the intestinal lumen and the apical membrane. White lines mark the basal membrane. Approximately four cells are present in each image. "n" denotes nucleus (A). Bar: (A) 10 μm.

Figure 17

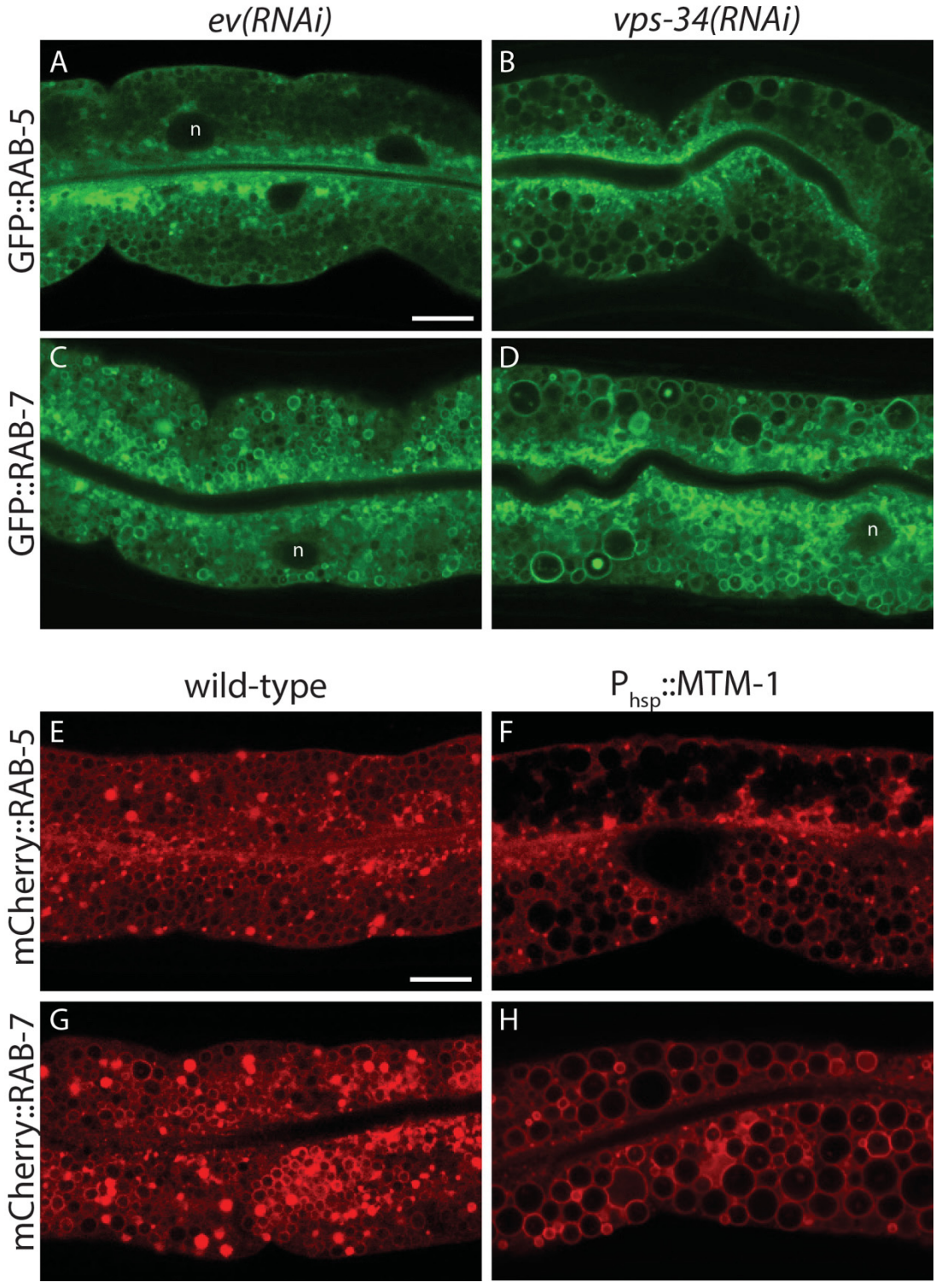
ev(RNAi)
vps-34(RNAi)
A
B
n
GFP::RAB-5
C
D
n
n
GFP::RAB-7
wild-type
P hsp ::MTM-1
E
F
mCherry::RAB-5
G
H
mCherry::RAB-7

Figure 17. Loss of VPS-34 or overexpression of MTM-1 induces the formation of enlarged endosomes. (A-D) Representative confocal images of GFP::RAB-5 (A and B) or GFP::RAB-7 (C and D) localization in wildtype worms treated with *ev(RNAi)* (A and C) or *vps-34(RNAi)* (B and D). (E-H) Representative confocal images of mCherry::RAB-5 (E and F) or mCherry::RAB-7 (G and H) in wildtype worms (E and G) or worms expressing *qxIs156* MTM-1 under the heat shock promoter (F and H). "n" denotes nuclei. All animals were imaged at L4 stage. Bar: (A and E) 10 μm.

Figure 18

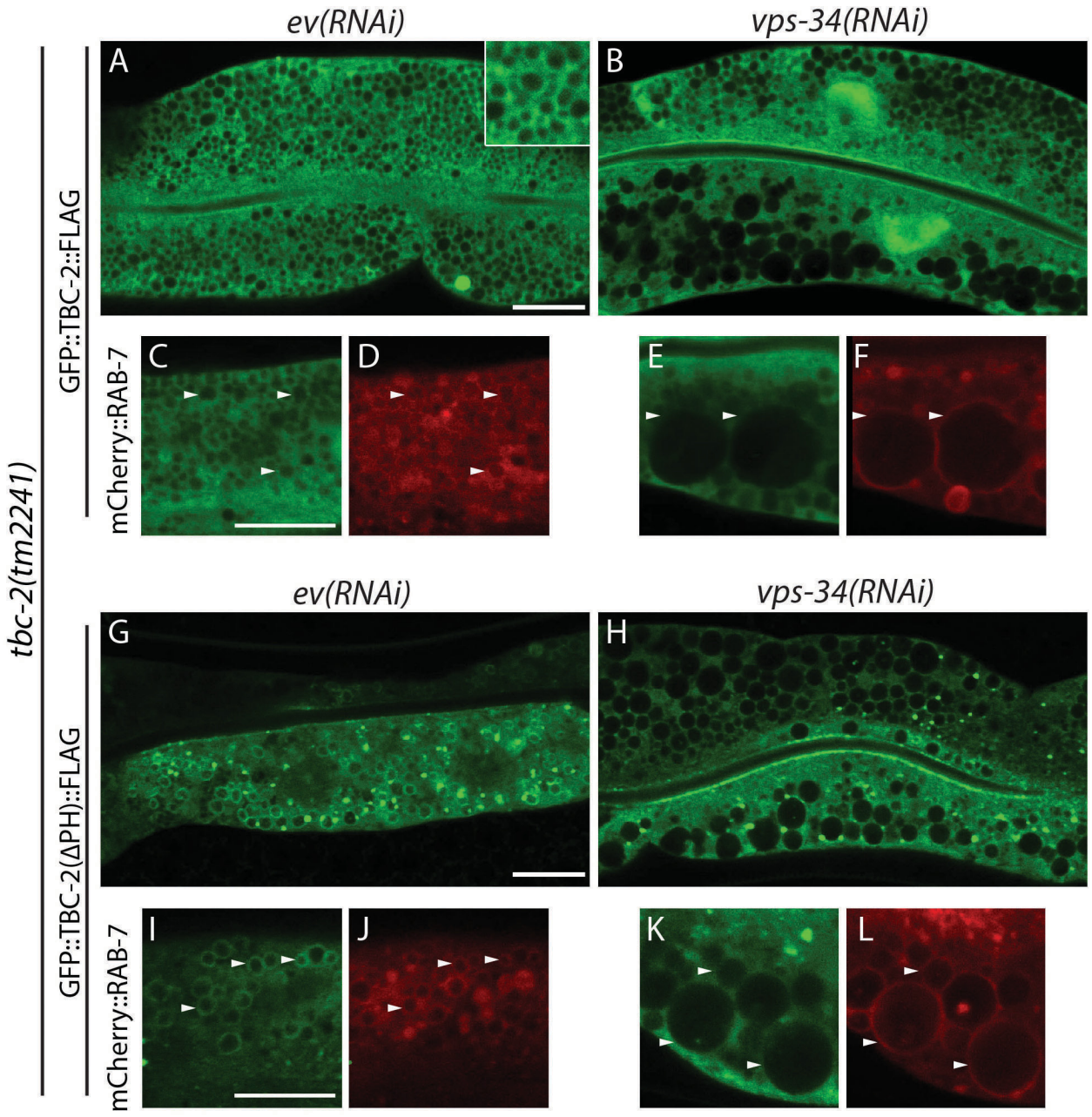
ev(RNAi)
vps-34(RNAi)
tbc-2(tm2241)
GFP::TBC-2::FLAG
mCherry::RAB-7
GFP::TBC-2(ΔPH)::FLAG
A
B
C
D
E
F
G
H
I
J
K
L

Figure 18. The Class III PI3K VPS-34 subunit regulates TBC-2 endosome localization. (A, B, G and H) Representative confocal images of GFP::TBC-2::FLAG (A and B) or GFP::TBC-2(ΔPH)::FLAG (G and H) intestinal expression in *tbc-2(tm2241)* L4 larvae treated with *ev(RNAi)* (A and G) or *vps-34(RNAi)* (B and H). In (B), the *vps-34(RNAi)* effect was less severe in the upper cell than in the lower. In (G), the upper cell had lower GFP signal than the bottom cell, which may be due to differences in expression and/or inheritance levels. (C-F, I-L) Representative confocal images of *tbc-2(tm2241)* L4 larvae co-expressing *pwIs429* mCherry::RAB-7 and either *vhEx12* GFP::TBC-2::FLAG (C-F), or *vhEx20* GFP::TBC-2(ΔPH)::FLAG (I-L) with treatment of either *ev(RNAi)* (C, D, I and J), or *vps-34(RNAi)* (E, F, K and L). GFP and mCherry signals are represented as green and red, respectively. White arrowheads denote examples of vesicles displaying signals from both channels. Bar: (A and J) 10 μm.

Figure 19

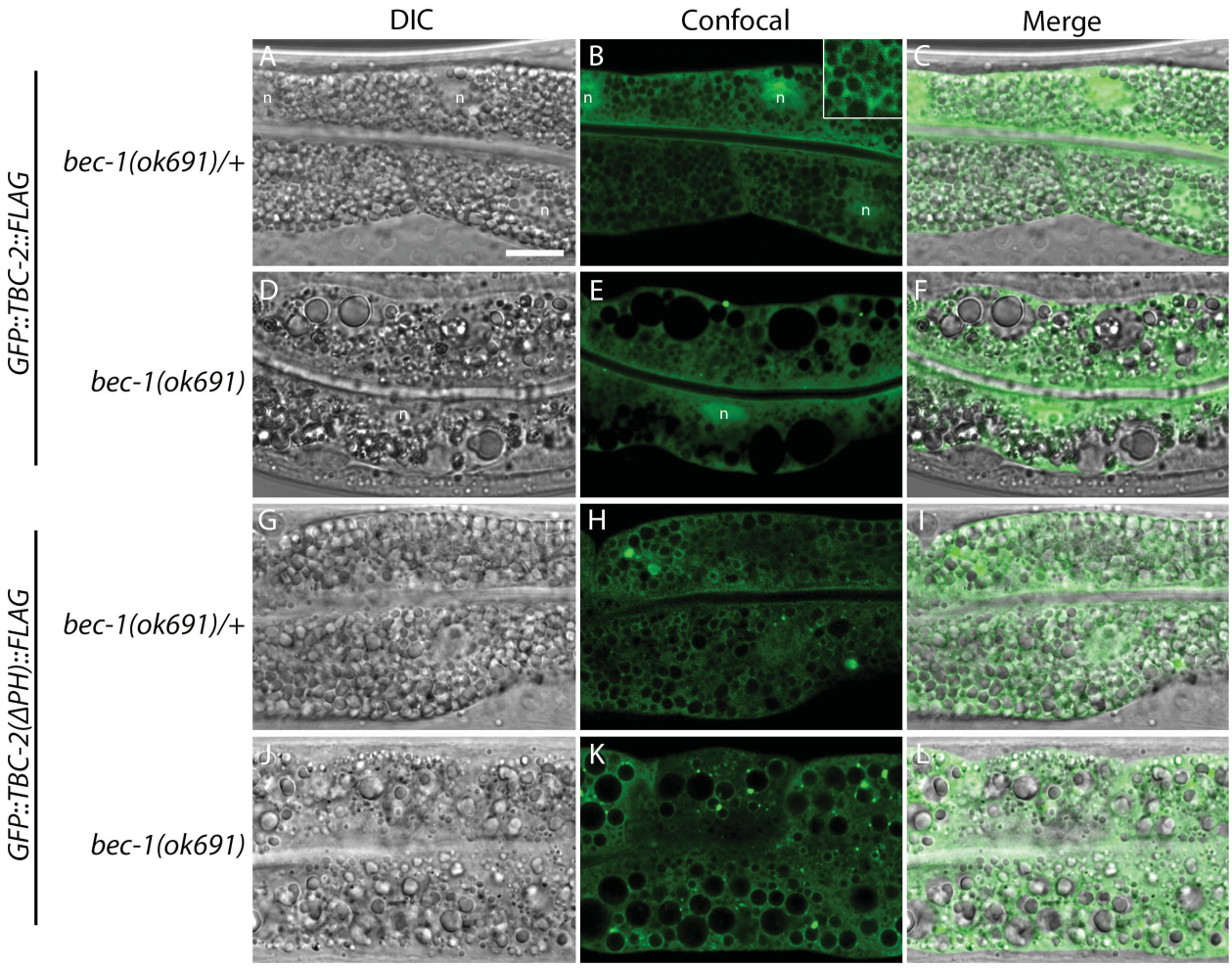
DIC
Confocal
Merge
GFP::TBC-2::FLAG
bec-1(ok691)/+
bec-1(ok691)
GFP::TBC-2(ΔPH)::FLAG
bec-1(ok691)/+
bec-1(ok691)
A
B
C
D
E
F
G
H
I
J
K
L
n

Figure 19. Loss-of-function *bec-1(ok691)* induces the formation of enlarged endosomes and reduces localization of TBC-2. (A-L) Representative images of heterozygous (A-C, G-I) and homozygous *bec-1(ok691)* (D-F, J-L) L4 worms expressing *vhEx12* GFP::TBC-2::FLAG (A-F) or *vhEx20* GFP::TBC-2(ΔPH)::FLAG (G-L). "n" denotes nucleus. Bar: (A) 10 μm.

Figure 20

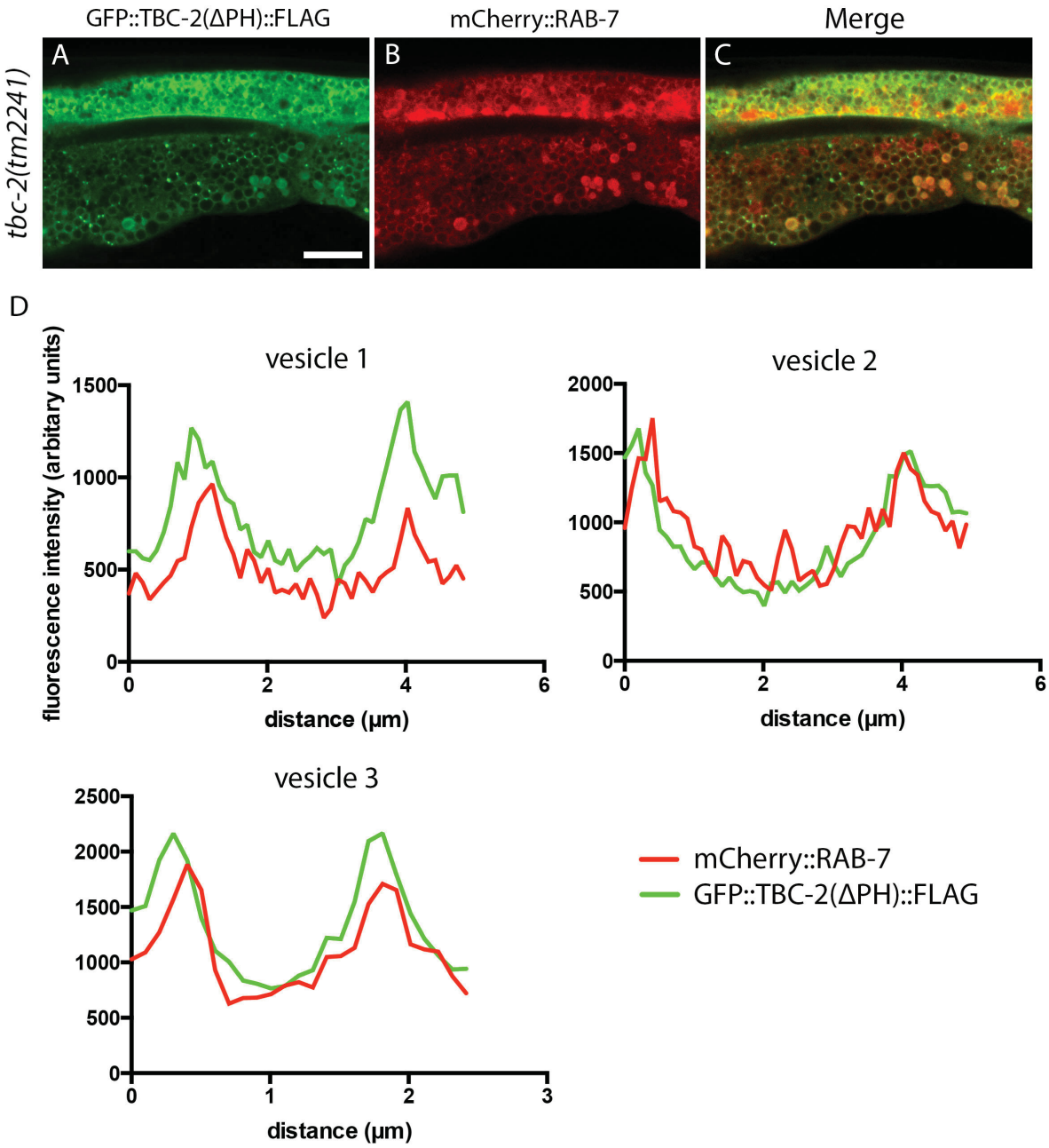
GFP::TBC-2(ΔPH)::FLAG
mCherry::RAB-7
Merge
A
B
C
tbc-2(tm2241)
D
vesicle 1
vesicle 2
vesicle 3
fluorescence intensity (arbitary units)
distance (μm)
mCherry::RAB-7
GFP::TBC-2(ΔPH)::FLAG

Figure 20. GFP::TBC-2(ΔPH)::FLAG localizes onto LEs. (A-C) Representative images of L4 *tbc-2(tm2241)* worms co-expressing *pwIs429* mCherry::RAB-7 and *vhEx20* GFP::TBC-2(ΔPH)::FLAG. The upper cell had stronger GFP signal due to higher *vhEx20* expression. (D) Fluorescence intensity profiles of three vesicles with GFP::TBC-2(ΔPH)::FLAG (green) and mCherry::RAB-7 (red) membrane localizations. The slight misalignments of red and green fluorescent peaks were due to minute movements from live worms during imaging. Bar (A) 10 μm.

Figure 21

A

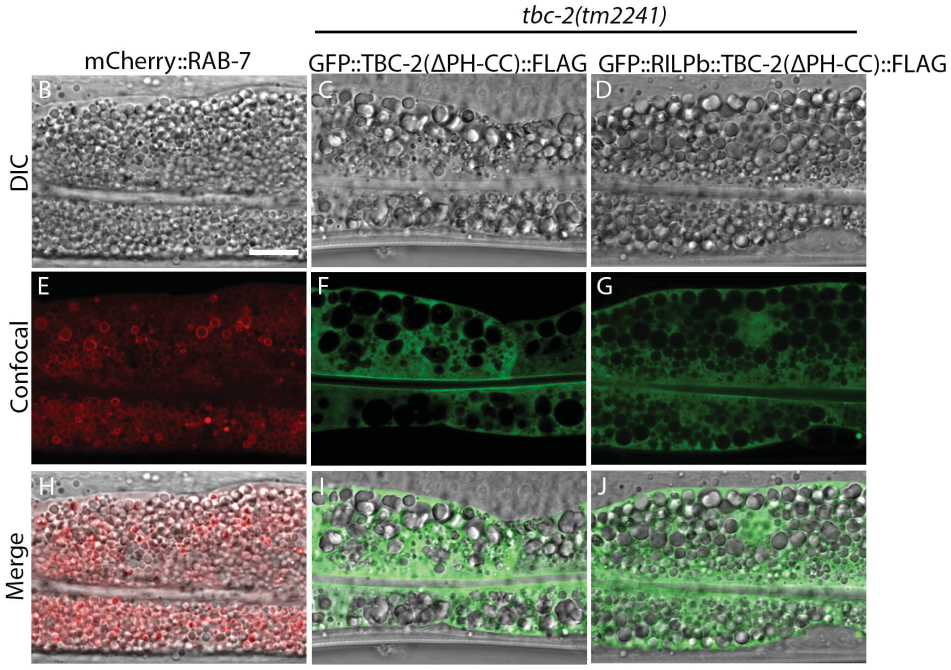

K

Genotype	Mean vesicular diameter (µm)	Std deviation (µm)	Mode (µm)	Min value (µm)	Max value (µm)
Wildtype (N2) (n=50)	1.70	0.26	1.93	1.11	2.36
***tbc-2(tm2241);* GFP::TBC-2(ΔPH-CC)::FLAG** (n=50)	5.93	1.19	4.85	3.91	9.2
***tbc-2(tm2241);* GFP::RILPb::TBC-2(ΔPH-CC)::FLAG** (n=51)	3.78	0.85	3.93	2.31	5.82

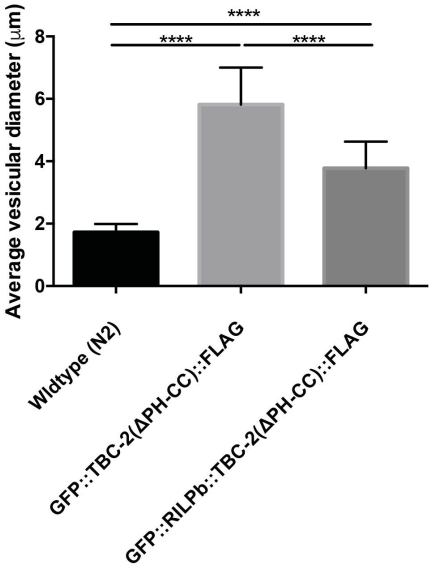

Figure 21. Targeted localization of GFP::TBC-2(ΔPH-CC)::FLAG by RILPb partially rescues the *tbc-2(tm2241)* enlarged vesicular phenotype. (A) Schematic diagram of where the Rab7-binding domain (referred to as RILPb) from mammalian RILP is inserted into GFP::TBC-2(ΔPH-CC)::FLAG for LE targeting. (B-J) Representative images of worms expressing *pwIs170* mCherry::RAB-7 alone (B, E, H), *tbc-2(tm2241)* mutants expressing either *vhEx22* GFP::TBC-2(ΔPH-CC)::FLAG (C, F, I), or *vhEx51* GFP:: RILPb::TBC-2(ΔPH-CC)::FLAG (D, G, J). All worms were imaged at L4 stage. (K) Quantitative summary of vesicular diameters measured from the three imaged genotypes. "n" denotes the number of vesicles measured per group. Decimal places of all values were rounded to the nearest hundredth place. Median vesicular diameters are represented in a frequency graph. Error bars represent standard deviations. ****, $P < 0.001$ (differences between treatments). Bar: (A) 10 μm.

Chapter 5. Characterization of *vh45*, a potential TBC-2 regulator

Preface

A mutant from a forward genetic screen displaying RAB-7-positive, enlarged basolateral endosomes in the intestine was isolated and named *vh45*. Phenotypes between *vh45 and tbc-2(tm2241)* worms share other similarities based on vesicular size and presence of globular material. These features distinguish *vh45* as a potential regulator for TBC-2 function. Further characterization of *vh45* revealed that it gives rise to a co-dominant allele affecting both sexes. The locus of the *vh45* mutation was mapped to a region on Chromosome II between 2-5 Mb (megabase pairs) using WGS-SNP (Whole Genome Sequencing-Single Nucleotide Polymorphism). So far, three candidates were tested via RNAi treatment for the *vh45* phenotype, but no *vh45* effect has been observed.

5.1 The *vh45* mutation gives rise to enlarged LEs

Mutations that give rise to *tbc-2(tm2241)*-like phenotypes can affect genes that encode for TBC-2 regulators, or for products that function in an alternative pathway to inactivate RAB-5. To this end, a former summer student named Shang Xiang performed a forward genetic screen using the chemical ethyl methanesulfonate (EMS) on worms expressing GFP::RAB-7. She then screened the mutagenized worms and isolated a mutant displaying large, RAB-7-positive vesicles that are restricted to the basolateral region of the intestine (**Figure 22 A-C**). The mutant was named *vh45*.

Mean vesicular diameters between *vh45* and *tbc-2(tm2241)* mutants were not statistically different (**Figure 22 D**, 6.22 μm versus 5 μm, $P<0.001$). Additionally, within the affected vesicles of *vh45* mutants, globular cargo similar to *tbc-2(tm2241)* worms can often be observed (**Figure 22 B, C**). Unlike the *tbc-2(tm2241)* phenotype, however, *vh45* oocytes do not have large yolk platelets (**Figure 22 A'-C'**).

5.2 The *vh45* mutation is sex-independent and co-dominant

Enlarged intestinal vesicles were detected from both *vh45* homozygous hermaphrodites and males (**Figure 23 C, D**). Not all individuals, however, displayed the mutant phenotype (undocumented observation), which suggests that the *vh45* effect is not fully penetrant. *vh45*/+ animals possessed an extremely mild intestinal phenotype where most basolateral vesicles were similarly sized to those of wildtype worms. Larger-sized vesicles were occasionally found (**Figure 23 B and caption**) and had diameters that fell within the range of enlarged *vh45* vesicles

(**Figure 22 D**). These data suggest that *vh45* produces a co-dominant allele that is not sex-linked. All further genetic characterizations of *vh45*, however, were treated as if the mutation were recessive. This approach has been previously applied elsewhere (Greenwald and Horvitz, 1980).

5.3 The *vh45* phenotype occurs from the effect at a single locus

If the *vh45* phenotype arises from the effect at a single locus, then the expected ratio of homozygous *vh45* progenies produced from a *vh45*/+ mother would be 25%. The remaining 75% would exhibit a wildtype or a mild intestinal phenotype (Griffiths, 2000).

From two *vh45*/+ mothers, inferred *vh45* homozygous progenies were found to comprise 19.3% and 19.6% of the population (**Table 3**). The slightly lowered values from the expected 25% may be caused by incomplete penetrance of the *vh45* phenotype. Despite the reduced percentages, the evidence suggests that the *vh45* phenotype arises from a mutation at a single locus.

5.4 The *vh45* locus is not an allele of *tbc-2*

To find if the *vh45* mutation occurs at the *tbc-2* locus, a complementation test was performed (Griffiths, 2000; Yook, 2005). As demonstrated in Chapter 3, this genetic test can provide information on whether two recessive mutations occur in alleles of the same gene. Individuals carrying two recessive alleles of the same gene are expected to exhibit a mutant phenotype, whereas those carrying recessive alleles located on different loci are phenotypically wildtype.

Worms carrying a single copy of both *tbc-2(tm2241)* and *vh45* in *trans* possessed small vesicles like those found in wildtype intestine (**Figure 23 E, F**). This successful complementation suggests that *vh45* is not an allele of *tbc-2,* but rather an allele of another gene that may regulate *tbc-2*.

5.5 Mapping the *vh45* mutation via Whole Genome Sequencing-Single Nucleotide Polymorphism

Whole genome sequencing (WGS) and single-nucleotide polymorphism (SNP) mapping have each been widely used for genetic mapping. However, while WGS is fast and cost-effective, it is limited by a lack of mapping information to pinpoint the locus of interest. On the other hand, SNP mapping can locate mutations to the chromosome interval, but it is laborious and time-consuming. By combining both WGS and SNP mapping into a single-step strategy (Doitsidou et al., 2010; Minevich et al., 2012), this novel method can rapidly and reliably determine the chromosome interval affected by the *vh45* mutation—for which no mapping information is known.

Mutagenized strains have been found to carry as many as 300 extraneous mutations per chromosome (Sarin et al., 2010). To reduce complications in identifying the *vh45* locus, mutant worms were outcrossed six times to the wildtype Bristol strain (N2). The final outcrossed strain does not retain the GFP::RAB-7 marker, yet enlarged intestinal vesicles are still observed (**Figure 22 C**). This indicates that GFP::RAB-7 does not contribute to the *vh45* phenotype.

To obtain unique SNPs for mapping, the outcrossed *vh45* worms were mated to a polymorphic Hawaiian variant (Doitsidou et al., 2010; Wicks et al., 2001) (**Figure 24 A**).

Several F1 *vh45*/Hawaiian hermaphrodites were chosen to produce self-progenies. F2 worms displaying the homozygous *vh45* phenotype were selected to establish clonal populations on separate feeding plates. Subsequent generations from each population were then pooled for genomic extraction. Genomic sequencing was performed by Genome Quebec.

After sequencing, the raw data were analyzed using a cloud-based, publicly available pipeline called CloudMap (Minevich et al., 2012). The pipeline aligned short sequenced reads from the raw data to a reference *C. elegans* genome template. Multiple reads covering a given region of the genome were stacked (i.e. in a pileup) (**Figure 24 B**). Pileups are particularly useful to determine if a detected nucleotide change reflects a true mutation or a sequencing error.

The distribution pattern of Hawaiian SNPs and their frequency in the genome provide information on where the *vh45* mutation is located. Normally, parental chromosomes undergo meiotic recombination in an unbiased manner at any given locus. For this reason, there is equal chance of inheriting either a Bristol or Hawaiian SNP in the next generation. Selection for the homozygous *vh45* phenotype in the F2 generation (**Figure 24 A**) exerted a bias against recombination at the *vh45* locus in order to preserve the phenotype. This effect caused nearby regions (and therefore SNP loci) to become "linked" to the *vh45* locus. As a result, regions approaching the *vh45* locus would have increasing rare opportunities to acquire recombinant Hawaiian SNPs (Doitsidou et al., 2010). The *vh45* locus would appear as a region of pure Bristol SNPs on distribution graphs (**Figure 24 C**).

Once the raw sequenced reads were aligned, CloudMap compiled three sets of data to identify the location of the causal *vh45* mutation:

(1) Ratios of Hawaiian SNPs to total runs at each known Hawaiian SNP loci (*y*-axis) were plotted against chromosome position (*x*-axis). Six scatter plots were made for

each of the six *C. elegans* chromosomes (**Figure 25 A-F**). To better visualize ratio trends, a smooth fitting LOESS (locally weighted smoothing) regression line was included in each plot. This regression line incorporates information from all scatter points, with greater weight given to local points over points located further away (Jacoby, 2000).

(2) Each scatter plot is accompanied by a frequency graph to indicate regions containing pure Bristol SNPs. For example, regions with a ratio of 0 on scatter plots have corresponding peaks on frequency graphs (**Figure 25 A'-F'**).

(3) All detected homozygous mutations shared between sequenced genomes are listed in an excel file. For each mutation, information on its genomic position, type of effect (non-synonymous, synonymous, frameshift) and location in relation to the affected gene (codon deletion, codon insertion, intron, 5'-UTR, 3'-UTR, splice-site acceptor, upstream, downstream) is provided.

5.6 The *vh45* mutation affects a locus on Chromosome II

Regions linked to the *vh45* locus would have increased retention of Bristol SNPs and at the chromosome interval very close to the *vh45* locus, there should be no meiotic recombination. On the Chromosome II scatter plot, the LOESS regression line approached the ratio value of 0 between the physical locations of 2-5 Mb. As observed from the accompanying frequency graph, pure Bristol SNPs were found in this segment (**Figure 25 B, B'**).

Six genes located in the 2-5 Mb interval that carry mutation(s) within their coding regions were selected from the excel file as *vh45* candidates. These candidates are: *K12H6.9* and *Y27F2A.11* with non-synonymous mutations; *Y110A2AM.1* and *Y46D2A.2* with frameshift

mutations; *Y8A9A.2* with both non-synonymous and frameshift mutations; and *ZK355.2* with a mutation at a splice-site acceptor (**Table 4, Figure 26 A**).

The *tbc-2* locus is located at the 5.8 Mb position and lies adjacent to the 2-5 Mb region of interest. From the provided excel file, *tbc-2* was not found to contain homologous mutations in *vh45* worms. The closest mutations to the *tbc-2* locus occur in the *dsh-2* locus (5.0 Mb) and the *B0034.5* locus (5.9 Mb). Both of these genes have not been functionally linked to endocytosis. This result confirms that the *vh45* mutation occurs away from the *tbc-2* locus.

Most *vh45* candidates are uncharacterized and have no known phenotypes (Wormbase.org). Two genes, *ZK355.2* and *Y46D2A.2,* have enriched expressions in the intestine (Wormbase.org). The products of both *Y27F2A.11* and *ZK355.2* are predicted to possess seven transmembrane domains and are putative G protein-coupled receptors (GPCRs) (Tuteja, 2009) **(Table 4)**.

Y8A9A.2 is the best characterized of all the candidates. It is expressed in the gland cells of the pharynx (Ghai et al., 2012), a neuromuscular organ for food intake (Albertson and Thomson, 1976). Unlike most pharynx gland genes, *Y8A9A.2* is not regulated by the HLH-6 (helix loop helix-6) transcription factor but rather by a *cis*-acting motif called HRL3 (Hlh-6 regulatory element 3) (Ghai et al., 2012). The exact function of *Y8A9A.2* is unknown. It is predicted to encode for a zinc metalloprotease (Ghai et al., 2012) that contains four type 1 thrombospondin domains (TSP1s). These domains have been shown to function in the extracellular matrix for cell-cell adhesion, cell-matrix adhesion and cell motility (Adams and Tucker, 2000). An NCBI protein BLAST search for the *Y8A9A.2* product revealed hemicentin as a top match (**Table 4**). Hemicentin is an extracellular protein of the immunoglobulin family that functions in cell attachment (Vogel and Hedgecock, 2001).

5.7 No *vh45* enlarged vesicles were observed from RNAi to *Y27F2A.11*, *K12H6.9* or *Y8A9A.2*

The chemical mutagen EMS preferentially induces G/C to A/T transitions. This nucleotide change has often been found to generate premature stop codons that result in strong loss-of-function or null mutations (Flibotte et al., 2010; Kutscher and Shaham, 2014). For this reason, candidates containing non-synonymous mutations—*Y27F2A.11*, *K12H6.9* and *Y8A9A.2*—were chosen first to test for a *vh45* phenotype.

RNAi treatment of *Y27F2A.11*, *K12H6.9* or *Y8A9A.2* in wildtype worms was unable to produce a *vh45* phenotype (**Figure 26 B-E**). Without further confirmation (i.e. through real-time PCR) to show that the mRNAs of interest were actually targeted, it remains unknown at this time whether any of the three candidates are responsible for the *vh45* effect.

Summary

This chapter presents initial work characterizing a mutation named *vh45*. Worms homozygous for *vh45* have enlarged LEs in the intestine that are basolaterally restricted. The *vh45* mutation is mapped to Chromosome II, at the 2-5 Mb interval. Six protein encoding genes were selected as *vh45* candidates. So far, three candidates carrying non-synonymous mutations were tested via knockdown, but none have yet produced a *vh45* phenotype.

Figure 22

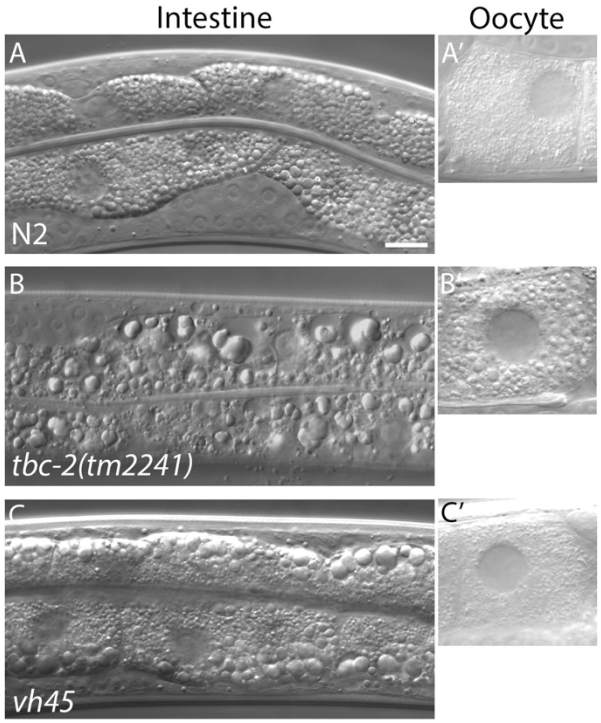

D

Genotype	Mean vesicular diameter (µm)	Std deviation (µm)	Mode (µm)	Min value (µm)	Max value (µm)
Wildtype (N2) (n=60)	1.74	0.19	1.76	1.34	2.26
tbc-2(tm2241) (n=51)	6.22	1.61	6.07	3	10.72
vh45 (n=78)	5.00	1.38	4.44	2.89	11.19

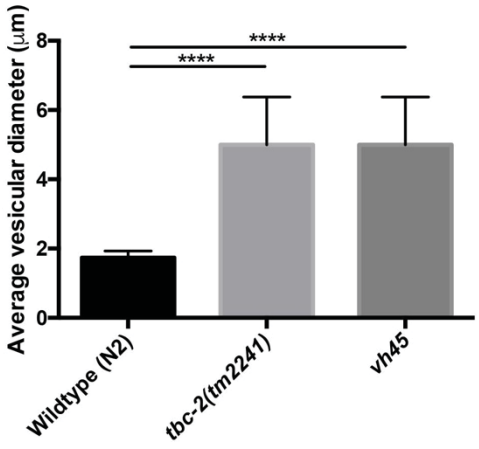

Figure 22. *vh45* homozygous worms display enlarged, basolateral endosomes in the intestine. (A-C, A'-C') Representative DIC images of intestine and the most proximal oocyte prior to fertilization in wildtype (A, A'), *tbc-2(tm2241)* (B, B') and *vh45* (C, C') worms. The imaged *vh45* worm was outcrossed to wildtype Bristol strain and has lost the GFP::RAB-7 marker. Intestinal images were taken at L4 stage, while oocytes were taken at adult stage. Bar: (A) 10 μm. (D) Quantitative summary of vesicular diameters measured from imaged worms. "n" denotes the number of vesicles measured per group. Decimal places of all values were rounded to the nearest hundredth place. A corresponding frequency graph of median vesicular diameters. Median vesicular diameters are represented in a frequency graph. Error bars represent standard deviations. ****, $P < 0.001$ (differences between treatments).

Figure 23

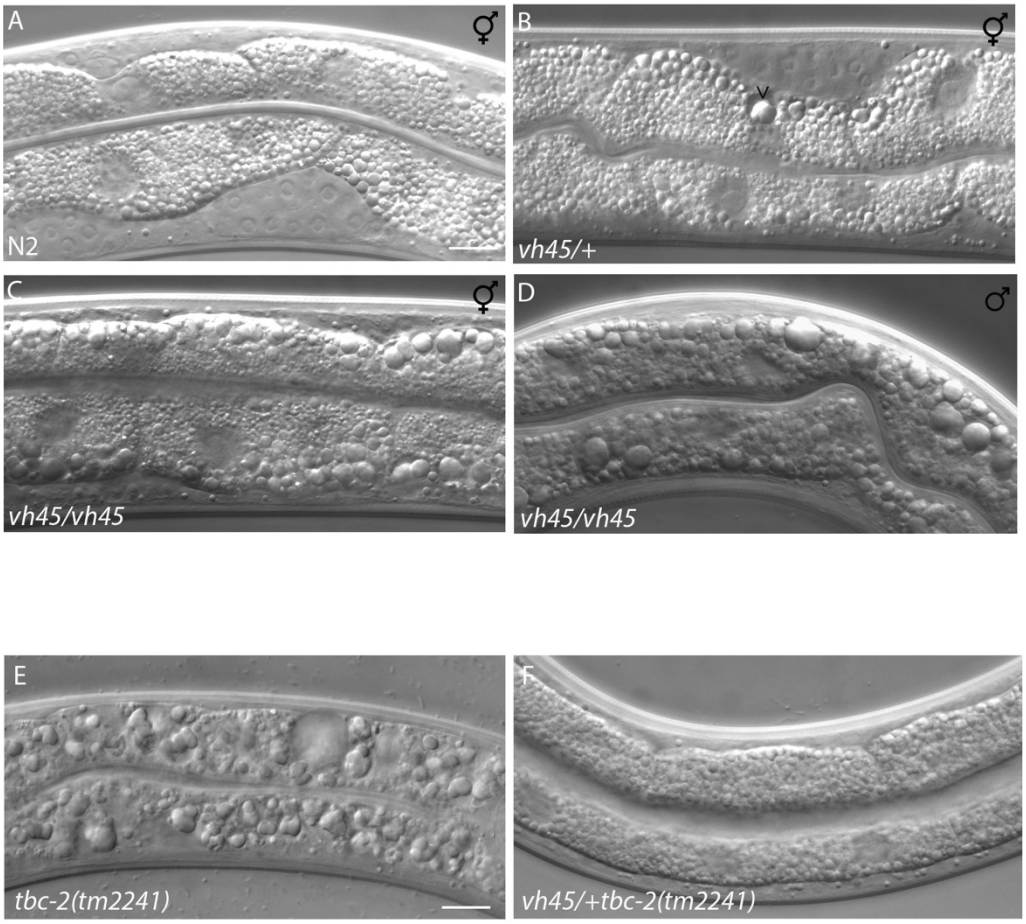
A
N2
B
V
vh45/+
C
vh45/vh45
D
vh45/vh45
E
tbc-2(tm2241)
F
vh45/+tbc-2(tm2241)

Figure 23. The *vh45* mutation likely occurs at a locus distinct from *tbc-2* and produces a co-dominant allele that affects both sexes. (A-D) Representative DIC images of L4 stage wildtype (A), *vh45*/+ (B), *vh45* hermaphrodite (C), and *vh45* male (D) intestine. The upside down arrowhead denotes a larger vesicle that was occasionally found in *vh45*/+ animals. This particular vesicle has a diameter of 6.91 μm. (E-F) Representative images from a complementation test. *tbc-2(tm2241)* worms exhibit enlarged vesicles in the intestine (E). *trans*-heterozygous progenies carrying *tbc-2(tm2241)* and *vh45* had no large vesicles (F). Bar: (A), (E) 10 μm.

Figure 24

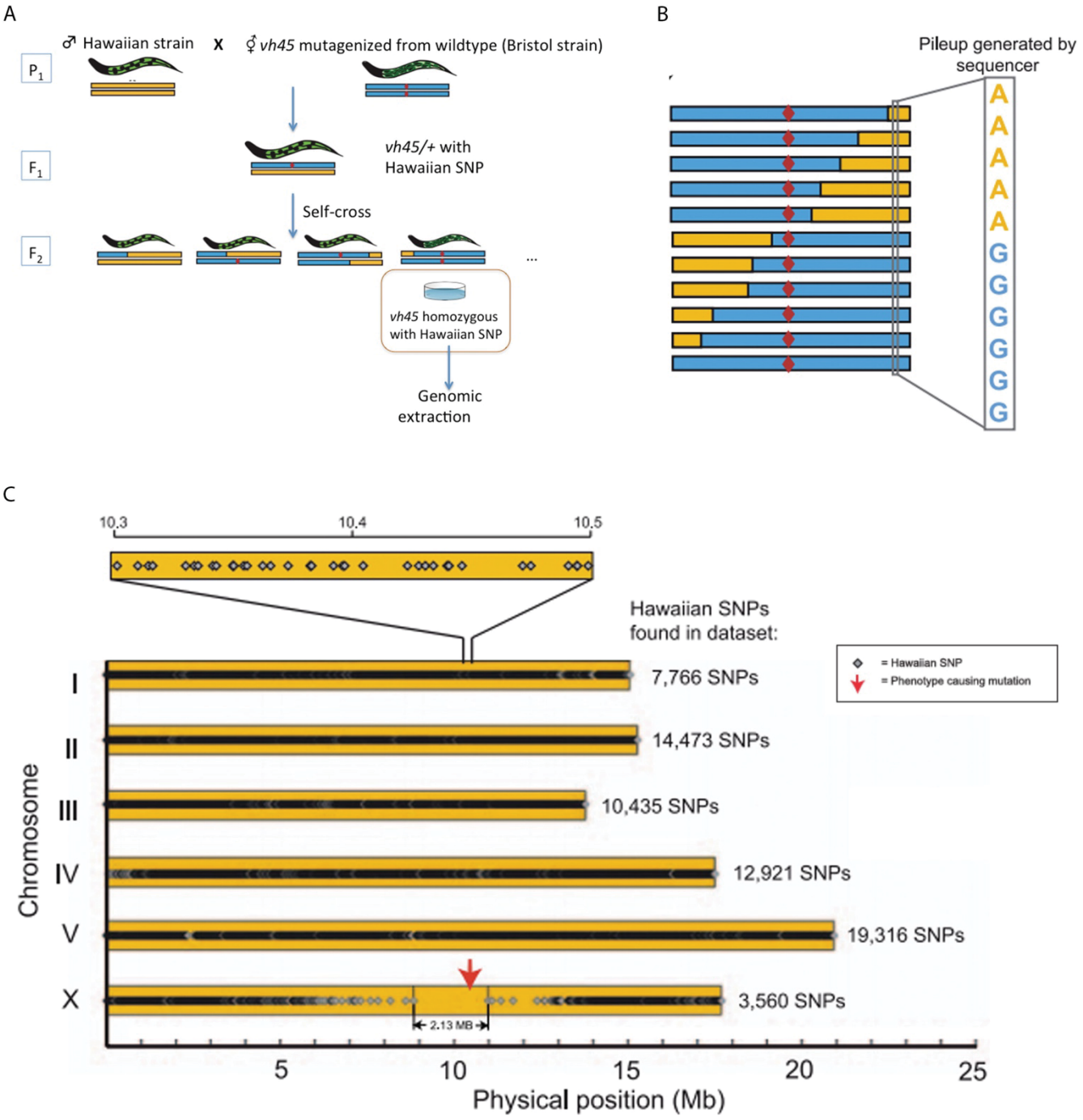
A
♂ Hawaiian strain
X
♀ vh45 mutagenized from wildtype (Bristol strain)
P1
F1
vh45/+ with Hawaiian SNP
Self-cross
F2
...
vh45 homozygous with Hawaiian SNP
Genomic extraction
B
Pileup generated by sequencer
A
A
A
A
A
G
G
G
G
G
G
C
10.3
10.4
10.5
Hawaiian SNPs found in dataset:
= Hawaiian SNP
= Phenotype causing mutation
I
II
III
IV
V
X
7,766 SNPs
14,473 SNPs
10,435 SNPs
12,921 SNPs
19,316 SNPs
3,560 SNPs
2.13 MB
Chromosome
5
10
15
20
25
Physical position (Mb)

Figure 24. Overview of the WGS-SNP mapping strategy. (A) Genetic scheme used for WGS-SNP mapping. The Bristol-derived *vh45* strain was crossed to the Hawaiian CB4856 strain to obtain polymorphic SNPs into the genome. The red dot symbolizes the *vh45* mutation. F1 *vh45*/Hawaiian mothers were allowed to self-cross. Those F2 progenies displaying the homozygous *vh45* phenotype were isolated for clonal propagation. Subsequent generations were pooled for genomic extraction. (B) Genomes were sequenced as short reads. The reads were aligned to a template genome and "piled up" using the CloudMap program. (C) A graph showing distributions of Hawaiian SNPs. Meiotic recombination normally occurs in an unbiased manner, where a given position has equal likelihood of inheriting either a Bristol or Hawaiian SNP in the next generation. However, selection for the *vh45* homozygous phenotype at F2 exerted a bias against meiotic recombinants carrying Hawaiian SNPs at the *vh45* locus. In the example shown, Hawaiian SNPs were absent in the mapping interval of 9-11 Mb of Chromosome X. The red arrow shows the position of where the mutation is actually located. Diagrams used in this figure were modified from Doitsidou *et al*. (Doitsidou et al., 2010).

Figure 25

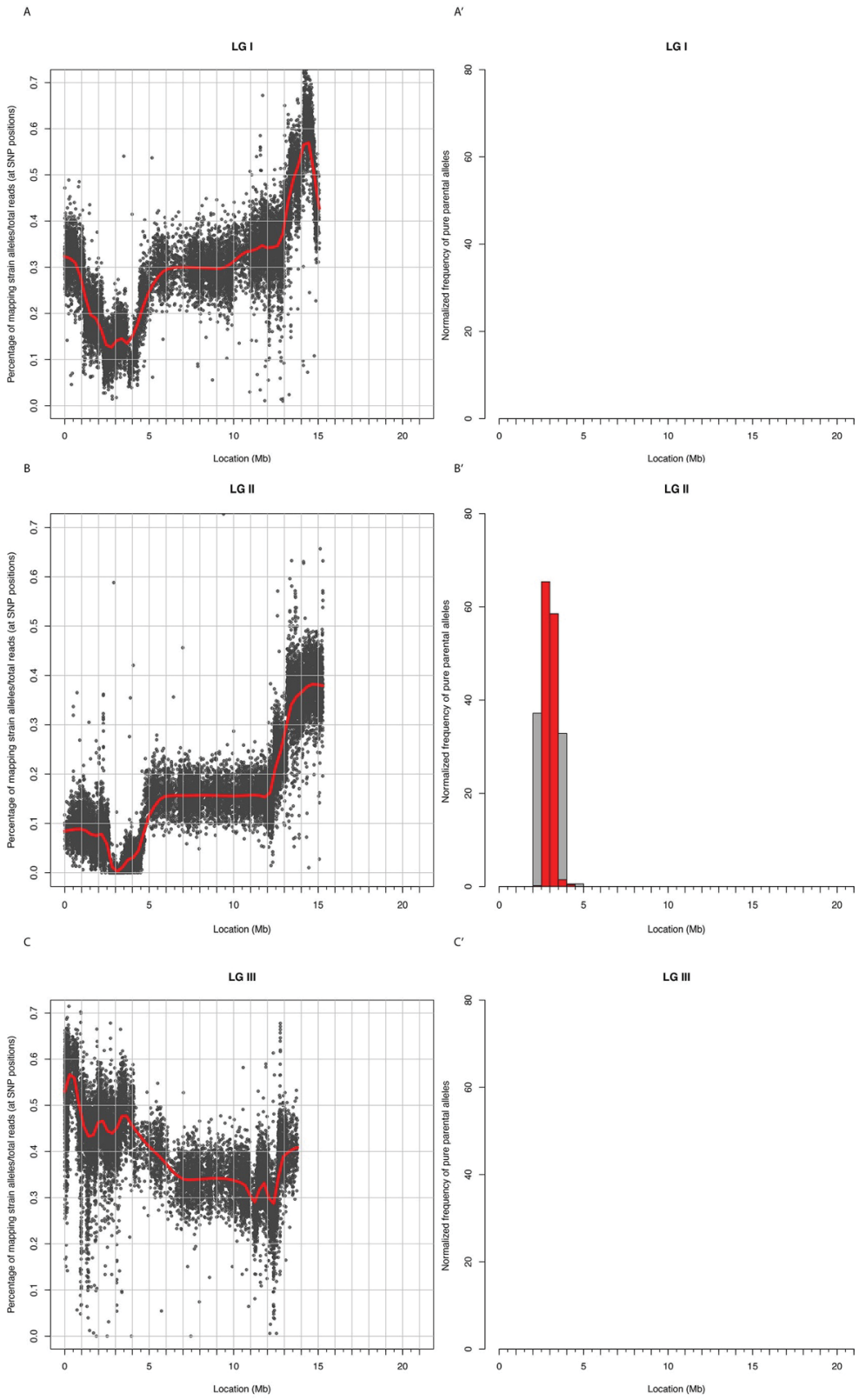
A
LG I
Percentage of mapping strain alleles/total reads (at SNP positions)
Location (Mb)
A′
LG I
Normalized frequency of pure parental alleles
Location (Mb)
B
LG II
Percentage of mapping strain alleles/total reads (at SNP positions)
Location (Mb)
B′
LG II
Normalized frequency of pure parental alleles
Location (Mb)
C
LG III
Percentage of mapping strain alleles/total reads (at SNP positions)
Location (Mb)
C′
LG III
Normalized frequency of pure parental alleles
Location (Mb)

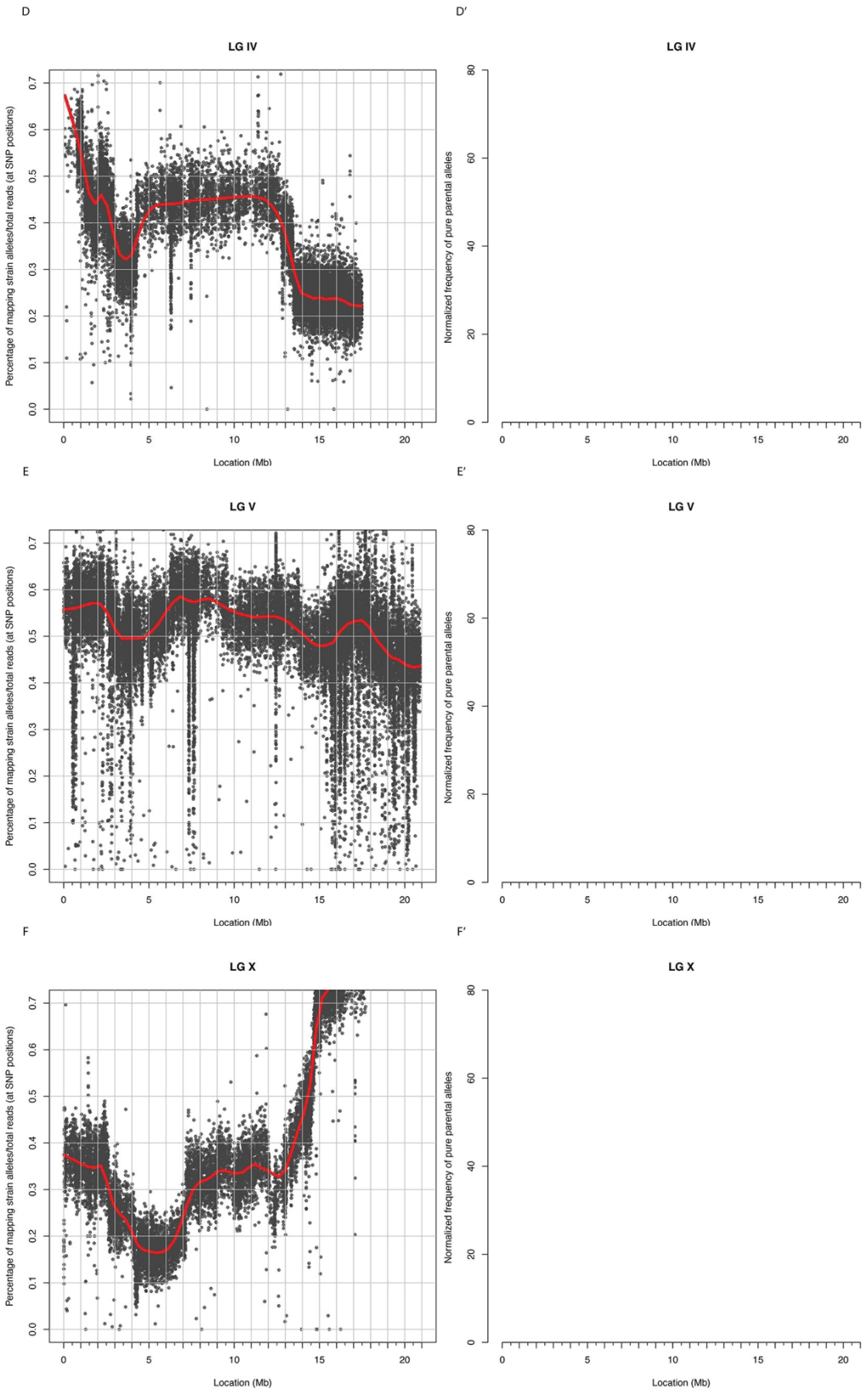
D
LG IV
Percentage of mapping strain alleles/total reads (at SNP positions)
Location (Mb)
D′
LG IV
Normalized frequency of pure parental alleles
Location (Mb)
E
LG V
Percentage of mapping strain alleles/total reads (at SNP positions)
Location (Mb)
E′
LG V
Normalized frequency of pure parental alleles
Location (Mb)
F
LG X
Percentage of mapping strain alleles/total reads (at SNP positions)
Location (Mb)
F′
LG X
Normalized frequency of pure parental alleles
Location (Mb)

Figure 25. The *vh45* locus is mapped to the 2-5 Mb position of Chromosome II. Scatter plots (A-F) and accompanying frequency graphs (A'-F') were compiled by CloudMap for *C. elegans* Chromosomes I-V and X. (A-F) Each data point is a ratio of Hawaiian SNPs/number of total runs (*y*-axis) that is plotted to a genomic position (*x*-axis). Values were normalized to remove false linkage and to improve mapping signal (Minevich et al., 2012). Genomic positions are measured in Mb. A red LOESS regression line is incorporated into each scatter plot to better visualize trend patterns. (A'-F') Regions on scatter plots with no Hawaiian SNPs have peaks of Bristol SNPs indicated on accompanying frequency graphs. Frequency bars are presented in bins of 1 Mb (gray) and 0.5 Mb (red).

Figure 26

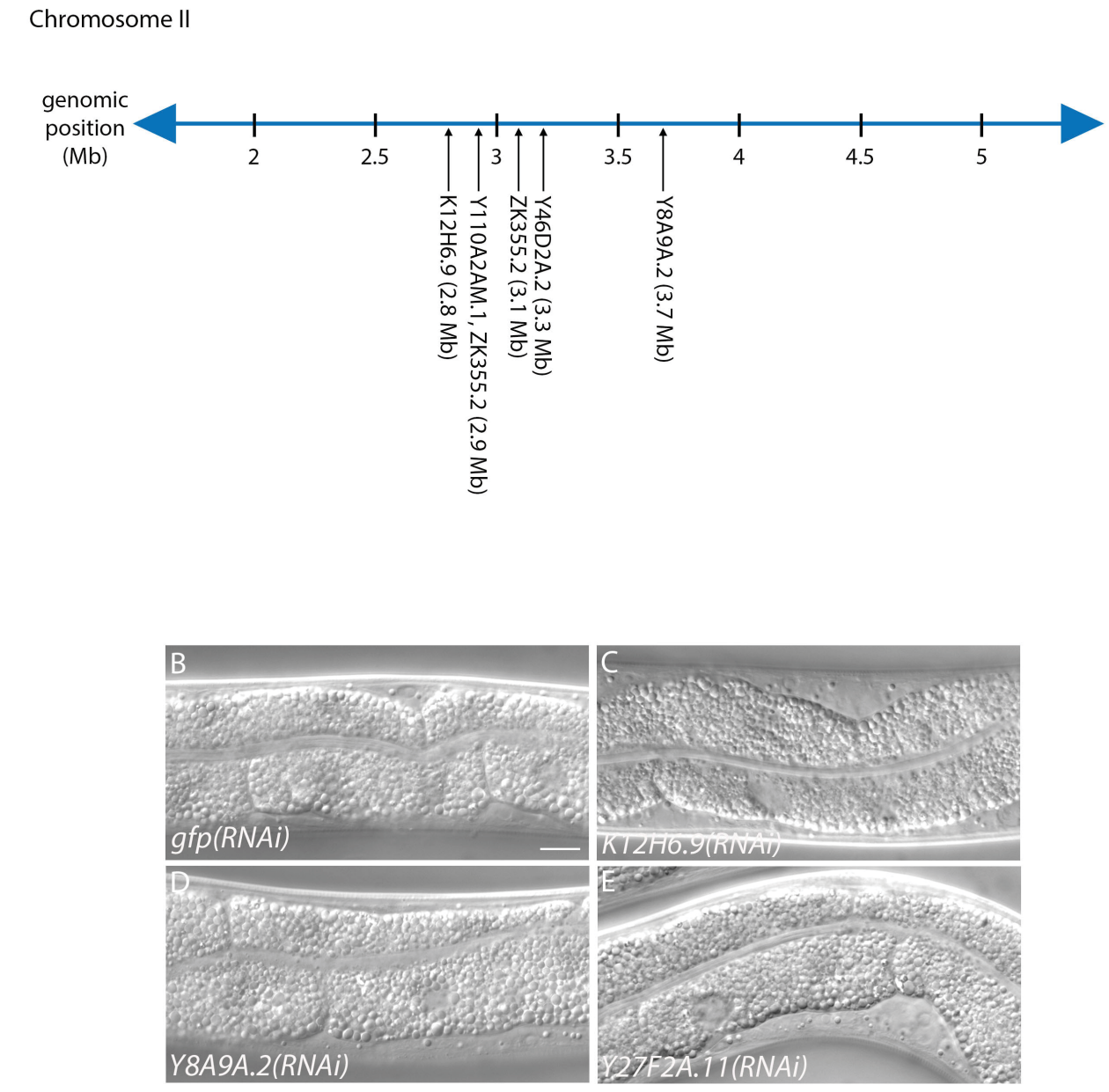
A
Chromosome II
genomic position (Mb)
2
2.5
3
3.5
4
4.5
5
K12H6.9 (2.8 Mb)
Y110A2AM.1, ZK355.2 (2.9 Mb)
ZK355.2 (3.1 Mb)
Y46D2A.2 (3.3 Mb)
Y8A9A.2 (3.7 Mb)
B
gfp(RNAi)
C
K12H6.9(RNAi)
D
Y8A9A.2(RNAi)
E
Y27F2A.11(RNAi)

Figure 26. No *vh45* phenotype is detected from RNAi knockdown to *K12H6.9*, *Y8A9A.2* or *Y27F2A.11*. (A) Schematic diagram of where the six *vh45* candidates are situated on Chromosome II. The blue axis represents the length of Chromosome II. Diagram is not to scale. (B-E) Representative images of L4 stage wildtype worms upon RNAi knockdown to *gfp* (control) (B), *K12H6.9* (C), *Y8A9A.2* (D) and *Y27F2A.11* (E). Bar: (A) 10 μm.

Table 3. The *vh45* phenotype arises from mutation at a single locus.

***vh45*/+ mother**	**Progenies**		
	Large vesicles (*vh45* homozygotes)	**Less severe or normal vesicles (*vh45*/+ or wildtype)**	**Total individuals**
1	63 (**19.3%**)	264 (80.7%)	327
2	56 (**19.6%**)	229 (80.4%)	285
Total	119 (**19.4%**)	493 (80.6%)	612

Table 4. *vh45* candidates with mutations at coding regions.

Gene	Genomic location on Chromosome II	Comments
K12H6.9	2.8 Mb	• Non-synonymous mutation, nucleotide G→A (A120T, 3rd exon) • No predictable domain or motifs (SMART) • No human homologs (NCBI BLASTp) • No protein domains (SMART)
Y110A2AM.1	2.9 Mb	• Deletion causing frameshift • Uncharacterized, no recorded phenotypes • No human homologs (NCBI BLASTp) • Contains a central coiled-coil domain (SMART)
ZK355.2	2.9 Mb	• Splice site acceptor mutation, nucleotide G→A • Uncharacterized, no recorded phenotypes • Enriched in intestine, body wall muscles (Wormbase.org) • No significant human homologs found from NCBI BLASTp* • 7 TM domains, putative serpentine receptor (SMART)
Y27F2A.11	3.1 Mb	• Non-synonymous, nucleotide G→A (G123R, 2nd exon) • No recorded phenotypes • Involved in body morphogenesis, embryo development, locomotion and nematode larval development (Wormbase.org) • No human homologs (NCBI BLASTp) • 7 TM domains, putative serpentine receptor (SMART)
Y46D2A.2	3.3 Mb	• Insertion causing frame shift • Uncharacterized, no recorded phenotypes • Enriched in the intestine (Wormbase.org) • No significant human homologs found from NCBI BLASTp* • No protein domains (SMART)
Y8A9A.2	3.7 Mb	• Insertion causing frameshift (at 3796675) • Non-synonymous, nucleotide A→T (N311I), T→C (L390P), T→C (L399P), C→T(P414L) • Closest human homolog is hemicentin (24% identity, 57% cover, accession number EAW91198, NCBI BLASTp) • Contains 4 thrombospondin type 1 domains

		(SMART)

*insufficient coverage is <15% identity

Chapter 6. Discussion

6.0 Discussion

Rab5 to Rab7 conversion represents an important step in endocytic trafficking for cargo degradation. Rab5 inactivation begins with the displacement of Rabaptin-5-Rabex5 by the Rab7 GEF Mon1/SAND-1-Ccz1 (Poteryaev et al., 2010) to stop the positive feedback of Rab5 activation. Then, a Rab5 GAP promotes the hydrolysis of the GTP bound to Rab5. This step promptly deactivates Rab5 and prevents it from re-establishing its positive feedback loop. Thus, Rab5 GAPs are important components for the regulation of Rab5 activity and for endosome maturation.

This thesis investigated mechanisms by which TBC-2, a *C. elegans* Rab5 GAP, is spatiotemporally targeted onto endosomal membranes. From structure-function analysis of TBC-2 transgenes, the ability for TBC-2 to localize onto membranes was determined on whether there was *tbc-2(tm2241)* phenotypic rescue; this is based on the premise that TBC-2 must be physically close to its cognate Rab for GAP function. Therefore, as exemplified by *tbc-2(tm2241)* rescue experiments, both GFP::TBC-2::FLAG (**Figure 8 A, D**) and GFP::TBC-2(ΔPH)::FLAG (**Figure 8 B, E**) retained their ability to localize onto membranes. GFP::TBC-2(ΔPH-CC)::FLAG had a cytoplasmic localization and was unable to rescue the *tbc-2(tm2241)* effect (**Figure 8 C, F**). While this fusion protein was not tested for GAP activity, a shorter version of TBC-2(ΔPH-CC) can catalyze the hydrolysis of GTP-bound RAB-5 and RAB-7 (Chotard et al., 2010a). The CC domain region is critical for TBC-2 endosome localization, which is consistent with the requirement for TBC-2 localization onto phagosomes (Li et al., 2009).

6.1 Regulatory role of the PH domain in TBC-2 localization

The loss of the PH domain or PH-CC segment have separate effects on TBC-2 localization, suggesting that the PH domain and the CC domain region play different functions. It also provides evidence that TBC-2 uses coincidence detection to target maturing endosomes in a spatiotemporal manner. While the CC domain region plays a critical role in this process (**Figure 8 L-M, Figure 20**), the PH domain is proposed to restrict membrane localization of TBC-2. This is demonstrated from the strong overlap observed between GFP::TBC-2(ΔPH)::FLAG and the LE marker RAB-7 (**Figure 8 L, M, Figure 20**). The PH domain likely prevents TBC-2 from membrane binding once the endosome has matured and PI3P/PI4P has turned over.

In another instance, strong colocalization has been found between the catalytically inactive TBC-2(R689K) and RAB-7 (Chotard et al., 2010a). However, this colocalization likely arises not from a loss of PH domain, but from the inability of TBC-2(R689K) to supply the catalytic arginine for GAP function (Pan et al., 2006; Tempel et al., 2008). As a result, the protein is likely locked in its transition state with a GTP-bound RAB-5. TBC-2 (R689K) can only dissociate from the membrane when Rab5 undergoes intrinsic GTP hydrolysis.

6.1.1 The PH domain binds to PI3P and PI4P

From *in vitro* assays, we showed that the TBC-2 PH domain binds to PI3P and PI4P (**Figure 15**). The PH domain of the TBC-2 human homolog Armus also binds to the same lipids (Jaber et al., 2016). While TBC-2 binding to PI3P is consistent with its GAP function for RAB-5 during the EE to LE transition (Chotard et al., 2010a; Gillooly et al., 2000), its binding to PI4P—

a PI that localizes on the sorting tubules of EEs (Henmi et al., 2016)—might reflect TBC-2 targeting to RAB-5 at regions where recycling vesicles bud off (Chen et al., 2006; Delevoye et al., 2014; Jovic et al., 2010; Sonnichsen et al., 2000). It would be interesting to find if PI4P cooperates with recycling proteins CED-10, RAB-10 and AMPH-1 for TBC-2 recruitment onto REs (Liu and Grant, 2015; Sun et al., 2012; Wilson et al., 2000). If so, this would provide evidence that the PH domain facilitates TBC-2 localization in both degradative and recycling pathways.

6.2 TBC-2 binds through its CC domain region

From GFP::TBC-2(ΔPH)::FLAG and RAB-7 colocalization data (**Figure 8 L,M, Figure 20**), the CC domain region is hypothesized to target TBC-2 onto membranes by binding to a LE-associated element. To artificially target TBC-2 to RAB-7-positive vesicles, the Rab7 targeting domain of mammalian RILPb was incorporated into GFP::TBC-2(ΔPH-CC)::FLAG and expressed in *tbc-2(tm2241)* worms. Unfortunately, this fusion protein not found on endosomes (**Figure 21**). This suggests that RILPb does not bind to RAB-7 and that this interaction is not evolutionary conserved (Shinde and Maddika, 2016; Wu et al., 2005). Alternative Rab7 binding domains from mammalian effectors can be used in future experiments to target GFP::TBC-2(ΔPH-CC)::FLAG to LEs. Such examples are ORP1L, Rabring7 (Rab7-interacting RING finger protein), and Rubicon (RUN domain and cysteine-rich domain containing, Beclin 1-interacting protein) (Johansson et al., 2005; Mizuno et al., 2003; Tabata et al., 2010).

Despite that GFP::RILPb::TBC-2(ΔPH-CC)::FLAG did not bind to membranes, the mean vesicular diameter of *tbc-2(tm2241)* worms expressing this transgene had a small, yet

significant reduction compared to the mean diameter from mutants expressing untargeted GFP::TBC-2(ΔPH-CC)::FLAG (**Figure 21 K**). This may be explained by higher GFP::RILPb::TBC-2(ΔPH-CC)::FLAG expression from differences in extrachromosomal inheritance. Alternatively, diameters were measured from worms that incidentally possessed smaller vesicles. As a result, the values fell in the lower range of *tbc-2(tm2241)* vesicular sizes. If this is the case, a better representative mean can be obtained by scoring a greater number of animals.

6.2.1 Binding target of the CC domain region

The CC domain region encompasses both the CC domain and the intervening region between the PH and CC domains. The CC domain was not found to bind to lipids (**Figure 15**). The intervening region was not investigated for membrane binding.

From the literature, the AMPH-1-RAB-10 complex recruits TBC-2 by binding onto both its CC domain and the intervening region (Liu and Grant, 2015). Another protein, CED-10, may recruit TBC-2 (Sun et al., 2012) in a manner that is similar to how its human homolog Rac1 binds to the CC domain of Armus (Frasa et al., 2010). It is unknown if the AMPH-1-RAB-10 complex and CED-10 act redundantly to recruit TBC-2: loss-of-function to any of the three proteins has not been reported to produce an enlarged vesicular phenotype in the intestine (Liu and Grant, 2015; Sun et al., 2012). If the binding partner for CC domain region is identified for TBC-2 endosome localization in future experiments, it would be interesting to find if its loss of function is sufficient to produce a *tbc-2(tm2241)* effect.

A possible interacting partner to the CC domain region is the Class III PI3K. This prediction is consistent with a reduced GFP::TBC-2(ΔPH)::FLAG membrane association observed from *vps-34(RNAi)* or loss-of-function *bec-1(ok691)* (**Figure 18 G-L, Figure 19 G-L**). Additionally, human Armus requires Vps34 for its LE targeting (Jaber et al., 2016; Stein et al., 2003). If the CC domain region binds to VPS-34 rather than to PI3P, GFP::TBC-2(ΔPH)::FLAG should remain on endosomal membranes despite overexpression of MTM-1. Further experiments can explore if the interaction is direct or indirect.

Novel binding partners to the CC domain region can be identified through BioID (proximity-dependent biotin identification) (Kim et al., 2016; Roux et al., 2012). This method labels neighbours of close proximity to a protein of interest by using a bacterial biotin ligase called BirA (Kim et al., 2016; Roux et al., 2012). Biotinylated targets are then isolated and identified through mass spectrometry. In mammals, biotinylation is a rare modification with few known targets, thus making BioID an excellent tool for mammalian systems (Roux et al., 2012). To study TBC-2 binding, worm homologs of those interacting partners identified from mammalian TBC1D2A/B can be used. Potential binding partners may be regulatory cytosolic proteins (**Figure 27 A**) or the *vh45* causative gene product (mentioned later in this discussion). These novel partners can provide exciting directions in examining how TBC-2 and its homologs are recruited or regulated.

6.3 PI3P is a positive regulator of endosome maturation

In a three-pronged strategy, PI3P facilitates Rab5 to Rab7 conversion by promoting the recruitment of (1) RAB-7 GEF Mon1/SAND-1-CCZ-1 (Cabrera et al., 2014; Lawrence et al.,

2014; Poteryaev et al., 2010), (2) TBC-2 (this thesis), and (3) the PI3P kinase pikFYVE for PI3P turnover and LE membrane identity (Dove et al., 2009; Nicot et al., 2006; Sbrissa et al., 2002).

6.3.1 The Class III PI3K and TBC-2 localization

vps-34(RNAi) or loss-of-function *bec-1(ok691)* reduced TBC-2 recruitment onto endosomes and resulted in a *tbc-2(tm2241)*-like vesicular morphology (**Figure 18, Figure 19**). This finding is consistent with the effects observed in mammalian cells: upon Vps34 silencing, vacuoles became enlarged and had a loss of Armus localization (Jaber et al., 2016). These cells also had elevated levels of the Armus GAP target, GTP-bound Rab7 (Jaber et al., 2016).

To provide greater evidence that TBC-2 requires the Class III PI3K for localization, differences in elevated levels of GTP-bound RAB-5 and/or RAB-7 can be compared. This can be done by fractionating wildtype and *vps-34(RNAi)* worm lysates into membrane-bound or cytosolic portions. Another method is to use GST Rab effector pulldown assays. GTP-bound RAB-5 can be captured using EEA-1. On the other hand, no *C. elegans* RAB-7 effectors have been identified; however, several characterized mammalian effectors (mentioned earlier) may be sufficient for this purpose.

In this thesis, the Class III PI3K subunits (*vps-34*, *vps-15* and *bec-1*) were targeted for study; however, disrupting the function of this lipid kinase also affects processes in autophagy and phagocytosis. While *vps-34(RNAi)* enlarged vesicles were not positive for the autophagic marker LGG-1 (LC3, GABARAP, and GATE-16-1; data not shown), specific targeting of the endocytic Class III PI3K complex may be considered for future experiments. Two conserved

BEC-1 binding factors called SORF (suppressor of organelle fusion)-1 and SORF-2 are components of an endosome-specific Class III PI3K. Both proteins have been found to negatively regulate PI3P levels and facilitate endosome maturation (Liu et al., 2016).

Understanding how the lipase kinase activity of Class III PI3K is regulated can unveil circumstances that promote TBC-2 localization. In mammalian cells, the Class III PI3K VPS15 subunit interacts with GTP-bound Rab5 (Christoforidis et al., 1999b; Murray et al., 2002), GDP-bound Rab7 (Backer, 2008; Cao et al., 2007a; Stein et al., 2003) and MTM1 (Cao et al., 2007a) in mutually exclusive complexes (Cao et al., 2007a). A member of the myotubularin-related family, MTMR2, localizes primarily onto LEs and also interacts with VPS15 (Cao et al., 2008).

Distinct VPS15-VPS34 complexes suggest a stepwise system to regulate the enzymatic activity of VPS34 and therefore, PI3P production (Cao et al., 2008; Murray et al., 2002; Stein et al., 2003; Sun et al., 2010). In *C. elegans*, spatiotemporal control of PI3P levels is essential for phagosome maturation. Two peaks of PI3P are produced by the concerted actions of Class II PI3K PIKI-1, Class III PI3K VPS-34 and phosphatase MTM-1 (Fratti et al., 2001; Gillooly et al., 2001; Lu et al., 2012; Wirawan et al., 2012). Loss-of-function *piki-1* reduces RAB-5 association on phagosome membranes (which likely inhibits TBC-2 recruitment (Li et al., 2009)) and leads to an accumulation of phagocytosed cargo (Lu et al., 2012). Cycles of PI3P levels have also been observed on mammalian phagosomes. Phagosomes containing the bacteria *Mycobacterium tuberculosis* do not exhibit the second PI3P peak or have associated Rab7 (Via et al., 1997). These effects are linked to the strategy used by *M. tuberculosis* to disrupt phagosome maturation for its survival in the cell (Chua and Deretic, 2004; Fratti et al., 2003; Vergne et al., 2004).

No studies have yet investigated if PI3P is spatiotemporally regulated on endosomes. If it

is, identifying when RAB-5, RAB-7, RAB-7 GEF and TBC-2 arrive at the endosomal membrane during changes in PI3P levels will enhance our understanding on the coordination of their recruitments during Rab conversion.

6.4 Working model for TBC-2 localization

From the findings presented in this thesis, a coincidence detection model for TBC-2 endosome localization is proposed. Our results suggest that the PH domain first interacts with PI3P/PI4P to release its inhibitory effect on the CC domain region. Inhibition of the CC domain region may occur through one of two ways: obstruction by a cytosolic factor (**Figure 27 A**) or sequestration by an intramolecular interaction (**Figure 27 B**). Once the CC domain region is liberated, it can bind to its LE-associated element. Simultaneous binding by both the PH domain and the CC domain region specifies TBC-2 localization to maturing endosomes (**Figure 27 C**).

Function of the THR domain was not sufficiently explored in this thesis; however, worms expressing a *tbc-2* allele that contains a missense mutation within the THR domain exhibit a weak *tbc-2(tm2241)*-like phenotype (**Figure 9 D**). This mutation is predicted to disrupt the helical structure within the THR domain (**Figure 10**), although it may also affect global TBC-2 misfolding. Further work is needed to determine if the phenotype arises from aberrant TBC-2 localization or its GAP function.

6.4.1 Intramolecular feature of TBC-2 regulation

An intramolecular role of the PH domain offers an elegant and minimalistic strategy for TBC-2 autoinhibition. This regulatory feature can be tested through several approaches. The open conformation of GFP::TBC-2(ΔPH)::FLAG should be able to bind to free PH domains; therefore, worms co-expressing GFP::TBC-2(ΔPH)::FLAG and an isolated PH domain would have reduced GFP::TBC-2(ΔPH)::FLAG membrane localization. To show that TBC-2 has open and closed conformations, a BRET (bioluminescence resonance energy transfer)-based biosensor assay can be used (Lima-Fernandes et al., 2014; Pfleger et al., 2006; Sleno et al., 2016). In such an experiment, the donor moiety is attached at the N-terminus (i.e. PH domain), while the acceptor moiety is attached at the C-terminus. Difference in BRET signal can be compared between TBC-2(ΔPH) and full length TBC-2. Alternatively, BRET can be used to find where the PH domain binds on TBC-2: on full length TBC-2, an acceptor moiety at the C-terminus is positioned progressively towards the amino end of the protein in a series of walks. The position of the acceptor moiety that yields the greatest amount of energy transfer signal would indicate the region where the PH domain binds (Lima-Fernandes et al., 2014; Pfleger et al., 2006; Sleno et al., 2016).

TBC-2 and its homologs likely share similar mechanisms of regulation due to conservations found in their domains and organization (Bernards, 2003). For instance, the PH domain of TBC1D2A interacts with the C-terminal region of the protein, which is where the GAP domain is located (Toyofuku et al., 2015). Dissociating this interaction is probably required for Rab7 GAP activity and may involve PI3P/PI4P binding by the PH domain (Jaber et al., 2016).

Releasing intramolecular interactions by PI binding is a regulatory feature that has been documented in other trafficking proteins. For example, the PH domain of Rho p120 GAP releases its interaction with the C-terminal GAP domain upon binding to $PI(3,4,5)P_3$ or $PI(4,5)P_2$ (Bos et al., 2007; Drugan et al., 2000; Pamonsinlapatham et al., 2009). Two Rho GEFs members, Sos (Sons of Sevenless) and Vav, possess a conserved PH domain that is believed to interact with the upstream catalytic DH (Dbl homology) domain (Zheng, 2001). This interaction dissociates upon PH domain binding to $PI(3,4,5)P_3$ (Han et al., 1998; Nimnual et al., 1998).

6.5 Other future experiments

Several more experiments are presented in this section to further explore and/or confirm the mechanisms behind the TBC-2 membrane localization model.

6.5.1 PH domain binding to PI4P

This thesis presents evidence that the PH domain binds to PI3P for TBC-2 localization on endosomal membranes; however, no work has been done to examine its binding to PI4P *in vivo*. Similar to the strategies used to reduce PI3P levels, PI4P levels can be manipulated through its kinase, the Class II PI4K α isoform (PI4KIIα) (Balla et al., 2002; Henmi et al., 2016), and phosphatase Sac2 (Nakatsu et al., 2015). Putative *C. elegans* homologs for PI4KIIα and Sac2 are encoded by *Y75B8A.24* and *W09C5.7* respectively (Wormbase.org). If changes to TBC-2 localization and/or vesicular sizes and morphologies are observed upon loss of PI4P, it suggests

that the interaction between PH domain and PI4P has physiological relevance on TBC-2 function.

6.5.2 Oligomerization of TBC-2

From the TBC-2 localization model, TBC-2 binds to membranes as a monomer. Despite this, several observations suggest the possibility for TBC-2 oligomerization. From lipid binding and liposome assays, the purified, monomeric PH domain was able to bind to both PI3P and PI4P with relatively equal affinity (**Figure 15**). However, as exemplified by the dynamin PH domain, binding to multiple PIs may simply imply for weak affinity (Narayan and Lemmon, 2006): the monomeric domain had similar preferences for PI3P, $PI(3,4)P_2$, $PI(4,5)P_2$, $PI(3,5)P_2$ and $PI(3,4,5)P_3$ (Narayan and Lemmon, 2006), but its oligomerized form was clearly specific for $PI(4,5)P_2$ (Klein et al., 1998; Salim et al., 1996). Consistent with this idea, TBC-2 PH-CC had a stronger binding for PI3P in two of three lipid binding experiments (**Figure 15 A', caption**). This segment may have oligomerized through spontaneous dimerization of the GST tag (Ji et al., 1992; Klein et al., 1998) or the CC domain.

Though there is currently little evidence that TBC-2 utilizes avidity binding, determining whether oligomerization occurs is important for understanding the mechanism behind TBC-2 localization. TBC-2 contains two coiled-coil domains—the CC domain (Chotard et al., 2010a) (**Figure 14**) and the THR domain (**Figure 11**)—through which oligomerization may occur. To investigate if TBC-2 assembles into dimers or higher-ordered oligomers, lysates from wildtype worms can be run on native gels to detect for the presence of higher-weighted, TBC-2-labelled bands. If such bands are found, the next step is to determine if artificial dimerization of the PH

domain (i.e. through a disulfide bond) will lead to a preference for PI3P or PI4P binding (Klein et al., 1998; Wang et al., 2011).

6.5.3 Posttranslational effects on TBC-2 membrane targeting

We did not test for effects of posttranslational modifications on TBC-2 localization. Phosphorylation, for instance, has been shown to regulate catalytic activity (Bernards and Settleman, 2004; Bos et al., 2007) and/or localization (Sordella et al., 2003) of GAP proteins. The LRRK1 kinase, a regulator of TBC1D2A, may phosphorylate TBC1D2A in order to dissociate its intramolecular bond for GAP function (Toyofuku et al., 2015). To test if TBC-2 is phosphorylated for its localization, residues identified as potential phosphorylation targets can be replaced with phosphomimetics through site-directed mutagenesis. The modified transgene can then be expressed in *tbc-2(tm2241)* mutant worms for observation.

6.6 The *vh45* mutation does not affect the *tbc-2* locus

Similarities in vesicular size, globular cargo and RAB-7 identity shared between *tbc-2(tm2241)* and *vh45* phenotypes suggest that *vh45* is a potential regulator of TBC-2 function in the intestines **(Figure 22)**. From a complementation test, the *vh45* mutation was not found to occur at the *tbc-2* locus (**Figure 23 E, F**). While this experiment may have provided a false negative result from intragenic complementation—an event where two mutated alleles of the same gene are able to complement each other (Yook, 2005)—the WGS-SNP mapping data confirms this finding.

6.6.1 Screening for the *vh45* affected gene

Six genes from Chromosome II (**Figure 25**) containing non-synonymous, frameshift and/or splice site mutations within their protein-coding regions were chosen as *vh45* candidates (**Table 4**). Three of these candidates—*Y27F2A.11*, *K12H6.9* and *Y8A9A.2*—were screened via RNAi in wildtype worms. No *vh45* phenotype was observed from the experiments (**Figure 26 B-E)**, suggesting that the tested genes contain benign mutations. Such mutations can originate spontaneously or from founder effect during worm maintenance (Denver et al., 2009; Sarin et al., 2010)), or perhaps from the forward genetic screen.

On the other hand, if the *vh45* mutation causes a gain-of-function or hypermorphic effect, knocking down expression of the affected gene will not reveal the phenotype: as a genetic silencing technique, RNAi is ineffective towards gain-of-function mutations, proteins with slow turnover, or proteins with functional/genetic redundancy (Boutros and Ahringer, 2008; Fraser, 2004; Jorgensen and Mango, 2002; Qu et al., 2011). At this point, no conclusions can be made on whether any of the three tested genes contain the causative mutation. Available mutants for *Y27F2A.11, K12H6.9* and *Y8A9A.2* can be used to confirm RNAi results.

Despite the limitations of RNAi, it should still be used as a powerful technique to rapidly test remaining candidates. However, if none of the candidates produces a *vh45* phenotype from either RNAi or available mutants, new candidates that carry mutations in non-coding regions (i.e. upstream and downstream regions of genes) should be considered.

6.6.2 Identifying future candidates

Identifying the *vh45* effect on gene expression or activity level of the encoded product can provide clues into how the phenotype arises. This analysis on gene function can be performed using a Chromosome II deficiency (*Df*) that spans the interval of where the *vh45* mutation is mapped (i.e. *C. elegans nDf2* [Wormbase.org]) (**Figure 25**). Assuming that the genes lost from the deficiency do not contribute to the phenotype, worms carrying *vh45* in *trans* to a deficiency (*vh45*/*Df*) are compared to homozygous *vh45* individuals for differences in phenotypic severity. If *vh45* causes an amorphic (null or loss-of-function) effect, the phenotypic severity between *vh45*/*Df* and homozygous *vh45* worms would be equal. This scenario can arise from no genetic transcription, premature degradation of a transcribed product or a non-functional translated product. If *vh45* causes a hypomorphic (partial loss-of-function) effect from reduction in either gene or protein expression, *vh45*/*Df* worms would display a more severe phenotype than *vh45* homozygous worms. Considering that enlarged vesicles were occasionally found in *vh45*/+ worms (**Figure 23 B**), it suggests that the *vh45* allele can compete with its wildtype form. For this reason, dominant gain-of-function scenarios, such as hypermorphic or neomorphic effects, should also be considered.

When a gene is identified to produce the *vh45* phenotype, results can be confirmed via transgenic rescue experiments. Additionally, available alleles of the gene would likely exhibit similar phenotypes to *vh45* and can be used as further validation. These alleles can also be ordered according to their phenotypic severity (i.e. in an allelic series) to extrapolate the consequence of the null phenotype should the *vh45* mutation only produce a hypomorphic effect. Finally, novel alleles of the identified gene can be constructed and engineered into the *C. elegans*

genome for future experimental manipulations. This may be done by a genome-targeting technique called the CRISPR (clustered regularly interspaced short palindromic repeats)-Cas9 system (Dickinson and Goldstein, 2016; Hsu et al., 2014; Paix et al., 2015).

6.6.3 Relationship between *tbc-2* and the *vh45* causative gene

The effect of *vh45* on TBC-2 localization has not been investigated. If TBC-2 localization is altered on *vh45* enlarged endosomes, it would suggest that TBC-2 is differentially regulated in basolateral and apical trafficking (Babbey et al., 2006; Chen et al., 2006; Stoops and Caplan, 2014; Weisz and Rodriguez-Boulan, 2009; Winter et al., 2012). If TBC-2 localization can still be detected on *vh45* enlarged endosomes, perhaps its GAP function is affected. To find if RAB-5 activation is elevated in *vh45* worms, a GST Rab effector pulldown assay can be performed.

If elevated RAB-5 activation is detected, it is possible for *vh45* worms to have increased GEF activity. This can be further investigated by targeting the Rab5 GEF and effector complex Rabex-5-Rabaptin-5 (Sann et al., 2012; Sato et al., 2005) through RNAi or available mutants. If *vh45* endosomes are found to be reduced, this would provide a helpful clue in narrowing the *vh45* candidate search.

Alternatively, the *vh45* causative gene may be regulated by TBC-2 and act downstream to it. To investigate their functional order, epistasis—a phenomenon in genetic interaction whereby one gene masks the phenotype of another (Huang and Sternberg, 2006; Wang and Sherwood, 2011)—can be used. Assuming that *tbc-2(tm2241)* and *vh45* have no functional contributions (i.e. both are null alleles) and that both function in a linear pathway, *vh45;tbc-2(tm2241)* worms

would either have a *tbc-2(tm2241)* phenotype or a *vh45* phenotype. In the former situation, *tbc-2* would function downstream to (is epistatic to) *vh45,* whereas in the latter situation, *vh45* would function downstream to *tbc-2*. If a more severe phenotype (synthetic phenotype) is detected in double mutant worms that is not found from either *tbc-2* or *vh45* mutants, it suggests that the two genes interact or function redundantly in parallel pathways.

6.7 Prospective roles of *vh45* candidates in endocytosis

Of the six *vh45* candidate genes, only three encode for products containing unique domains and/or features from which function may be inferred (**Table 5**). Y27F2A.11 and ZK355.2 contain seven transmembrane domains and are putative GPCRs (G-protein coupled receptors). Y8A9A.2 contains four thrombospondin repeats, which are commonly found in metalloproteases (Ghai et al., 2012).

6.7.1 GPCRs in endocytic trafficking

GPCRs have been shown to regulate PI3K activity. While studies have reported their roles in Class I and II PI3K membrane recruitment and/or activation (Thorpe et al., 2015; Vanhaesebroeck et al., 2010), there is little evidence for GPCR function towards the Class III PI3K. One of the few examples demonstrating this relationship is in the yeast pheromone signalling pathway, where the GPCR Ste2 directly binds to Vps34 for PI3P production (Slessareva et al., 2006).

In polarized mammalian cells, PI3P on EEs has been found to be differentially regulated in apical and basolateral trafficking (Tuma et al., 2001). Drawing from the function of yeast Ste2 on PI3P production, perhaps Y27F2A.11 or ZK355.2 is involved in regulating Class III PI3K in basolateral EEs. To test the validity of this hypothesis, levels of PI3P on *vh45* endosomes can be assessed *in vivo* using the PI3P reporter 2XFYVE.

6.7.2 Metalloproteases in endocytic trafficking

Y8A9A.2 has been reported to be expressed in the *C. elegans* pharynx (Ghai et al., 2012), a muscular organ responsible for the mechanical digestion of food and its transport into the intestine (Pilon and Morck, 2005). Its exact role is unknown; however, from the presence of its thrombospondin domains and its involvement in pharyngeal gland development, Y8A9A.2 may have roles that are related to a family of secreted zinc metalloproteases called ADAMTS (a disintegrin and metalloproteinase with thrombospondin motifs). The ADAMTS family functions in tissue development and maintenance (Kelwick et al., 2015), and remodels the extracellular matrix (ECM) (Lu et al., 2011).

There is emerging evidence that ADAMTS members are involved in intracellular trafficking. Loss of function to human ADAMTS9 or to the *C. elegans* homolog GON-1 (abnormal gonad development-1) affects ER morphology and ER-to-Golgi trafficking in protein secretion (Yoshina et al., 2012). Mammalian ADAMTS7 and ADAMTS12 interact with progranulin, a secreted glycoprotein that is implicated in tissue repair, tumour growth, and immunological responses (Cenik et al., 2012; Eriksen and Mackenzie, 2008; Kollmann et al., 2013).

If *vh45* is an allele of *Y8A9A*.2, it would be interesting to understand how metalloproteases can cause an accumulation of RAB-7-positive vesicles in endocytic trafficking. The link between ADAMTS members and progranulin is an exciting topic to pursue, as progranulin is implicated in lysosome biogenesis and function (Belcastro et al., 2011; Tanaka et al., 2014; Tanaka et al., 2013). In humans, homozygous loss of function to the gene encoding progranulin leads to a fatal lysosomal storage disease called neuronal ceroid lipofuscinoses (NCL) (Smith et al., 2012). The characteristic lysosomal aggregates of proteins and lipids found in NCL patients (Ahmed et al., 2010; Carpenter et al., 1977; Jung et al., 2007; Petkau and Leavitt, 2014; Shacka, 2012) are reminiscent to the aggregates observed from *tbc-2(tm2241)* and *vh45* mutant vesicles.

Progranulin is targeted to LEs either directly from the TGN (Braulke and Bonifacino, 2009; Hu et al., 2010; Zhou et al., 2015) or indirectly from the ECM (Hu et al., 2010; Zhou et al., 2015). In *C. elegans,* progranulin is secreted from the intestine to the pseudocoelom (Kao et al., 2011), a body cavity which faces the intestinal basolateral surface (Altun, (ed.s) 2002-2016.). Perhaps Y8A9A.2 is involved in the trafficking of progranulin to lysosomes from the basolateral cell surface. In this possibility, Y8A9A.2 dysfunction may negatively interfere with cargo degradation and/or the endosome maturation program. However, despite these speculations, it is important to note that the *Y8A9A.2* allele carried by *vh45* worms contains multiple mutations (**Table 4**). As a result, the expressed protein may have altered activities.

6.8 Significance of work

The mechanisms governing trafficking proteins to their site of function are intricately regulated. From the data presented in this thesis, membrane association of *C. elegans* TBC-2 requires two binding components: the PH domain and the CC domain region. Both elements interact with separate targets, suggesting that TBC-2 relies on a coincidence detection strategy to limit its localization to endosomes undergoing the early-to-late transition. Colleagues and I revealed that TBC-2 recruitment is dependent upon the Class III PI3K and its generated PI3P.

Knowledge gained from this work has applicable relevance in human health, especially in etiologies that arise from defects in endocytic degradation. In pathogen invasion, a strategy to escape destruction in the lysosome is to disrupt the endosome maturation process. For instance, the facultative, intracellular bacteria of the genus *Salmonella* invade intestinal cells through endocytosis (Fabrega and Vila, 2013). The bacteria alter the identity of the *Salmonella*-containing vesicle (SCV) by secreting a virulence phosphatase called SopB into the cytosol. This protein maintains an elevated and prolonged level of PI3P on the SCV membrane (Hernandez et al., 2004; Marcus et al., 2001; Scott et al., 2002). The SCV later acquires Rab7 and LAMP1 and is translocated to the perinuclear region of the cell (Garcia-del Portillo et al., 1993; Harrison et al., 2004; Meresse et al., 1999; Steele-Mortimer et al., 1999). At this point, another bacterial protein called SopD2 is secreted to suppress effectors from further binding to the GTP-bound Rab7. This action arrests the SCV at the late maturation stage and prevents it fusing with the lysosome (D'Costa et al., 2015).

Tuberous sclerosis complex (TSC) is a disease characterized by tumorous growth on multiple organs (Bernards and Settleman, 2004; Roach and Sparagana, 2004). It occurs from defects to a bipartite GAP, which is reported to have high activity towards GTP-bound Rab5

(Xiao et al., 1997). Another disease, called Charcot-Marie-Tooth, is characterized by muscle weakness and atrophy. The 2B subtype occurs from mutations that give rise to a Rab7 that is predominantly in its GTP-bound form (Cogli et al., 2009). The 4B subtype arises from defects in PI3P production or its turnover (Berger et al., 2002; Kim et al., 2002). Finally, LRRK1, which regulates TBC1D2A GAP function, is a paralog of LRRK2 (Toyofuku et al., 2015). Mutant forms of LRRK2 are often found to give rise to an inherited form of Parkinson's disease (Di Fonzo et al., 2006; Mata et al., 2006).

Figure 27

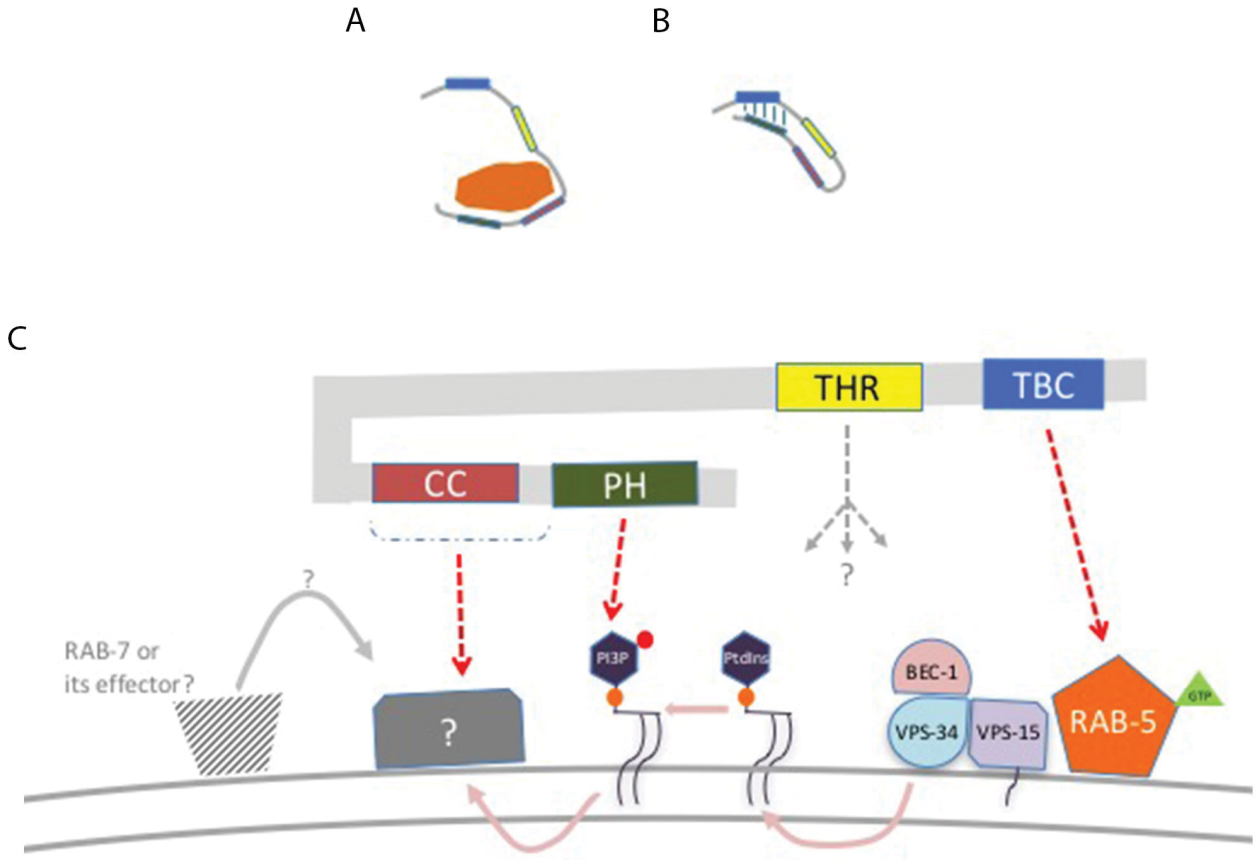
A
B
C
THR
TBC
CC
PH
?
RAB-7 or
its effector?
?
PI3P
PtdIns
BEC-1
VPS-34
VPS-15
RAB-5
GTP

Figure 27. Model of TBC-2 localization. In the cytoplasm, the CC domain region is blocked from binding to its LE-associated target through either a cytosolic, regulatory protein (orange) (A) or a conformational change involving the PH domain (B). The hatched portion in (B) symbolizes regions of where an intramolecular interaction may occur. In either situation, inhibition of the CC domain region can only be lifted when PH domain interacts with PI3P/PI4P. (C) TBC-2 utilizes both domain components to localize onto endosomes undergoing RAB-5 to RAB-7 conversion. For simplicity, only PI3P is shown. The CC domain region is believed to bind to a LE-associated target, which may be recruited by RAB-7 or through its effector. Red arrows with dotted lines denote interactions reported in this thesis and from the literature. Grey arrows with dotted lines denote unknown binding and/or function.

References

Adams, J.C., and R.P. Tucker. 2000. The thrombospondin type 1 repeat (TSR) superfamily: diverse proteins with related roles in neuronal development. *Dev Dyn*. 218:280-299.

Adams, M.D., S.E. Celniker, R.A. Holt, C.A. Evans, J.D. Gocayne, P.G. Amanatides, S.E. Scherer, P.W. Li, R.A. Hoskins, R.F. Galle, R.A. George, S.E. Lewis, S. Richards, M. Ashburner, S.N. Henderson, G.G. Sutton, J.R. Wortman, M.D. Yandell, Q. Zhang, L.X. Chen, R.C. Brandon, Y.H. Rogers, R.G. Blazej, M. Champe, B.D. Pfeiffer, K.H. Wan, C. Doyle, E.G. Baxter, G. Helt, C.R. Nelson, G.L. Gabor, J.F. Abril, A. Agbayani, H.J. An, C. Andrews-Pfannkoch, D. Baldwin, R.M. Ballew, A. Basu, J. Baxendale, L. Bayraktaroglu, E.M. Beasley, K.Y. Beeson, P.V. Benos, B.P. Berman, D. Bhandari, S. Bolshakov, D. Borkova, M.R. Botchan, J. Bouck, P. Brokstein, P. Brottier, K.C. Burtis, D.A. Busam, H. Butler, E. Cadieu, A. Center, I. Chandra, J.M. Cherry, S. Cawley, C. Dahlke, L.B. Davenport, P. Davies, B. de Pablos, A. Delcher, Z. Deng, A.D. Mays, I. Dew, S.M. Dietz, K. Dodson, L.E. Doup, M. Downes, S. Dugan-Rocha, B.C. Dunkov, P. Dunn, K.J. Durbin, C.C. Evangelista, C. Ferraz, S. Ferriera, W. Fleischmann, C. Fosler, A.E. Gabrielian, N.S. Garg, W.M. Gelbart, K. Glasser, A. Glodek, F. Gong, J.H. Gorrell, Z. Gu, P. Guan, M. Harris, N.L. Harris, D. Harvey, T.J. Heiman, J.R. Hernandez, J. Houck, D. Hostin, K.A. Houston, T.J. Howland, M.H. Wei, C. Ibegwam, et al. 2000. The genome sequence of Drosophila melanogaster. *Science*. 287:2185-2195.

Ahmed, Z., H. Sheng, Y.F. Xu, W.L. Lin, A.E. Innes, J. Gass, X. Yu, C.A. Wuertzer, H. Hou, S. Chiba, K. Yamanouchi, M. Leissring, L. Petrucelli, M. Nishihara, M.L. Hutton, E. McGowan, D.W. Dickson, and J. Lewis. 2010. Accelerated lipofuscinosis and ubiquitination in granulin knockout mice suggest a role for progranulin in successful aging. *Am J Pathol*. 177:311-324.

Albert, S., E. Will, and D. Gallwitz. 1999. Identification of the catalytic domains and their functionally critical arginine residues of two yeast GTPase-activating proteins specific for Ypt/Rab transport GTPases. *The EMBO journal*. 18:5216-5225.

Albertson, D.G., and J.N. Thomson. 1976. The pharynx of Caenorhabditis elegans. *Philos Trans R Soc Lond B Biol Sci*. 275:299-325.

Ali, B.R., C. Wasmeier, L. Lamoreux, M. Strom, and M.C. Seabra. 2004. Multiple regions contribute to membrane targeting of Rab GTPases. *Journal of cell science*. 117:6401-6412.

Altun, Z.F., Herndon, L.A., Wolkow, C.A., Crocker, C., Lints, R. and Hall, D.H. (ed.s) 2002-2016. . WormAtlas.

Aluru, S. 2006. Handbook of computational molecular biology. Chapman & Hall/CRC, Boca Raton, FL. ca. 965 p. in various pagings pp.

An, Y., Y. Shao, C. Alory, J. Matteson, T. Sakisaka, W. Chen, R.A. Gibbs, I.A. Wilson, and W.E. Balch. 2003. Geranylgeranyl switching regulates GDI-Rab GTPase recycling. *Structure*. 11:347-357.

Andres, D.A., M.C. Seabra, M.S. Brown, S.A. Armstrong, T.E. Smeland, F.P. Cremers, and J.L. Goldstein. 1993. cDNA cloning of component A of Rab geranylgeranyl transferase and demonstration of its role as a Rab escort protein. *Cell*. 73:1091-1099.

Avinoam, O., M. Schorb, C.J. Beese, J.A. Briggs, and M. Kaksonen. 2015. ENDOCYTOSIS. Endocytic sites mature by continuous bending and remodeling of the clathrin coat. *Science*. 348:1369-1372.

Babbey, C.M., N. Ahktar, E. Wang, C.C. Chen, B.D. Grant, and K.W. Dunn. 2006. Rab10 regulates membrane transport through early endosomes of polarized Madin-Darby canine kidney cells. *Molecular biology of the cell*. 17:3156-3175.

Backer, J.M. 2008. The regulation and function of Class III PI3Ks: novel roles for Vps34. *The Biochemical journal*. 410:1-17.

Balderhaar, H.J., and C. Ungermann. 2013. CORVET and HOPS tethering complexes - coordinators of endosome and lysosome fusion. *Journal of cell science*. 126:1307-1316.

Balla, A., G. Tuymetova, M. Barshishat, M. Geiszt, and T. Balla. 2002. Characterization of type II phosphatidylinositol 4-kinase isoforms reveals association of the enzymes with endosomal vesicular compartments. *The Journal of biological chemistry*. 277:20041-20050.

Barr, F., and D.G. Lambright. 2010. Rab GEFs and GAPs. *Current opinion in cell biology*. 22:461-470.

Barrowman, J., D. Bhandari, K. Reinisch, and S. Ferro-Novick. 2010. TRAPP complexes in membrane traffic: convergence through a common Rab. *Nature reviews. Molecular cell biology*. 11:759-763.

Behrends, C., M.E. Sowa, S.P. Gygi, and J.W. Harper. 2010. Network organization of the human autophagy system. *Nature*. 466:68-76.

Belcastro, V., V. Siciliano, F. Gregoretti, P. Mithbaokar, G. Dharmalingam, S. Berlingieri, F. Iorio, G. Oliva, R. Polishchuck, N. Brunetti-Pierri, and D. di Bernardo. 2011. Transcriptional gene network inference from a massive dataset elucidates transcriptome organization and gene function. *Nucleic acids research*. 39:8677-8688.

Berg, J.M., J.L. Tymoczko, and L. Stryer. 2002. Biochemistry. W. H. Freeman and Co., New York. xxxviii, 894, 872 p. pp.

Berger, P., S. Bonneick, S. Willi, M. Wymann, and U. Suter. 2002. Loss of phosphatase activity in myotubularin-related protein 2 is associated with Charcot-Marie-Tooth disease type 4B1. *Hum Mol Genet*. 11:1569-1579.

Berkowitz, L.A., A.L. Knight, G.A. Caldwell, and K.A. Caldwell. 2008. Generation of stable transgenic C. elegans using microinjection. *J Vis Exp*.

Bernards, A. 2003. GAPs galore! A survey of putative Ras superfamily GTPase activating proteins in man and Drosophila. *Biochimica et biophysica acta*. 1603:47-82.

Bernards, A., and J. Settleman. 2004. GAP control: regulating the regulators of small GTPases. *Trends in cell biology*. 14:377-385.

Blomberg, N., E. Baraldi, M. Sattler, M. Saraste, and M. Nilges. 2000. Structure of a PH domain from the C. elegans muscle protein UNC-89 suggests a novel function. *Structure*. 8:1079-1087.

Blumer, J., J. Rey, L. Dehmelt, T. Mazel, Y.W. Wu, P. Bastiaens, R.S. Goody, and A. Itzen. 2013. RabGEFs are a major determinant for specific Rab membrane targeting. *The Journal of cell biology*. 200:287-300.

Bos, J.L., H. Rehmann, and A. Wittinghofer. 2007. GEFs and GAPs: critical elements in the control of small G proteins. *Cell*. 129:865-877.

Boutros, M., and J. Ahringer. 2008. The art and design of genetic screens: RNA interference. *Nat Rev Genet*. 9:554-566.

Boya, P., R.A. Gonzalez-Polo, N. Casares, J.L. Perfettini, P. Dessen, N. Larochette, D. Metivier, D. Meley, S. Souquere, T. Yoshimori, G. Pierron, P. Codogno, and G. Kroemer. 2005.

Inhibition of macroautophagy triggers apoptosis. *Molecular and cellular biology*. 25:1025-1040.
Braulke, T., and J.S. Bonifacino. 2009. Sorting of lysosomal proteins. *Biochimica et biophysica acta*. 1793:605-614.
Brenner, S. 1974. The genetics of Caenorhabditis elegans. *Genetics*. 77:71-94.
Bucci, C., P. Thomsen, P. Nicoziani, J. McCarthy, and B. van Deurs. 2000. Rab7: a key to lysosome biogenesis. *Molecular biology of the cell*. 11:467-480.
Budovskaya, Y.V., H. Hama, D.B. DeWald, and P.K. Herman. 2002. The C terminus of the Vps34p phosphoinositide 3-kinase is necessary and sufficient for the interaction with the Vps15p protein kinase. *The Journal of biological chemistry*. 277:287-294.
Burkhard, P., J. Stetefeld, and S.V. Strelkov. 2001. Coiled coils: a highly versatile protein folding motif. *Trends in cell biology*. 11:82-88.
Burstein, E.S., and I.G. Macara. 1992. Interactions of the ras-like protein p25rab3A with Mg2+ and guanine nucleotides. *The Biochemical journal*. 282 (Pt 2):387-392.
Cabrera, M., M. Nordmann, A. Perz, D. Schmedt, A. Gerondopoulos, F. Barr, J. Piehler, S. Engelbrecht-Vandre, and C. Ungermann. 2014. The Mon1-Ccz1 GEF activates the Rab7 GTPase Ypt7 via a longin-fold-Rab interface and association with PI3P-positive membranes. *Journal of cell science*. 127:1043-1051.
Cabrera, M., and C. Ungermann. 2013. Guanine nucleotide exchange factors (GEFs) have a critical but not exclusive role in organelle localization of Rab GTPases. *The Journal of biological chemistry*. 288:28704-28712.
Cantalupo, G., P. Alifano, V. Roberti, C.B. Bruni, and C. Bucci. 2001. Rab-interacting lysosomal protein (RILP): the Rab7 effector required for transport to lysosomes. *The EMBO journal*. 20:683-693.
Cao, C., J.M. Backer, J. Laporte, E.J. Bedrick, and A. Wandinger-Ness. 2008. Sequential actions of myotubularin lipid phosphatases regulate endosomal PI(3)P and growth factor receptor trafficking. *Molecular biology of the cell*. 19:3334-3346.
Cao, C., J. Laporte, J.M. Backer, A. Wandinger-Ness, and M.P. Stein. 2007a. Myotubularin lipid phosphatase binds the hVPS15/hVPS34 lipid kinase complex on endosomes. *Traffic*. 8:1052-1067.
Cao, H., J. Chen, M. Awoniyi, J.R. Henley, and M.A. McNiven. 2007b. Dynamin 2 mediates fluid-phase micropinocytosis in epithelial cells. *Journal of cell science*. 120:4167-4177.
Carlton, J., M. Bujny, B.J. Peter, V.M. Oorschot, A. Rutherford, H. Mellor, J. Klumperman, H.T. McMahon, and P.J. Cullen. 2004. Sorting nexin-1 mediates tubular endosome-to-TGN transport through coincidence sensing of high- curvature membranes and 3-phosphoinositides. *Current biology : CB*. 14:1791-1800.
Carlton, J.G., and P.J. Cullen. 2005. Coincidence detection in phosphoinositide signaling. *Trends in cell biology*. 15:540-547.
Carney, D.S., B.A. Davies, and B.F. Horazdovsky. 2006. Vps9 domain-containing proteins: activators of Rab5 GTPases from yeast to neurons. *Trends in cell biology*. 16:27-35.
Carpenter, S., G. Karpati, F. Andermann, J.C. Jacob, and E. Andermann. 1977. The ultrastructural characteristics of the abnormal cytosomes in Batten-Kufs' disease. *Brain*. 100 Pt 1:137-156.
Carr, C.M., and J. Rizo. 2010. At the junction of SNARE and SM protein function. *Current opinion in cell biology*. 22:488-495.

Carroll, B., N. Mohd-Naim, F. Maximiano, M.A. Frasa, J. McCormack, M. Finelli, S.B. Thoresen, L. Perdios, R. Daigaku, R.E. Francis, C. Futter, I. Dikic, and V.M. Braga. 2013. The TBC/RabGAP Armus coordinates Rac1 and Rab7 functions during autophagy. *Developmental cell*. 25:15-28.

Cavanillas, M.L., O. Fernandez, M. Comabella, A. Alcina, M. Fedetz, G. Izquierdo, M. Lucas, M.C. Cenit, R. Arroyo, K. Vandenbroeck, I. Alloza, M. Garcia-Barcina, A. Antiguedad, L. Leyva, C.L. Gomez, J. Olascoaga, D. Otaegui, Y. Blanco, A. Saiz, X. Montalban, F. Matesanz, and E. Urcelay. 2011. Replication of top markers of a genome-wide association study in multiple sclerosis in Spain. *Genes Immun*. 12:110-115.

Cenik, B., C.F. Sephton, B. Kutluk Cenik, J. Herz, and G. Yu. 2012. Progranulin: a proteolytically processed protein at the crossroads of inflammation and neurodegeneration. *The Journal of biological chemistry*. 287:32298-32306.

Chakrabarti, P., and S. Chakrabarti. 1998. C--H...O hydrogen bond involving proline residues in alpha-helices. *Journal of molecular biology*. 284:867-873.

Chavrier, P., J.P. Gorvel, E. Stelzer, K. Simons, J. Gruenberg, and M. Zerial. 1991. Hypervariable C-terminal domain of rab proteins acts as a targeting signal. *Nature*. 353:769-772.

Chen, C.C., P.J. Schweinsberg, S. Vashist, D.P. Mareiniss, E.J. Lambie, and B.D. Grant. 2006. RAB-10 is required for endocytic recycling in the Caenorhabditis elegans intestine. *Molecular biology of the cell*. 17:1286-1297.

Chen, R.H., S. Corbalan-Garcia, and D. Bar-Sagi. 1997. The role of the PH domain in the signal-dependent membrane targeting of Sos. *The EMBO journal*. 16:1351-1359.

Cheng, Z.J., R.D. Singh, D.K. Sharma, E.L. Holicky, K. Hanada, D.L. Marks, and R.E. Pagano. 2006. Distinct mechanisms of clathrin-independent endocytosis have unique sphingolipid requirements. *Molecular biology of the cell*. 17:3197-3210.

Cherfils, J., and M. Zeghouf. 2013. Regulation of small GTPases by GEFs, GAPs, and GDIs. *Physiological reviews*. 93:269-309.

Chotard, L., A.K. Mishra, M.A. Sylvain, S. Tuck, D.G. Lambright, and C.E. Rocheleau. 2010a. TBC-2 regulates RAB-5/RAB-7-mediated endosomal trafficking in Caenorhabditis elegans. *Molecular biology of the cell*. 21:2285-2296.

Chotard, L., O. Skorobogata, M.A. Sylvain, S. Shrivastava, and C.E. Rocheleau. 2010b. TBC-2 is required for embryonic yolk protein storage and larval survival during L1 diapause in Caenorhabditis elegans. *PloS one*. 5:e15662.

Christoforidis, S., H.M. McBride, R.D. Burgoyne, and M. Zerial. 1999a. The Rab5 effector EEA1 is a core component of endosome docking. *Nature*. 397:621-625.

Christoforidis, S., M. Miaczynska, K. Ashman, M. Wilm, L. Zhao, S.C. Yip, M.D. Waterfield, J.M. Backer, and M. Zerial. 1999b. Phosphatidylinositol-3-OH kinases are Rab5 effectors. *Nature cell biology*. 1:249-252.

Chua, J., and V. Deretic. 2004. Mycobacterium tuberculosis reprograms waves of phosphatidylinositol 3-phosphate on phagosomal organelles. *The Journal of biological chemistry*. 279:36982-36992.

Clabecq, A., J.P. Henry, and F. Darchen. 2000. Biochemical characterization of Rab3-GTPase-activating protein reveals a mechanism similar to that of Ras-GAP. *The Journal of biological chemistry*. 275:31786-31791.

Clague, M.J., and O. Lorenzo. 2005. The myotubularin family of lipid phosphatases. *Traffic*. 6:1063-1069.

Cogli, L., F. Piro, and C. Bucci. 2009. Rab7 and the CMT2B disease. *Biochem Soc Trans*. 37:1027-1031.
Cole, B.J., and C. Bystroff. 2009. Alpha helical crossovers favor right-handed supersecondary structures by kinetic trapping: the phone cord effect in protein folding. *Protein Sci*. 18:1602-1608.
Conner, S.D., and S.L. Schmid. 2003. Regulated portals of entry into the cell. *Nature*. 422:37-44.
Consortium, C.e.S. 1998. Genome sequence of the nematode C. elegans: a platform for investigating biology. *Science*. 282:2012-2018.
Cooper, G.M., and R.E. Hausman. 2004. The cell : a molecular approach. ASM Press ;
Sinauer Associates, Washington, D.C.
Sunderland, Mass. xx, 713 p. pp.
Cureton, D.K., R.H. Massol, S. Saffarian, T.L. Kirchhausen, and S.P. Whelan. 2009. Vesicular stomatitis virus enters cells through vesicles incompletely coated with clathrin that depend upon actin for internalization. *PLoS pathogens*. 5:e1000394.
D'Costa, V.M., V. Braun, M. Landekic, R. Shi, A. Proteau, L. McDonald, M. Cygler, S. Grinstein, and J.H. Brumell. 2015. Salmonella Disrupts Host Endocytic Trafficking by SopD2-Mediated Inhibition of Rab7. *Cell reports*. 12:1508-1518.
De Matteis, M.A., and A. Godi. 2004. PI-loting membrane traffic. *Nature cell biology*. 6:487-492.
De Matteis, M.A., and J.S. Morrow. 2000. Spectrin tethers and mesh in the biosynthetic pathway. *Journal of cell science*. 113 (Pt 13):2331-2343.
De Matteis, M.A., C. Wilson, and G. D'Angelo. 2013. Phosphatidylinositol-4-phosphate: the Golgi and beyond. *Bioessays*. 35:612-622.
de Renzis, S., B. Sonnichsen, and M. Zerial. 2002. Divalent Rab effectors regulate the sub-compartmental organization and sorting of early endosomes. *Nature cell biology*. 4:124-133.
Del Conte-Zerial, P., L. Brusch, J.C. Rink, C. Collinet, Y. Kalaidzidis, M. Zerial, and A. Deutsch. 2008. Membrane identity and GTPase cascades regulated by toggle and cut-out switches. *Mol Syst Biol*. 4:206.
Delevoye, C., S. Miserey-Lenkei, G. Montagnac, F. Gilles-Marsens, P. Paul-Gilloteaux, F. Giordano, F. Waharte, M.S. Marks, B. Goud, and G. Raposo. 2014. Recycling endosome tubule morphogenesis from sorting endosomes requires the kinesin motor KIF13A. *Cell reports*. 6:445-454.
Denver, D.R., P.C. Dolan, L.J. Wilhelm, W. Sung, J.I. Lucas-Lledo, D.K. Howe, S.C. Lewis, K. Okamoto, W.K. Thomas, M. Lynch, and C.F. Baer. 2009. A genome-wide view of Caenorhabditis elegans base-substitution mutation processes. *Proceedings of the National Academy of Sciences of the United States of America*. 106:16310-16314.
Di Fonzo, A., C. Tassorelli, M. De Mari, H.F. Chien, J. Ferreira, C.F. Rohe, G. Riboldazzi, A. Antonini, G. Albani, A. Mauro, R. Marconi, G. Abbruzzese, L. Lopiano, E. Fincati, M. Guidi, P. Marini, F. Stocchi, M. Onofrj, V. Toni, M. Tinazzi, G. Fabbrini, P. Lamberti, N. Vanacore, G. Meco, P. Leitner, R.J. Uitti, Z.K. Wszolek, T. Gasser, E.J. Simons, G.J. Breedveld, S. Goldwurm, G. Pezzoli, C. Sampaio, E. Barbosa, E. Martignoni, B.A. Oostra, V. Bonifati, and N. Italian Parkinson's Genetics. 2006. Comprehensive analysis of the LRRK2 gene in sixty families with Parkinson's disease. *European journal of human genetics : EJHG*. 14:322-331.

Dickinson, D.J., and B. Goldstein. 2016. CRISPR-Based Methods for Caenorhabditis elegans Genome Engineering. *Genetics*. 202:885-901.
Dirac-Svejstrup, A.B., T. Sumizawa, and S.R. Pfeffer. 1997. Identification of a GDI displacement factor that releases endosomal Rab GTPases from Rab-GDI. *The EMBO journal*. 16:465-472.
Doherty, G.J., and H.T. McMahon. 2009. Mechanisms of endocytosis. *Annual review of biochemistry*. 78:857-902.
Doitsidou, M., R.J. Poole, S. Sarin, H. Bigelow, and O. Hobert. 2010. C. elegans mutant identification with a one-step whole-genome-sequencing and SNP mapping strategy. *PloS one*. 5:e15435.
Donaldson, J.G., and C.L. Jackson. 2011. ARF family G proteins and their regulators: roles in membrane transport, development and disease. *Nature reviews. Molecular cell biology*. 12:362-375.
Dove, S.K., K. Dong, T. Kobayashi, F.K. Williams, and R.H. Michell. 2009. Phosphatidylinositol 3,5-bisphosphate and Fab1p/PIKfyve underPPIn endo-lysosome function. *The Biochemical journal*. 419:1-13.
Dove, S.K., R.K. McEwen, A. Mayes, D.C. Hughes, J.D. Beggs, and R.H. Michell. 2002. Vac14 controls PtdIns(3,5)P(2) synthesis and Fab1-dependent protein trafficking to the multivesicular body. *Current biology : CB*. 12:885-893.
Drugan, J.K., K. Rogers-Graham, T. Gilmer, S. Campbell, and G.J. Clark. 2000. The Ras/p120 GTPase-activating protein (GAP) interaction is regulated by the p120 GAP pleckstrin homology domain. *The Journal of biological chemistry*. 275:35021-35027.
Echard, A., F.J. Opdam, H.J. de Leeuw, F. Jollivet, P. Savelkoul, W. Hendriks, J. Voorberg, B. Goud, and J.A. Fransen. 2000. Alternative splicing of the human Rab6A gene generates two close but functionally different isoforms. *Molecular biology of the cell*. 11:3819-3833.
Edgley, M.L., and D.L. Riddle. 2001. LG II balancer chromosomes in Caenorhabditis elegans: mT1(II;III) and the mIn1 set of dominantly and recessively marked inversions. *Mol Genet Genomics*. 266:385-395.
Eriksen, J.L., and I.R. Mackenzie. 2008. Progranulin: normal function and role in neurodegeneration. *J Neurochem*. 104:287-297.
Eskelinen, E.L., and P. Saftig. 2009. Autophagy: a lysosomal degradation pathway with a central role in health and disease. *Biochimica et biophysica acta*. 1793:664-673.
Fabrega, A., and J. Vila. 2013. Salmonella enterica serovar Typhimurium skills to succeed in the host: virulence and regulation. *Clin Microbiol Rev*. 26:308-341.
Falasca, M., and T. Maffucci. 2012. Regulation and cellular functions of class II phosphoinositide 3-kinases. *The Biochemical journal*. 443:587-601.
Farnsworth, C.C., M.C. Seabra, L.H. Ericsson, M.H. Gelb, and J.A. Glomset. 1994. Rab geranylgeranyl transferase catalyzes the geranylgeranylation of adjacent cysteines in the small GTPases Rab1A, Rab3A, and Rab5A. *Proceedings of the National Academy of Sciences of the United States of America*. 91:11963-11967.
Flannagan, R.S., V. Jaumouille, and S. Grinstein. 2012. The cell biology of phagocytosis. *Annu Rev Pathol*. 7:61-98.
Flibotte, S., M.L. Edgley, I. Chaudhry, J. Taylor, S.E. Neil, A. Rogula, R. Zapf, M. Hirst, Y. Butterfield, S.J. Jones, M.A. Marra, R.J. Barstead, and D.G. Moerman. 2010. Whole-genome profiling of mutagenesis in Caenorhabditis elegans. *Genetics*. 185:431-441.

Frasa, M.A., K.T. Koessmeier, M.R. Ahmadian, and V.M. Braga. 2012. Illuminating the functional and structural repertoire of human TBC/RABGAPs. *Nature reviews. Molecular cell biology*. 13:67-73.

Frasa, M.A., F.C. Maximiano, K. Smolarczyk, R.E. Francis, M.E. Betson, E. Lozano, J. Goldenring, M.C. Seabra, A. Rak, M.R. Ahmadian, and V.M. Braga. 2010. Armus is a Rac1 effector that inactivates Rab7 and regulates E-cadherin degradation. *Current biology : CB*. 20:198-208.

Fraser, A. 2004. Towards full employment: using RNAi to find roles for the redundant. *Oncogene*. 23:8346-8352.

Fratti, R.A., J.M. Backer, J. Gruenberg, S. Corvera, and V. Deretic. 2001. Role of phosphatidylinositol 3-kinase and Rab5 effectors in phagosomal biogenesis and mycobacterial phagosome maturation arrest. *The Journal of cell biology*. 154:631-644.

Fratti, R.A., J. Chua, I. Vergne, and V. Deretic. 2003. Mycobacterium tuberculosis glycosylated phosphatidylinositol causes phagosome maturation arrest. *Proceedings of the National Academy of Sciences of the United States of America*. 100:5437-5442.

Frick, M., N.A. Bright, K. Riento, A. Bray, C. Merrified, and B.J. Nichols. 2007. Coassembly of flotillins induces formation of membrane microdomains, membrane curvature, and vesicle budding. *Current biology : CB*. 17:1151-1156.

Fukuda, M. 2011. TBC proteins: GAPs for mammalian small GTPase Rab? *Biosci Rep*. 31:159-168.

Fukui, K., T. Sasaki, K. Imazumi, Y. Matsuura, H. Nakanishi, and Y. Takai. 1997. Isolation and characterization of a GTPase activating protein specific for the Rab3 subfamily of small G proteins. *The Journal of biological chemistry*. 272:4655-4658.

Funderburk, S.F., Q.J. Wang, and Z. Yue. 2010. The Beclin 1-VPS34 complex--at the crossroads of autophagy and beyond. *Trends in cell biology*. 20:355-362.

Futter, C.E., L.M. Collinson, J.M. Backer, and C.R. Hopkins. 2001. Human VPS34 is required for internal vesicle formation within multivesicular endosomes. *The Journal of cell biology*. 155:1251-1264.

Gabernet-Castello, C., A.J. O'Reilly, J.B. Dacks, and M.C. Field. 2013. Evolution of Tre-2/Bub2/Cdc16 (TBC) Rab GTPase-activating proteins. *Molecular biology of the cell*. 24:1574-1583.

Garcia-del Portillo, F., M.B. Zwick, K.Y. Leung, and B.B. Finlay. 1993. Salmonella induces the formation of filamentous structures containing lysosomal membrane glycoproteins in epithelial cells. *Proceedings of the National Academy of Sciences of the United States of America*. 90:10544-10548.

Gary, J.D., A.E. Wurmser, C.J. Bonangelino, L.S. Weisman, and S.D. Emr. 1998. Fab1p is essential for PtdIns(3)P 5-kinase activity and the maintenance of vacuolar size and membrane homeostasis. *The Journal of cell biology*. 143:65-79.

Gene Ontology, C. 2015. Gene Ontology Consortium: going forward. *Nucleic acids research*. 43:D1049-1056.

Gerondopoulos, A., L. Langemeyer, J.R. Liang, A. Linford, and F.A. Barr. 2012. BLOC-3 mutated in Hermansky-Pudlak syndrome is a Rab32/38 guanine nucleotide exchange factor. *Current biology : CB*. 22:2135-2139.

Ghai, V., R.B. Smit, and J. Gaudet. 2012. Transcriptional regulation of HLH-6-independent and subtype-specific genes expressed in the Caenorhabditis elegans pharyngeal glands. *Mechanisms of development*. 129:284-297.

Gillooly, D.J., I.C. Morrow, M. Lindsay, R. Gould, N.J. Bryant, J.M. Gaullier, R.G. Parton, and H. Stenmark. 2000. Localization of phosphatidylinositol 3-phosphate in yeast and mammalian cells. *The EMBO journal*. 19:4577-4588.

Gillooly, D.J., A. Simonsen, and H. Stenmark. 2001. Phosphoinositides and phagocytosis. *The Journal of cell biology*. 155:15-17.

Glebov, O.O., N.A. Bright, and B.J. Nichols. 2006. Flotillin-1 defines a clathrin-independent endocytic pathway in mammalian cells. *Nature cell biology*. 8:46-54.

Grant, B., Y. Zhang, M.C. Paupard, S.X. Lin, D.H. Hall, and D. Hirsh. 2001. Evidence that RME-1, a conserved C. elegans EH-domain protein, functions in endocytic recycling. *Nature cell biology*. 3:573-579.

Grant, B.D., and M. Sato. 2006. Intracellular trafficking. *WormBook*:1-9.

Greenwald, I.S., and H.R. Horvitz. 1980. unc-93(e1500): A behavioral mutant of Caenorhabditis elegans that defines a gene with a wild-type null phenotype. *Genetics*. 96:147-164.

Griffiths, A.J.F. 2000. An introduction to genetic analysis. W.H. Freeman, New York. xvii, 860 p. pp.

Griffiths, G., and J. Gruenberg. 1991. The arguments for pre-existing early and late endosomes. *Trends in cell biology*. 1:5-9.

Haglund, K., S. Sigismund, S. Polo, I. Szymkiewicz, P.P. Di Fiore, and I. Dikic. 2003. Multiple monoubiquitination of RTKs is sufficient for their endocytosis and degradation. *Nature cell biology*. 5:461-466.

Hammond, G.R., M.J. Fischer, K.E. Anderson, J. Holdich, A. Koteci, T. Balla, and R.F. Irvine. 2012. PI4P and PI(4,5)P2 are essential but independent lipid determinants of membrane identity. *Science*. 337:727-730.

Han, J., K. Luby-Phelps, B. Das, X. Shu, Y. Xia, R.D. Mosteller, U.M. Krishna, J.R. Falck, M.A. White, and D. Broek. 1998. Role of substrates and products of PI 3-kinase in regulating activation of Rac-related guanosine triphosphatases by Vav. *Science*. 279:558-560.

Harlan, J.E., P.J. Hajduk, H.S. Yoon, and S.W. Fesik. 1994. Pleckstrin homology domains bind to phosphatidylinositol-4,5-bisphosphate. *Nature*. 371:168-170.

Harrison, R.E., J.H. Brumell, A. Khandani, C. Bucci, C.C. Scott, X. Jiang, B.B. Finlay, and S. Grinstein. 2004. Salmonella impairs RILP recruitment to Rab7 during maturation of invasion vacuoles. *Molecular biology of the cell*. 15:3146-3154.

Haslam, R.J., H.B. Koide, and B.A. Hemmings. 1993. Pleckstrin domain homology. *Nature*. 363:309-310.

He, L., J.M. Thomson, M.T. Hemann, E. Hernando-Monge, D. Mu, S. Goodson, S. Powers, C. Cordon-Cardo, S.W. Lowe, G.J. Hannon, and S.M. Hammond. 2005. A microRNA polycistron as a potential human oncogene. *Nature*. 435:828-833.

Heasman, S.J., and A.J. Ridley. 2008. Mammalian Rho GTPases: new insights into their functions from in vivo studies. *Nature reviews. Molecular cell biology*. 9:690-701.

Henmi, Y., Y. Morikawa, N. Oe, N. Ikeda, A. Fujita, K. Takei, S. Minogue, and K. Tanabe. 2016. PtdIns4KIIalpha generates endosomal PtdIns(4)P and is required for receptor sorting at early endosomes. *Molecular biology of the cell*. 27:990-1001.

Herman, P.K., and S.D. Emr. 1990. Characterization of VPS34, a gene required for vacuolar protein sorting and vacuole segregation in Saccharomyces cerevisiae. *Molecular and cellular biology*. 10:6742-6754.

Herman, P.K., J.H. Stack, and S.D. Emr. 1991. A genetic and structural analysis of the yeast Vps15 protein kinase: evidence for a direct role of Vps15p in vacuolar protein delivery. *The EMBO journal*. 10:4049-4060.

Hernandez, L.D., K. Hueffer, M.R. Wenk, and J.E. Galan. 2004. Salmonella modulates vesicular traffic by altering phosphoinositide metabolism. *Science*. 304:1805-1807.

Hoeller, O., P. Bolourani, J. Clark, L.R. Stephens, P.T. Hawkins, O.D. Weiner, G. Weeks, and R.R. Kay. 2013. Two distinct functions for PI3-kinases in macropinocytosis. *Journal of cell science*. 126:4296-4307.

Hoepfner, S., F. Severin, A. Cabezas, B. Habermann, A. Runge, D. Gillooly, H. Stenmark, and M. Zerial. 2005. Modulation of receptor recycling and degradation by the endosomal kinesin KIF16B. *Cell*. 121:437-450.

Holleran, E.A., L.A. Ligon, M. Tokito, M.C. Stankewich, J.S. Morrow, and E.L. Holzbaur. 2001. beta III spectrin binds to the Arp1 subunit of dynactin. *The Journal of biological chemistry*. 276:36598-36605.

Horiuchi, H., R. Lippe, H.M. McBride, M. Rubino, P. Woodman, H. Stenmark, V. Rybin, M. Wilm, K. Ashman, M. Mann, and M. Zerial. 1997. A novel Rab5 GDP/GTP exchange factor complexed to Rabaptin-5 links nucleotide exchange to effector recruitment and function. *Cell*. 90:1149-1159.

Howe, K.L., B.J. Bolt, S. Cain, J. Chan, W.J. Chen, P. Davis, J. Done, T. Down, S. Gao, C. Grove, T.W. Harris, R. Kishore, R. Lee, J. Lomax, Y. Li, H.M. Muller, C. Nakamura, P. Nuin, M. Paulini, D. Raciti, G. Schindelman, E. Stanley, M.A. Tuli, K. Van Auken, D. Wang, X. Wang, G. Williams, A. Wright, K. Yook, M. Berriman, P. Kersey, T. Schedl, L. Stein, and P.W. Sternberg. 2016. WormBase 2016: expanding to enable helminth genomic research. *Nucleic acids research*. 44:D774-780.

Howes, M.T., M. Kirkham, J. Riches, K. Cortese, P.J. Walser, F. Simpson, M.M. Hill, A. Jones, R. Lundmark, M.R. Lindsay, D.J. Hernandez-Deviez, G. Hadzic, A. McCluskey, R. Bashir, L. Liu, P. Pilch, H. McMahon, P.J. Robinson, J.F. Hancock, S. Mayor, and R.G. Parton. 2010. Clathrin-independent carriers form a high capacity endocytic sorting system at the leading edge of migrating cells. *The Journal of cell biology*. 190:675-691.

Hsu, P.D., E.S. Lander, and F. Zhang. 2014. Development and applications of CRISPR-Cas9 for genome engineering. *Cell*. 157:1262-1278.

Hu, F., T. Padukkavidana, C.B. Vaegter, O.A. Brady, Y. Zheng, I.R. Mackenzie, H.H. Feldman, A. Nykjaer, and S.M. Strittmatter. 2010. Sortilin-mediated endocytosis determines levels of the frontotemporal dementia protein, progranulin. *Neuron*. 68:654-667.

Huang, L.S., and P.W. Sternberg. 2006. Genetic dissection of developmental pathways. *WormBook*:1-19.

Huotari, J., and A. Helenius. 2011. Endosome maturation. *The EMBO journal*. 30:3481-3500.

Hurley, J.H., and S. Misra. 2000. Signaling and subcellular targeting by membrane-binding domains. *Annu Rev Biophys Biomol Struct*. 29:49-79.

Hutagalung, A.H., and P.J. Novick. 2011. Role of Rab GTPases in membrane traffic and cell physiology. *Physiological reviews*. 91:119-149.

Hyvonen, M., M.J. Macias, M. Nilges, H. Oschkinat, M. Saraste, and M. Wilmanns. 1995. Structure of the binding site for inositol phosphates in a PH domain. *The EMBO journal*. 14:4676-4685.

Ikonomov, O.C., D. Sbrissa, and A. Shisheva. 2001. Mammalian cell morphology and endocytic membrane homeostasis require enzymatically active phosphoinositide 5-kinase PIKfyve. *The Journal of biological chemistry*. 276:26141-26147.

IRybin, V., O. Ullrich, M. Rubino, K. Alexandrov, I. Simon, M.C. Seabra, R. Goody, and M. Zerial. 1996. GTPase activity of Rab5 acts as a timer for endocytic membrane fusion. *Nature*. 383:266-269.

Jaber, N., N. Mohd-Naim, Z. Wang, J.L. DeLeon, S. Kim, H. Zhong, N. Sheshadri, Z. Dou, A.L. Edinger, G. Du, V.M. Braga, and W.X. Zong. 2016. Vps34 regulates Rab7 and late endocytic trafficking through recruitment of the GTPase activating protein Armus. *Journal of cell science*.

Jacoby, W.G. 2000. Loess: a nonparametric, graphical tool for depicting relationships between variables. *Elect Stud*. 19:577-613.

Jahn, R., and R.H. Scheller. 2006. SNAREs--engines for membrane fusion. *Nature reviews. Molecular cell biology*. 7:631-643.

Jean, S., and A.A. Kiger. 2012. Coordination between RAB GTPase and phosphoinositide regulation and functions. *Nature reviews. Molecular cell biology*. 13:463-470.

Ji, X., P. Zhang, R.N. Armstrong, and G.L. Gilliland. 1992. The three-dimensional structure of a glutathione S-transferase from the mu gene class. Structural analysis of the binary complex of isoenzyme 3-3 and glutathione at 2.2-A resolution. *Biochemistry*. 31:10169-10184.

Johannes, L., R.G. Parton, P. Bassereau, and S. Mayor. 2015. Building endocytic pits without clathrin. *Nature reviews. Molecular cell biology*. 16:311-321.

Johansson, M., M. Lehto, K. Tanhuanpaa, T.L. Cover, and V.M. Olkkonen. 2005. The oxysterol-binding protein homologue ORP1L interacts with Rab7 and alters functional properties of late endocytic compartments. *Molecular biology of the cell*. 16:5480-5492.

Johansson, M., N. Rocha, W. Zwart, I. Jordens, L. Janssen, C. Kuijl, V.M. Olkkonen, and J. Neefjes. 2007. Activation of endosomal dynein motors by stepwise assembly of Rab7-RILP-p150Glued, ORP1L, and the receptor betalll spectrin. *The Journal of cell biology*. 176:459-471.

Jordens, I., M. Fernandez-Borja, M. Marsman, S. Dusseljee, L. Janssen, J. Calafat, H. Janssen, R. Wubbolts, and J. Neefjes. 2001. The Rab7 effector protein RILP controls lysosomal transport by inducing the recruitment of dynein-dynactin motors. *Current biology : CB*. 11:1680-1685.

Jorgensen, E.M., and S.E. Mango. 2002. The art and design of genetic screens: caenorhabditis elegans. *Nat Rev Genet*. 3:356-369.

Jovic, M., M. Sharma, J. Rahajeng, and S. Caplan. 2010. The early endosome: a busy sorting station for proteins at the crossroads. *Histol Histopathol*. 25:99-112.

Jung, T., N. Bader, and T. Grune. 2007. Lipofuscin: formation, distribution, and metabolic consequences. *Annals of the New York Academy of Sciences*. 1119:97-111.

Kamath, R.S., and J. Ahringer. 2003. Genome-wide RNAi screening in Caenorhabditis elegans. *Methods*. 30:313-321.

Kamath, R.S., M. Martinez-Campos, P. Zipperlen, A.G. Fraser, and J. Ahringer. 2001. Effectiveness of specific RNA-mediated interference through ingested double-stranded RNA in Caenorhabditis elegans. *Genome Biol*. 2:RESEARCH0002.

Kang, R., H.J. Zeh, M.T. Lotze, and D. Tang. 2011. The Beclin 1 network regulates autophagy and apoptosis. *Cell Death Differ*. 18:571-580.

Kanno, E., K. Ishibashi, H. Kobayashi, T. Matsui, N. Ohbayashi, and M. Fukuda. 2010. Comprehensive screening for novel rab-binding proteins by GST pull-down assay using 60 different mammalian Rabs. *Traffic*. 11:491-507.

Kao, A.W., R.J. Eisenhut, L.H. Martens, A. Nakamura, A. Huang, J.A. Bagley, P. Zhou, A. de Luis, L.J. Neukomm, J. Cabello, R.V. Farese, Jr., and C. Kenyon. 2011. A neurodegenerative disease mutation that accelerates the clearance of apoptotic cells. *Proceedings of the National Academy of Sciences of the United States of America*. 108:4441-4446.

Karnoub, A.E., and R.A. Weinberg. 2008. Ras oncogenes: split personalities. *Nature reviews. Molecular cell biology*. 9:517-531.

Kaur, J., and J. Debnath. 2015. Autophagy at the crossroads of catabolism and anabolism. *Nature reviews. Molecular cell biology*. 16:461-472.

Kelwick, R., I. Desanlis, G.N. Wheeler, and D.R. Edwards. 2015. The ADAMTS (A Disintegrin and Metalloproteinase with Thrombospondin motifs) family. *Genome Biol*. 16:113.

Khosravi-Far, R., R.J. Lutz, A.D. Cox, L. Conroy, J.R. Bourne, M. Sinensky, W.E. Balch, J.E. Buss, and C.J. Der. 1991. Isoprenoid modification of rab proteins terminating in CC or CXC motifs. *Proceedings of the National Academy of Sciences of the United States of America*. 88:6264-6268.

Kihara, A., Y. Kabeya, Y. Ohsumi, and T. Yoshimori. 2001a. Beclin-phosphatidylinositol 3-kinase complex functions at the trans-Golgi network. *EMBO Rep*. 2:330-335.

Kihara, A., T. Noda, N. Ishihara, and Y. Ohsumi. 2001b. Two distinct Vps34 phosphatidylinositol 3-kinase complexes function in autophagy and carboxypeptidase Y sorting in Saccharomyces cerevisiae. *The Journal of cell biology*. 152:519-530.

Kim, D.I., S.C. Jensen, K.A. Noble, B. Kc, K.H. Roux, K. Motamedchaboki, and K.J. Roux. 2016. An improved smaller biotin ligase for BioID proximity labeling. *Molecular biology of the cell*. 27:1188-1196.

Kim, M.K., and Y.K. Kang. 1999. Positional preference of proline in alpha-helices. *Protein Sci*. 8:1492-1499.

Kim, S.A., G.S. Taylor, K.M. Torgersen, and J.E. Dixon. 2002. Myotubularin and MTMR2, phosphatidylinositol 3-phosphatases mutated in myotubular myopathy and type 4B Charcot-Marie-Tooth disease. *The Journal of biological chemistry*. 277:4526-4531.

Kirkham, M., A. Fujita, R. Chadda, S.J. Nixon, T.V. Kurzchalia, D.K. Sharma, R.E. Pagano, J.F. Hancock, S. Mayor, and R.G. Parton. 2005. Ultrastructural identification of uncoated caveolin-independent early endocytic vehicles. *The Journal of cell biology*. 168:465-476.

Klein, D.E., A. Lee, D.W. Frank, M.S. Marks, and M.A. Lemmon. 1998. The pleckstrin homology domains of dynamin isoforms require oligomerization for high affinity phosphoinositide binding. *The Journal of biological chemistry*. 273:27725-27733.

Klopper, T.H., N. Kienle, D. Fasshauer, and S. Munro. 2012. Untangling the evolution of Rab G proteins: implications of a comprehensive genomic analysis. *BMC Biol*. 10:71.

Kollmann, K., K. Uusi-Rauva, E. Scifo, J. Tyynela, A. Jalanko, and T. Braulke. 2013. Cell biology and function of neuronal ceroid lipofuscinosis-related proteins. *Biochimica et biophysica acta*. 1832:1866-1881.

Koshiba, S., T. Kigawa, J.H. Kim, M. Shirouzu, D. Bowtell, and S. Yokoyama. 1997. The solution structure of the pleckstrin homology domain of mouse Son-of-sevenless 1 (mSos1). *Journal of molecular biology*. 269:579-591.

Kovacs, J.M., C.T. Mant, and R.S. Hodges. 2006. Determination of intrinsic hydrophilicity/hydrophobicity of amino acid side chains in peptides in the absence of nearest-neighbor or conformational effects. *Biopolymers*. 84:283-297.

Kowanetz, K., K. Husnjak, D. Holler, M. Kowanetz, P. Soubeyran, D. Hirsch, M.H. Schmidt, K. Pavelic, P. De Camilli, P.A. Randazzo, and I. Dikic. 2004. CIN85 associates with multiple effectors controlling intracellular trafficking of epidermal growth factor receptors. *Molecular biology of the cell*. 15:3155-3166.

Kundra, R., and S. Kornfeld. 1999. Asparagine-linked oligosaccharides protect Lamp-1 and Lamp-2 from intracellular proteolysis. *The Journal of biological chemistry*. 274:31039-31046.

Kutateladze, T.G. 2010. Translation of the phosphoinositide code by PI effectors. *Nature chemical biology*. 6:507-513.

Kutscher, L.M., and S. Shaham. 2014. Forward and reverse mutagenesis in C. elegans. *WormBook*:1-26.

Lai, C.H., C.Y. Chou, L.Y. Ch'ang, C.S. Liu, and W. Lin. 2000. Identification of novel human genes evolutionarily conserved in Caenorhabditis elegans by comparative proteomics. *Genome Res*. 10:703-713.

Laporte, J., L.J. Hu, C. Kretz, J.L. Mandel, P. Kioschis, J.F. Coy, S.M. Klauck, A. Poustka, and N. Dahl. 1996. A gene mutated in X-linked myotubular myopathy defines a new putative tyrosine phosphatase family conserved in yeast. *Nat Genet*. 13:175-182.

Laporte, J., L. Liaubet, F. Blondeau, H. Tronchere, J.L. Mandel, and B. Payrastre. 2002. Functional redundancy in the myotubularin family. *Biochemical and biophysical research communications*. 291:305-312.

Lawrence, G., C.C. Brown, B.A. Flood, S. Karunakaran, M. Cabrera, M. Nordmann, C. Ungermann, and R.A. Fratti. 2014. Dynamic association of the PI3P-interacting Mon1-Ccz1 GEF with vacuoles is controlled through its phosphorylation by the type 1 casein kinase Yck3. *Molecular biology of the cell*. 25:1608-1619.

Lemmon, M.A. 2007. Pleckstrin homology (PH) domains and phosphoinositides. *Biochemical Society symposium*:81-93.

Lemmon, M.A. 2008. Membrane recognition by phospholipid-binding domains. *Nature reviews. Molecular cell biology*. 9:99-111.

Lemmon, M.A., and K.M. Ferguson. 2000. Signal-dependent membrane targeting by pleckstrin homology (PH) domains. *The Biochemical journal*. 350 Pt 1:1-18.

Letunic, I., T. Doerks, and P. Bork. 2015. SMART: recent updates, new developments and status in 2015. *Nucleic acids research*. 43:D257-260.

Li, J.Q., L. Tan, and J.T. Yu. 2014. The role of the LRRK2 gene in Parkinsonism. *Mol Neurodegener*. 9:47.

Li, W., W. Zou, D. Zhao, J. Yan, Z. Zhu, J. Lu, and X. Wang. 2009. C. elegans Rab GTPase activating protein TBC-2 promotes cell corpse degradation by regulating the small GTPase RAB-5. *Development*. 136:2445-2455.

Liang, X.H., S. Jackson, M. Seaman, K. Brown, B. Kempkes, H. Hibshoosh, and B. Levine. 1999. Induction of autophagy and inhibition of tumorigenesis by beclin 1. *Nature*. 402:672-676.

Liang, X.H., L.K. Kleeman, H.H. Jiang, G. Gordon, J.E. Goldman, G. Berry, B. Herman, and B. Levine. 1998. Protection against fatal Sindbis virus encephalitis by beclin, a novel Bcl-2-interacting protein. *J Virol*. 72:8586-8596.

Lim, J.P., and P.A. Gleeson. 2011. Macropinocytosis: an endocytic pathway for internalising large gulps. *Immunol Cell Biol*. 89:836-843.
Lima-Fernandes, E., S. Misticone, C. Boularan, J.S. Paradis, H. Enslen, P.P. Roux, M. Bouvier, G.S. Baillie, S. Marullo, and M.G. Scott. 2014. A biosensor to monitor dynamic regulation and function of tumour suppressor PTEN in living cells. *Nat Commun*. 5:4431.
Lippe, R., M. Miaczynska, V. Rybin, A. Runge, and M. Zerial. 2001. Functional synergy between Rab5 effector Rabaptin-5 and exchange factor Rabex-5 when physically associated in a complex. *Molecular biology of the cell*. 12:2219-2228.
Liu, K., Y. Jian, X. Sun, C. Yang, Z. Gao, Z. Zhang, X. Liu, Y. Li, J. Xu, Y. Jing, S. Mitani, S. He, and C. Yang. 2016. Negative regulation of phosphatidylinositol 3-phosphate levels in early-to-late endosome conversion. *The Journal of cell biology*. 212:181-198.
Liu, O., and B.D. Grant. 2015. Basolateral Endocytic Recycling Requires RAB-10 and AMPH-1 Mediated Recruitment of RAB-5 GAP TBC-2 to Endosomes. *PLoS genetics*. 11:e1005514.
Lodowski, D.T., J.A. Pitcher, W.D. Capel, R.J. Lefkowitz, and J.J. Tesmer. 2003. Keeping G proteins at bay: a complex between G protein-coupled receptor kinase 2 and Gbetagamma. *Science*. 300:1256-1262.
Lu, N., Q. Shen, T.R. Mahoney, L.J. Neukomm, Y. Wang, and Z. Zhou. 2012. Two PI 3-kinases and one PI 3-phosphatase together establish the cyclic waves of phagosomal PtdIns(3)P critical for the degradation of apoptotic cells. *PLoS biology*. 10:e1001245.
Lu, P., K. Takai, V.M. Weaver, and Z. Werb. 2011. Extracellular matrix degradation and remodeling in development and disease. *Cold Spring Harbor perspectives in biology*. 3.
Lupas, A. 1996. Prediction and analysis of coiled-coil structures. *Methods in enzymology*. 266:513-525.
Lupas, A., M. Van Dyke, and J. Stock. 1991. Predicting coiled coils from protein sequences. *Science*. 252:1162-1164.
Lupas, A.a.L., J. COILS version 2.2.
Luzio, J.P., P.R. Pryor, and N.A. Bright. 2007. Lysosomes: fusion and function. *Nature reviews. Molecular cell biology*. 8:622-632.
Macara, I.G. 2001. Transport into and out of the nucleus. *Microbiol Mol Biol Rev*. 65:570-594, table of contents.
Maffucci, T., and M. Falasca. 2001. Specificity in pleckstrin homology (PH) domain membrane targeting: a role for a phosphoinositide-protein co-operative mechanism. *FEBS Lett*. 506:173-179.
Marat, A.L., and V. Haucke. 2016. Phosphatidylinositol 3-phosphates-at the interface between cell signalling and membrane traffic. *The EMBO journal*. 35:561-579.
Marcus, S.L., M.R. Wenk, O. Steele-Mortimer, and B.B. Finlay. 2001. A synaptojanin-homologous region of Salmonella typhimurium SigD is essential for inositol phosphatase activity and Akt activation. *FEBS Lett*. 494:201-207.
Marquez, R.T., and L. Xu. 2012. Bcl-2:Beclin 1 complex: multiple, mechanisms regulating autophagy/apoptosis toggle switch. *Am J Cancer Res*. 2:214-221.
Marshansky, V., and M. Futai. 2008. The V-type H+-ATPase in vesicular trafficking: targeting, regulation and function. *Current opinion in cell biology*. 20:415-426.
Mason, J.M., and K.M. Arndt. 2004. Coiled coil domains: stability, specificity, and biological implications. *Chembiochem*. 5:170-176.

Masters, T.A., B. Pontes, V. Viasnoff, Y. Li, and N.C. Gauthier. 2013. Plasma membrane tension orchestrates membrane trafficking, cytoskeletal remodeling, and biochemical signaling during phagocytosis. *Proceedings of the National Academy of Sciences of the United States of America*. 110:11875-11880.

Mata, I.F., W.J. Wedemeyer, M.J. Farrer, J.P. Taylor, and K.A. Gallo. 2006. LRRK2 in Parkinson's disease: protein domains and functional insights. *Trends Neurosci*. 29:286-293.

Mayinger, P. 2012. Phosphoinositides and vesicular membrane traffic. *Biochimica et biophysica acta*. 1821:1104-1113.

Mayor, S., and R.E. Pagano. 2007. Pathways of clathrin-independent endocytosis. *Nature reviews. Molecular cell biology*. 8:603-612.

Mayor, S., R.G. Parton, and J.G. Donaldson. 2014. Clathrin-independent pathways of endocytosis. *Cold Spring Harbor perspectives in biology*. 6.

McBride, H.M., V. Rybin, C. Murphy, A. Giner, R. Teasdale, and M. Zerial. 1999. Oligomeric complexes link Rab5 effectors with NSF and drive membrane fusion via interactions between EEA1 and syntaxin 13. *Cell*. 98:377-386.

McKnight, N.C., Y. Zhong, M.S. Wold, S. Gong, G.R. Phillips, Z. Dou, Y. Zhao, N. Heintz, W.X. Zong, and Z. Yue. 2014. Beclin 1 is required for neuron viability and regulates endosome pathways via the UVRAG-VPS34 complex. *PLoS genetics*. 10:e1004626.

McLachlan, A.D., and J. Karn. 1983. Periodic features in the amino acid sequence of nematode myosin rod. *Journal of molecular biology*. 164:605-626.

McLaughlin, S., and D. Murray. 2005. Plasma membrane phosphoinositide organization by protein electrostatics. *Nature*. 438:605-611.

McMahon, H.T., and E. Boucrot. 2011. Molecular mechanism and physiological functions of clathrin-mediated endocytosis. *Nature reviews. Molecular cell biology*. 12:517-533.

McWilliam, H., W. Li, M. Uludag, S. Squizzato, Y.M. Park, N. Buso, A.P. Cowley, and R. Lopez. 2013. Analysis Tool Web Services from the EMBL-EBI. *Nucleic acids research*. 41:W597-600.

Meresse, S., O. Steele-Mortimer, B.B. Finlay, and J.P. Gorvel. 1999. The rab7 GTPase controls the maturation of Salmonella typhimurium-containing vacuoles in HeLa cells. *The EMBO journal*. 18:4394-4403.

Mills, I.G., A.T. Jones, and M.J. Clague. 1998. Involvement of the endosomal autoantigen EEA1 in homotypic fusion of early endosomes. *Current biology : CB*. 8:881-884.

Minevich, G., D.S. Park, D. Blankenberg, R.J. Poole, and O. Hobert. 2012. CloudMap: a cloud-based pipeline for analysis of mutant genome sequences. *Genetics*. 192:1249-1269.

Mironov, A.A., and M. Pavelka. 2008. The Golgi apparatus : state of the art 110 years after Camillo Golgi's discovery. Springer, Wien ; New York. viii, 716 p. pp.

Mizuno, K., A. Kitamura, and T. Sasaki. 2003. Rabring7, a novel Rab7 target protein with a RING finger motif. *Molecular biology of the cell*. 14:3741-3752.

Morris, D.H., C.K. Yip, Y. Shi, B.T. Chait, and Q.J. Wang. 2015. Beclin 1-Vps34 Complex Architecture: Understanding the Nuts and Bolts of Therapeutic Targets. *Front Biol (Beijing)*. 10:398-426.

Mott, H.R., and D. Owen. 2015. Structures of Ras superfamily effector complexes: What have we learnt in two decades? *Critical reviews in biochemistry and molecular biology*. 50:85-133.

Muresan, V., M.C. Stankewich, W. Steffen, J.S. Morrow, E.L. Holzbaur, and B.J. Schnapp. 2001. Dynactin-dependent, dynein-driven vesicle transport in the absence of membrane proteins: a role for spectrin and acidic phospholipids. *Molecular cell*. 7:173-183.

Murphy, R.F. 1991. Maturation models for endosome and lysosome biogenesis. *Trends in cell biology*. 1:77-82.

Murray, J.T., C. Panaretou, H. Stenmark, M. Miaczynska, and J.M. Backer. 2002. Role of Rab5 in the recruitment of hVps34/p150 to the early endosome. *Traffic*. 3:416-427.

Nagano, F., T. Sasaki, K. Fukui, T. Asakura, K. Imazumi, and Y. Takai. 1998. Molecular cloning and characterization of the noncatalytic subunit of the Rab3 subfamily-specific GTPase-activating protein. *The Journal of biological chemistry*. 273:24781-24785.

Nakatsu, F., M. Messa, R. Nandez, H. Czapla, Y. Zou, S.M. Strittmatter, and P. De Camilli. 2015. Sac2/INPP5F is an inositol 4-phosphatase that functions in the endocytic pathway. *The Journal of cell biology*. 209:85-95.

Narayan, K., and M.A. Lemmon. 2006. Determining selectivity of phosphoinositide-binding domains. *Methods*. 39:122-133.

Nassar, N., G.R. Hoffman, D. Manor, J.C. Clardy, and R.A. Cerione. 1998. Structures of Cdc42 bound to the active and catalytically compromised forms of Cdc42GAP. *Nat Struct Biol*. 5:1047-1052.

Nicot, A.S., H. Fares, B. Payrastre, A.D. Chisholm, M. Labouesse, and J. Laporte. 2006. The phosphoinositide kinase PIKfyve/Fab1p regulates terminal lysosome maturation in Caenorhabditis elegans. *Molecular biology of the cell*. 17:3062-3074.

Nielsen, E., S. Christoforidis, S. Uttenweiler-Joseph, M. Miaczynska, F. Dewitte, M. Wilm, B. Hoflack, and M. Zerial. 2000. Rabenosyn-5, a novel Rab5 effector, is complexed with hVPS45 and recruited to endosomes through a FYVE finger domain. *Journal of Cell Biology*. 151:601-612.

Nielsen, E., F. Severin, J.M. Backer, A.A. Hyman, and M. Zerial. 1999. Rab5 regulates motility of early endosomes on microtubules. *Nature cell biology*. 1:376-382.

Nimnual, A.S., B.A. Yatsula, and D. Bar-Sagi. 1998. Coupling of Ras and Rac guanosine triphosphatases through the Ras exchanger Sos. *Science*. 279:560-563.

Nordmann, M., M. Cabrera, A. Perz, C. Brocker, C. Ostrowicz, S. Engelbrecht-Vandre, and C. Ungermann. 2010. The Mon1-Ccz1 complex is the GEF of the late endosomal Rab7 homolog Ypt7. *Current biology : CB*. 20:1654-1659.

O'Brien, K.P., I. Westerlund, and E.L. Sonnhammer. 2004. OrthoDisease: a database of human disease orthologs. *Hum Mutat*. 24:112-119.

Opdam, F.J., A. Echard, H.J. Croes, J.A. van den Hurk, R.A. van de Vorstenbosch, L.A. Ginsel, B. Goud, and J.A. Fransen. 2000. The small GTPase Rab6B, a novel Rab6 subfamily member, is cell-type specifically expressed and localised to the Golgi apparatus. *Journal of cell science*. 113 (Pt 15):2725-2735.

Pace, C.N., and J.M. Scholtz. 1998. A helix propensity scale based on experimental studies of peptides and proteins. *Biophys J*. 75:422-427.

Paix, A., A. Folkmann, D. Rasoloson, and G. Seydoux. 2015. High Efficiency, Homology-Directed Genome Editing in Caenorhabditis elegans Using CRISPR-Cas9 Ribonucleoprotein Complexes. *Genetics*. 201:47-54.

Pamonsinlapatham, P., R. Hadj-Slimane, Y. Lepelletier, B. Allain, M. Toccafondi, C. Garbay, and F. Raynaud. 2009. p120-Ras GTPase activating protein (RasGAP): a multi-interacting protein in downstream signaling. *Biochimie*. 91:320-328.

Pan, X., S. Eathiraj, M. Munson, and D.G. Lambright. 2006. TBC-domain GAPs for Rab GTPases accelerate GTP hydrolysis by a dual-finger mechanism. *Nature*. 442:303-306.
Panaretou, C., J. Domin, S. Cockcroft, and M.D. Waterfield. 1997. Characterization of p150, an adaptor protein for the human phosphatidylinositol (PtdIns) 3-kinase. Substrate presentation by phosphatidylinositol transfer protein to the p150.Ptdins 3-kinase complex. *The Journal of biological chemistry*. 272:2477-2485.
Pandey, U.B., and C.D. Nichols. 2011. Human disease models in Drosophila melanogaster and the role of the fly in therapeutic drug discovery. *Pharmacological reviews*. 63:411-436.
Park, S.Y., W. Jin, J.R. Woo, and S.E. Shoelson. 2011. Crystal structures of human TBC1D1 and TBC1D4 (AS160) RabGTPase-activating protein (RabGAP) domains reveal critical elements for GLUT4 translocation. *The Journal of biological chemistry*. 286:18130-18138.
Parry, D.A. 1982. Coiled-coils in alpha-helix-containing proteins: analysis of the residue types within the heptad repeat and the use of these data in the prediction of coiled-coils in other proteins. *Biosci Rep*. 2:1017-1024.
Parton, R.G., and K. Simons. 2007. The multiple faces of caveolae. *Nature reviews. Molecular cell biology*. 8:185-194.
Pattingre, S., A. Tassa, X. Qu, R. Garuti, X.H. Liang, N. Mizushima, M. Packer, M.D. Schneider, and B. Levine. 2005. Bcl-2 antiapoptotic proteins inhibit Beclin 1-dependent autophagy. *Cell*. 122:927-939.
Payne, C.K., S.A. Jones, C. Chen, and X. Zhuang. 2007. Internalization and trafficking of cell surface proteoglycans and proteoglycan-binding ligands. *Traffic*. 8:389-401.
Pereira-Leal, J.B., and M.C. Seabra. 2000. The mammalian Rab family of small GTPases: definition of family and subfamily sequence motifs suggests a mechanism for functional specificity in the Ras superfamily. *Journal of molecular biology*. 301:1077-1087.
Pereira-Leal, J.B., and M.C. Seabra. 2001. Evolution of the Rab family of small GTP-binding proteins. *Journal of molecular biology*. 313:889-901.
Petkau, T.L., and B.R. Leavitt. 2014. Progranulin in neurodegenerative disease. *Trends Neurosci*. 37:388-398.
Pfleger, K.D., R.M. Seeber, and K.A. Eidne. 2006. Bioluminescence resonance energy transfer (BRET) for the real-time detection of protein-protein interactions. *Nat Protoc*. 1:337-345.
Phillips, M.J., and G.K. Voeltz. 2016. Structure and function of ER membrane contact sites with other organelles. *Nature reviews. Molecular cell biology*. 17:69-82.
Pilon, M., and C. Morck. 2005. Development of Caenorhabditis elegans pharynx, with emphasis on its nervous system. *Acta Pharmacol Sin*. 26:396-404.
Popovic, D., M. Akutsu, I. Novak, J.W. Harper, C. Behrends, and I. Dikic. 2012. Rab GTPase-activating proteins in autophagy: regulation of endocytic and autophagy pathways by direct binding to human ATG8 modifiers. *Molecular and cellular biology*. 32:1733-1744.
Posor, Y., M. Eichhorn-Gruenig, D. Puchkov, J. Schoneberg, A. Ullrich, A. Lampe, R. Muller, S. Zarbakhsh, F. Gulluni, E. Hirsch, M. Krauss, C. Schultz, J. Schmoranzer, F. Noe, and V. Haucke. 2013. Spatiotemporal control of endocytosis by phosphatidylinositol-3,4-bisphosphate. *Nature*. 499:233-237.
Poteryaev, D., S. Datta, K. Ackema, M. Zerial, and A. Spang. 2010. Identification of the switch in early-to-late endosome transition. *Cell*. 141:497-508.
Poteryaev, D., H. Fares, B. Bowerman, and A. Spang. 2007. Caenorhabditis elegans SAND-1 is essential for RAB-7 function in endosomal traffic. *The EMBO journal*. 26:301-312.

Qu, W., C. Ren, Y. Li, J. Shi, J. Zhang, X. Wang, X. Hang, Y. Lu, D. Zhao, and C. Zhang. 2011. Reliability analysis of the Ahringer Caenorhabditis elegans RNAi feeding library: a guide for genome-wide screens. *BMC Genomics*. 12:170.

Raiborg, C., K.G. Bache, D.J. Gillooly, I.H. Madshus, E. Stang, and H. Stenmark. 2002. Hrs sorts ubiquitinated proteins into clathrin-coated microdomains of early endosomes. *Nature cell biology*. 4:394-398.

Raiborg, C., B. Bremnes, A. Mehlum, D.J. Gillooly, A. D'Arrigo, E. Stang, and H. Stenmark. 2001. FYVE and coiled-coil domains determine the specific localisation of Hrs to early endosomes. *Journal of cell science*. 114:2255-2263.

Rak, A., R. Fedorov, K. Alexandrov, S. Albert, R.S. Goody, D. Gallwitz, and A.J. Scheidig. 2000. Crystal structure of the GAP domain of Gyp1p: first insights into interaction with Ypt/Rab proteins. *The EMBO journal*. 19:5105-5113.

Richardson, J.S., and D.C. Richardson. 1988. Amino acid preferences for specific locations at the ends of alpha helices. *Science*. 240:1648-1652.

Riddle, D.L. 1997. C. elegans II. Cold Spring Harbor Laboratory Press, Plainview, N.Y. xvii, 1222 p. pp.

Rink, J., E. Ghigo, Y. Kalaidzidis, and M. Zerial. 2005. Rab conversion as a mechanism of progression from early to late endosomes. *Cell*. 122:735-749.

Rittinger, K., P.A. Walker, J.F. Eccleston, S.J. Smerdon, and S.J. Gamblin. 1997. Structure at 1.65 A of RhoA and its GTPase-activating protein in complex with a transition-state analogue. *Nature*. 389:758-762.

Roach, E.S., and S.P. Sparagana. 2004. Diagnosis of tuberous sclerosis complex. *J Child Neurol*. 19:643-649.

Roberts, R., and N.T. Ktistakis. 2013. Omegasomes: PI3P platforms that manufacture autophagosomes. *Essays Biochem*. 55:17-27.

Rocha, N., C. Kuijl, R. van der Kant, L. Janssen, D. Houben, H. Janssen, W. Zwart, and J. Neefjes. 2009. Cholesterol sensor ORP1L contacts the ER protein VAP to control Rab7-RILP-p150 Glued and late endosome positioning. *The Journal of cell biology*. 185:1209-1225.

Roggo, L., V. Bernard, A.L. Kovacs, A.M. Rose, F. Savoy, M. Zetka, M.P. Wymann, and F. Muller. 2002. Membrane transport in Caenorhabditis elegans: an essential role for VPS34 at the nuclear membrane. *The EMBO journal*. 21:1673-1683.

Romero Rosales, K., E.R. Peralta, G.G. Guenther, S.Y. Wong, and A.L. Edinger. 2009. Rab7 activation by growth factor withdrawal contributes to the induction of apoptosis. *Molecular biology of the cell*. 20:2831-2840.

Rost, B. 1996. PHD: predicting one-dimensional protein structure by profile-based neural networks. *Methods in enzymology*. 266:525-539.

Rost, B., and J. Liu. 2003. The PredictProtein server. *Nucleic acids research*. 31:3300-3304.

Rost, B., and C. Sander. 1993. Prediction of protein secondary structure at better than 70% accuracy. *Journal of molecular biology*. 232:584-599.

Roux, K.J., D.I. Kim, M. Raida, and B. Burke. 2012. A promiscuous biotin ligase fusion protein identifies proximal and interacting proteins in mammalian cells. *The Journal of cell biology*. 196:801-810.

Royle, S.J. 2006. The cellular functions of clathrin. *Cellular and molecular life sciences : CMLS*. 63:1823-1832.

Ruck, A., J. Attonito, K.T. Garces, L. Nunez, N.J. Palmisano, Z. Rubel, Z. Bai, K.C. Nguyen, L. Sun, B.D. Grant, D.H. Hall, and A. Melendez. 2011. The Atg6/Vps30/Beclin 1 ortholog BEC-1 mediates endocytic retrograde transport in addition to autophagy in C. elegans. *Autophagy*. 7:386-400.

Russo, C., Y. Gao, P. Mancini, C. Vanni, M. Porotto, M. Falasca, M.R. Torrisi, Y. Zheng, and A. Eva. 2001. Modulation of oncogenic DBL activity by phosphoinositol phosphate binding to pleckstrin homology domain. *The Journal of biological chemistry*. 276:19524-19531.

Sabharanjak, S., P. Sharma, R.G. Parton, and S. Mayor. 2002. GPI-anchored proteins are delivered to recycling endosomes via a distinct cdc42-regulated, clathrin-independent pinocytic pathway. *Developmental cell*. 2:411-423.

Salim, K., M.J. Bottomley, E. Querfurth, M.J. Zvelebil, I. Gout, R. Scaife, R.L. Margolis, R. Gigg, C.I. Smith, P.C. Driscoll, M.D. Waterfield, and G. Panayotou. 1996. Distinct specificity in the recognition of phosphoinositides by the pleckstrin homology domains of dynamin and Bruton's tyrosine kinase. *The EMBO journal*. 15:6241-6250.

Sandvig, K., S. Pust, T. Skotland, and B. van Deurs. 2011. Clathrin-independent endocytosis: mechanisms and function. *Current opinion in cell biology*. 23:413-420.

Sann, S.B., M.M. Crane, H. Lu, and Y. Jin. 2012. Rabx-5 regulates RAB-5 early endosomal compartments and synaptic vesicles in C. elegans. *PloS one*. 7:e37930.

Sarin, S., V. Bertrand, H. Bigelow, A. Boyanov, M. Doitsidou, R.J. Poole, S. Narula, and O. Hobert. 2010. Analysis of multiple ethyl methanesulfonate-mutagenized Caenorhabditis elegans strains by whole-genome sequencing. *Genetics*. 185:417-430.

Sasaki, T., A. Kikuchi, S. Araki, Y. Hata, M. Isomura, S. Kuroda, and Y. Takai. 1990. Purification and characterization from bovine brain cytosol of a protein that inhibits the dissociation of GDP from and the subsequent binding of GTP to smg p25A, a ras p21-like GTP-binding protein. *The Journal of biological chemistry*. 265:2333-2337.

Sato, K., A. Norris, M. Sato, and B.D. Grant. 2014. C. elegans as a model for membrane traffic. *WormBook*:1-47.

Sato, M., K. Sato, P. Fonarev, C.J. Huang, W. Liou, and B.D. Grant. 2005. Caenorhabditis elegans RME-6 is a novel regulator of RAB-5 at the clathrin-coated pit. *Nature cell biology*. 7:559-569.

Sbrissa, D., O.C. Ikonomov, and A. Shisheva. 2002. Phosphatidylinositol 3-phosphate-interacting domains in PIKfyve. Binding specificity and role in PIKfyve. Endomenbrane localization. *The Journal of biological chemistry*. 277:6073-6079.

Sbrissa, D., O.C. Ikonomov, J. Strakova, R. Dondapati, K. Mlak, R. Deeb, R. Silver, and A. Shisheva. 2004. A mammalian ortholog of Saccharomyces cerevisiae Vac14 that associates with and up-regulates PIKfyve phosphoinositide 5-kinase activity. *Molecular and cellular biology*. 24:10437-10447.

Scheffzek, K., M.R. Ahmadian, L. Wiesmuller, W. Kabsch, P. Stege, F. Schmitz, and A. Wittinghofer. 1998. Structural analysis of the GAP-related domain from neurofibromin and its implications. *The EMBO journal*. 17:4313-4327.

Scheffzek, K., A. Lautwein, W. Kabsch, M.R. Ahmadian, and A. Wittinghofer. 1996. Crystal structure of the GTPase-activating domain of human p120GAP and implications for the interaction with Ras. *Nature*. 384:591-596.

Schindelin, J., I. Arganda-Carreras, E. Frise, V. Kaynig, M. Longair, T. Pietzsch, S. Preibisch, C. Rueden, S. Saalfeld, B. Schmid, J.Y. Tinevez, D.J. White, V. Hartenstein, K. Eliceiri, P.

Tomancak, and A. Cardona. 2012. Fiji: an open-source platform for biological-image analysis. *Nature methods*. 9:676-682.
Schink, K.O., C. Raiborg, and H. Stenmark. 2013. Phosphatidylinositol 3-phosphate, a lipid that regulates membrane dynamics, protein sorting and cell signalling. *Bioessays*. 35:900-912.
Schmidt, O., and D. Teis. 2012. The ESCRT machinery. *Current biology : CB*. 22:R116-120.
Schneider, C.A., W.S. Rasband, and K.W. Eliceiri. 2012. NIH Image to ImageJ: 25 years of image analysis. *Nature methods*. 9:671-675.
Schroeder, B., S.G. Weller, J. Chen, D. Billadeau, and M.A. McNiven. 2010. A Dyn2-CIN85 complex mediates degradative traffic of the EGFR by regulation of late endosomal budding. *The EMBO journal*. 29:3039-3053.
Schroer, T.A. 2004. Dynactin. *Annual review of cell and developmental biology*. 20:759-779.
Schu, P.V., K. Takegawa, M.J. Fry, J.H. Stack, M.D. Waterfield, and S.D. Emr. 1993. Phosphatidylinositol 3-kinase encoded by yeast VPS34 gene essential for protein sorting. *Science*. 260:88-91.
Schubert, W., P.G. Frank, B. Razani, D.S. Park, C.W. Chow, and M.P. Lisanti. 2001. Caveolae-deficient endothelial cells show defects in the uptake and transport of albumin in vivo. *The Journal of biological chemistry*. 276:48619-48622.
Scott, C.C., P. Cuellar-Mata, T. Matsuo, H.W. Davidson, and S. Grinstein. 2002. Role of 3-phosphoinositides in the maturation of Salmonella-containing vacuoles within host cells. *The Journal of biological chemistry*. 277:12770-12776.
Seals, D.F., G. Eitzen, N. Margolis, W.T. Wickner, and A. Price. 2000. A Ypt/Rab effector complex containing the Sec1 homolog Vps33p is required for homotypic vacuole fusion. *Proceedings of the National Academy of Sciences of the United States of America*. 97:9402-9407.
Seaman, M.N. 2012. The retromer complex - endosomal protein recycling and beyond. *Journal of cell science*. 125:4693-4702.
Serva, A., B. Knapp, Y.T. Tsai, C. Claas, T. Lisauskas, P. Matula, N. Harder, L. Kaderali, K. Rohr, H. Erfle, R. Eils, V. Braga, and V. Starkuviene. 2012. miR-17-5p regulates endocytic trafficking through targeting TBC1D2/Armus. *PloS one*. 7:e52555.
Shacka, J.J. 2012. Mouse models of neuronal ceroid lipofuscinoses: useful pre-clinical tools to delineate disease pathophysiology and validate therapeutics. *Brain Res Bull*. 88:43-57.
Shaw, G. 1996. The pleckstrin homology domain: an intriguing multifunctional protein module. *Bioessays*. 18:35-46.
Shin, H.W., M. Hayashi, S. Christoforidis, S. Lacas-Gervais, S. Hoepfner, M.R. Wenk, J. Modregger, S. Uttenweiler-Joseph, M. Wilm, A. Nystuen, W.N. Frankel, M. Solimena, P. De Camilli, and M. Zerial. 2005. An enzymatic cascade of Rab5 effectors regulates phosphoinositide turnover in the endocytic pathway. *The Journal of cell biology*. 170:607-618.
Shinde, S.R., and S. Maddika. 2016. PTEN modulates EGFR late endocytic trafficking and degradation by dephosphorylating Rab7. *Nat Commun*. 7:10689.
Shirane, M., and K.I. Nakayama. 2006. Protrudin induces neurite formation by directional membrane trafficking. *Science*. 314:818-821.
Sigismund, S., V. Algisi, G. Nappo, A. Conte, R. Pascolutti, A. Cuomo, T. Bonaldi, E. Argenzio, L.G. Verhoef, E. Maspero, F. Bianchi, F. Capuani, A. Ciliberto, S. Polo, and P.P. Di Fiore. 2013. Threshold-controlled ubiquitination of the EGFR directs receptor fate. *The EMBO journal*. 32:2140-2157.

Sigismund, S., E. Argenzio, D. Tosoni, E. Cavallaro, S. Polo, and P.P. Di Fiore. 2008. Clathrin-mediated internalization is essential for sustained EGFR signaling but dispensable for degradation. *Developmental cell*. 15:209-219.
Simonsen, A., J.M. Gaullier, A. D'Arrigo, and H. Stenmark. 1999. The Rab5 effector EEA1 interacts directly with syntaxin-6. *The Journal of biological chemistry*. 274:28857-28860.
Simonsen, A., R. Lippe, S. Christoforidis, J.M. Gaullier, A. Brech, J. Callaghan, B.H. Toh, C. Murphy, M. Zerial, and H. Stenmark. 1998. EEA1 links PI(3)K function to Rab5 regulation of endosome fusion. *Nature*. 394:494-498.
Sin, O., H. Michels, and E.A. Nollen. 2014. Genetic screens in Caenorhabditis elegans models for neurodegenerative diseases. *Biochimica et biophysica acta*. 1842:1951-1959.
Sinha, S., and B. Levine. 2008. The autophagy effector Beclin 1: a novel BH3-only protein. *Oncogene*. 27 Suppl 1:S137-148.
Sleno, R., D. Petrin, D. Devost, E. Goupil, A. Zhang, and T.E. Hebert. 2016. Designing BRET-based conformational biosensors for G protein-coupled receptors. *Methods*. 92:11-18.
Slessareva, J.E., S.M. Routt, B. Temple, V.A. Bankaitis, and H.G. Dohlman. 2006. Activation of the phosphatidylinositol 3-kinase Vps34 by a G protein alpha subunit at the endosome. *Cell*. 126:191-203.
Smith, K.R., J. Damiano, S. Franceschetti, S. Carpenter, L. Canafoglia, M. Morbin, G. Rossi, D. Pareyson, S.E. Mole, J.F. Staropoli, K.B. Sims, J. Lewis, W.L. Lin, D.W. Dickson, H.H. Dahl, M. Bahlo, and S.F. Berkovic. 2012. Strikingly different clinicopathological phenotypes determined by progranulin-mutation dosage. *American journal of human genetics*. 90:1102-1107.
Soisson, S.M., A.S. Nimnual, M. Uy, D. Bar-Sagi, and J. Kuriyan. 1998. Crystal structure of the Dbl and pleckstrin homology domains from the human Son of sevenless protein. *Cell*. 95:259-268.
Sollner, T., S.W. Whiteheart, M. Brunner, H. Erdjument-Bromage, S. Geromanos, P. Tempst, and J.E. Rothman. 1993. SNAP receptors implicated in vesicle targeting and fusion. *Nature*. 362:318-324.
Sonnichsen, B., S. De Renzis, E. Nielsen, J. Rietdorf, and M. Zerial. 2000. Distinct membrane domains on endosomes in the recycling pathway visualized by multicolor imaging of Rab4, Rab5, and Rab11. *The Journal of cell biology*. 149:901-914.
Sordella, R., W. Jiang, G.C. Chen, M. Curto, and J. Settleman. 2003. Modulation of Rho GTPase signaling regulates a switch between adipogenesis and myogenesis. *Cell*. 113:147-158.
St Johnston, D. 2002. The art and design of genetic screens: Drosophila melanogaster. *Nat Rev Genet*. 3:176-188.
Stack, J.H., D.B. DeWald, K. Takegawa, and S.D. Emr. 1995. Vesicle-mediated protein transport: regulatory interactions between the Vps15 protein kinase and the Vps34 PtdIns 3-kinase essential for protein sorting to the vacuole in yeast. *The Journal of cell biology*. 129:321-334.
Stack, J.H., P.K. Herman, P.V. Schu, and S.D. Emr. 1993. A membrane-associated complex containing the Vps15 protein kinase and the Vps34 PI 3-kinase is essential for protein sorting to the yeast lysosome-like vacuole. *The EMBO journal*. 12:2195-2204.
Steele-Mortimer, O., S. Meresse, J.P. Gorvel, B.H. Toh, and B.B. Finlay. 1999. Biogenesis of Salmonella typhimurium-containing vacuoles in epithelial cells involves interactions with the early endocytic pathway. *Cellular microbiology*. 1:33-49.

Stein, M.P., Y. Feng, K.L. Cooper, A.M. Welford, and A. Wandinger-Ness. 2003. Human VPS34 and p150 are Rab7 interacting partners. *Traffic*. 4:754-771.
Stenmark, H. 2009. Rab GTPases as coordinators of vesicle traffic. *Nature reviews. Molecular cell biology*. 10:513-525.
Stenmark, H., and V.M. Olkkonen. 2001. The Rab GTPase family. *Genome Biol*. 2:REVIEWS3007.
Stiernagle, T. 2006. Maintenance of C. elegans. *WormBook*:1-11.
Stoops, E.H., and M.J. Caplan. 2014. Trafficking to the apical and basolateral membranes in polarized epithelial cells. *Journal of the American Society of Nephrology : JASN*. 25:1375-1386.
Suh, B.C., T. Inoue, T. Meyer, and B. Hille. 2006. Rapid chemically induced changes of PtdIns(4,5)P2 gate KCNQ ion channels. *Science*. 314:1454-1457.
Sun, L., O. Liu, J. Desai, F. Karbassi, M.A. Sylvain, A. Shi, Z. Zhou, C.E. Rocheleau, and B.D. Grant. 2012. CED-10/Rac1 regulates endocytic recycling through the RAB-5 GAP TBC-2. *PLoS genetics*. 8:e1002785.
Sun, Q., W. Westphal, K.N. Wong, I. Tan, and Q. Zhong. 2010. Rubicon controls endosome maturation as a Rab7 effector. *Proceedings of the National Academy of Sciences of the United States of America*. 107:19338-19343.
Tabata, K., K. Matsunaga, A. Sakane, T. Sasaki, T. Noda, and T. Yoshimori. 2010. Rubicon and PLEKHM1 negatively regulate the endocytic/autophagic pathway via a novel Rab7-binding domain. *Molecular biology of the cell*. 21:4162-4172.
Takacs-Vellai, K., T. Vellai, A. Puoti, M. Passannante, C. Wicky, A. Streit, A.L. Kovacs, and F. Muller. 2005. Inactivation of the autophagy gene bec-1 triggers apoptotic cell death in C. elegans. *Current biology : CB*. 15:1513-1517.
Tanaka, D., K. Kameyama, H. Okamoto, and M. Doi. 2008. Caenorhabditis elegans Rab escort protein (REP-1) differently regulates each Rab protein function and localization in a tissue-dependent manner. *Genes Cells*. 13:1141-1157.
Tanaka, Y., J.K. Chambers, T. Matsuwaki, K. Yamanouchi, and M. Nishihara. 2014. Possible involvement of lysosomal dysfunction in pathological changes of the brain in aged progranulin-deficient mice. *Acta Neuropathol Commun*. 2:78.
Tanaka, Y., T. Matsuwaki, K. Yamanouchi, and M. Nishihara. 2013. Increased lysosomal biogenesis in activated microglia and exacerbated neuronal damage after traumatic brain injury in progranulin-deficient mice. *Neuroscience*. 250:8-19.
Taylor, G.S., T. Maehama, and J.E. Dixon. 2000. Myotubularin, a protein tyrosine phosphatase mutated in myotubular myopathy, dephosphorylates the lipid second messenger, phosphatidylinositol 3-phosphate. *Proceedings of the National Academy of Sciences of the United States of America*. 97:8910-8915.
Tempel, W., Y. Tong, S. Dimov, A. Bochkarev, and H. Park. 2008. First crystallographic models of human TBC domains in the context of a family-wide structural analysis. *Proteins*. 71:497-502.
Thompson, O., M. Edgley, P. Strasbourger, S. Flibotte, B. Ewing, R. Adair, V. Au, I. Chaudhry, L. Fernando, H. Hutter, A. Kieffer, J. Lau, N. Lee, A. Miller, G. Raymant, B. Shen, J. Shendure, J. Taylor, E.H. Turner, L.W. Hillier, D.G. Moerman, and R.H. Waterston. 2013. The million mutation project: a new approach to genetics in Caenorhabditis elegans. *Genome Res*. 23:1749-1762.

Thorpe, L.M., H. Yuzugullu, and J.J. Zhao. 2015. PI3K in cancer: divergent roles of isoforms, modes of activation and therapeutic targeting. *Nat Rev Cancer*. 15:7-24.
Toolkit, M.-P.I.f.D.B.B. 2008-2016. About COILS/PCOILS.
Touhara, K., J. Inglese, J.A. Pitcher, G. Shaw, and R.J. Lefkowitz. 1994. Binding of G protein beta gamma-subunits to pleckstrin homology domains. *The Journal of biological chemistry*. 269:10217-10220.
Toyofuku, T., K. Morimoto, S. Sasawatari, and A. Kumanogoh. 2015. Leucine-Rich Repeat Kinase 1 Regulates Autophagy through Turning On TBC1D2-Dependent Rab7 Inactivation. *Molecular and cellular biology*. 35:3044-3058.
Tsujita, K., T. Itoh, T. Ijuin, A. Yamamoto, A. Shisheva, J. Laporte, and T. Takenawa. 2004. Myotubularin regulates the function of the late endosome through the gram domain-phosphatidylinositol 3,5-bisphosphate interaction. *The Journal of biological chemistry*. 279:13817-13824.
Tuma, P.L., L.K. Nyasae, J.M. Backer, and A.L. Hubbard. 2001. Vps34p differentially regulates endocytosis from the apical and basolateral domains in polarized hepatic cells. *The Journal of cell biology*. 154:1197-1208.
Tuteja, N. 2009. Signaling through G protein coupled receptors. *Plant Signal Behav*. 4:942-947.
Ullrich, O., H. Stenmark, K. Alexandrov, L.A. Huber, K. Kaibuchi, T. Sasaki, Y. Takai, and M. Zerial. 1993. Rab GDP dissociation inhibitor as a general regulator for the membrane association of rab proteins. *The Journal of biological chemistry*. 268:18143-18150.
van der Kant, R., A. Fish, L. Janssen, H. Janssen, S. Krom, N. Ho, T. Brummelkamp, J. Carette, N. Rocha, and J. Neefjes. 2013. Late endosomal transport and tethering are coupled processes controlled by RILP and the cholesterol sensor ORP1L. *Journal of cell science*. 126:3462-3474.
Vanhaesebroeck, B., J. Guillermet-Guibert, M. Graupera, and B. Bilanges. 2010. The emerging mechanisms of isoform-specific PI3K signalling. *Nature reviews. Molecular cell biology*. 11:329-341.
Vergne, I., J. Chua, S.B. Singh, and V. Deretic. 2004. Cell biology of mycobacterium tuberculosis phagosome. *Annual review of cell and developmental biology*. 20:367-394.
Via, L.E., D. Deretic, R.J. Ulmer, N.S. Hibler, L.A. Huber, and V. Deretic. 1997. Arrest of mycobacterial phagosome maturation is caused by a block in vesicle fusion between stages controlled by rab5 and rab7. *The Journal of biological chemistry*. 272:13326-13331.
Viaud, J., R. Mansour, A. Antkowiak, A. Mujalli, C. Valet, G. Chicanne, J.M. Xuereb, A.D. Terrisse, S. Severin, M.P. Gratacap, F. Gaits-Iacovoni, and B. Payrastre. 2016. Phosphoinositides: Important lipids in the coordination of cell dynamics. *Biochimie*. 125:250-258.
Vogel, B.E., and E.M. Hedgecock. 2001. Hemicentin, a conserved extracellular member of the immunoglobulin superfamily, organizes epithelial and other cell attachments into oriented line-shaped junctions. *Development*. 128:883-894.
Volinia, S., R. Dhand, B. Vanhaesebroeck, L.K. MacDougall, R. Stein, M.J. Zvelebil, J. Domin, C. Panaretou, and M.D. Waterfield. 1995. A human phosphatidylinositol 3-kinase complex related to the yeast Vps34p-Vps15p protein sorting system. *The EMBO journal*. 14:3339-3348.
Vonderheit, A., and A. Helenius. 2005. Rab7 associates with early endosomes to mediate sorting and transport of Semliki forest virus to late endosomes. *PLoS biology*. 3:e233.

Waguri, S., F. Dewitte, R. Le Borgne, Y. Rouille, Y. Uchiyama, J.F. Dubremetz, and B. Hoflack. 2003. Visualization of TGN to endosome trafficking through fluorescently labeled MPR and AP-1 in living cells. *Molecular biology of the cell*. 14:142-155.

Wandinger-Ness, A., and M. Zerial. 2014. Rab proteins and the compartmentalization of the endosomal system. *Cold Spring Harbor perspectives in biology*. 6:a022616.

Wang, C.W., P.E. Stromhaug, E.J. Kauffman, L.S. Weisman, and D.J. Klionsky. 2003. Yeast homotypic vacuole fusion requires the Ccz1-Mon1 complex during the tethering/docking stage. *The Journal of cell biology*. 163:973-985.

Wang, L., and A. Audhya. 2014. In vivo imaging of C. elegans endocytosis. *Methods*. 68:518-528.

Wang, W., J. Zhu, T.A. Springer, and B.H. Luo. 2011. Tests of integrin transmembrane domain homo-oligomerization during integrin ligand binding and signaling. *The Journal of biological chemistry*. 286:1860-1867.

Wang, Z., and D.R. Sherwood. 2011. Dissection of genetic pathways in C. elegans. *Methods Cell Biol*. 106:113-157.

Weigert, R., A.C. Yeung, J. Li, and J.G. Donaldson. 2004. Rab22a regulates the recycling of membrane proteins internalized independently of clathrin. *Molecular biology of the cell*. 15:3758-3770.

Weisz, O.A., and E. Rodriguez-Boulan. 2009. Apical trafficking in epithelial cells: signals, clusters and motors. *Journal of cell science*. 122:4253-4266.

Wen, W., J. Yan, and M. Zhang. 2006. Structural characterization of the split pleckstrin homology domain in phospholipase C-gamma1 and its interaction with TRPC3. *The Journal of biological chemistry*. 281:12060-12068.

Wickner, W. 2010. Membrane fusion: five lipids, four SNAREs, three chaperones, two nucleotides, and a Rab, all dancing in a ring on yeast vacuoles. *Annual review of cell and developmental biology*. 26:115-136.

Wickner, W., and R. Schekman. 2008. Membrane fusion. *Nat Struct Mol Biol*. 15:658-664.

Wicks, S.R., R.T. Yeh, W.R. Gish, R.H. Waterston, and R.H. Plasterk. 2001. Rapid gene mapping in Caenorhabditis elegans using a high density polymorphism map. *Nat Genet*. 28:160-164.

Wilson, J.M., M. de Hoop, N. Zorzi, B.H. Toh, C.G. Dotti, and R.G. Parton. 2000. EEA1, a tethering protein of the early sorting endosome, shows a polarized distribution in hippocampal neurons, epithelial cells, and fibroblasts. *Molecular biology of the cell*. 11:2657-2671.

Winter, J.F., S. Hopfner, K. Korn, B.O. Farnung, C.R. Bradshaw, G. Marsico, M. Volkmer, B. Habermann, and M. Zerial. 2012. Caenorhabditis elegans screen reveals role of PAR-5 in RAB-11-recycling endosome positioning and apicobasal cell polarity. *Nature cell biology*. 14:666-676.

Wirawan, E., S. Lippens, T. Vanden Berghe, A. Romagnoli, G.M. Fimia, M. Piacentini, and P. Vandenabeele. 2012. Beclin1: a role in membrane dynamics and beyond. *Autophagy*. 8:6-17.

Wittinghofer, A. 2014. Ras Superfamily Small G Proteins: Biology and Mechanisms.

Woolfson, D.N. 2005. The design of coiled-coil structures and assemblies. *Adv Protein Chem*. 70:79-112.

Wu, M., T. Wang, E. Loh, W. Hong, and H. Song. 2005. Structural basis for recruitment of RILP by small GTPase Rab7. *The EMBO journal*. 24:1491-1501.

Wu, Y.W., R.S. Goody, R. Abagyan, and K. Alexandrov. 2009. Structure of the disordered C terminus of Rab7 GTPase induced by binding to the Rab geranylgeranyl transferase catalytic complex reveals the mechanism of Rab prenylation. *The Journal of biological chemistry*. 284:13185-13192.

Xiao, G.H., F. Shoarinejad, F. Jin, E.A. Golemis, and R.S. Yeung. 1997. The tuberous sclerosis 2 gene product, tuberin, functions as a Rab5 GTPase activating protein (GAP) in modulating endocytosis. *The Journal of biological chemistry*. 272:6097-6100.

Xue, Y., H. Fares, B. Grant, Z. Li, A.M. Rose, S.G. Clark, and E.Y. Skolnik. 2003. Genetic analysis of the myotubularin family of phosphatases in Caenorhabditis elegans. *The Journal of biological chemistry*. 278:34380-34386.

Yachdav, G., E. Kloppmann, L. Kajan, M. Hecht, T. Goldberg, T. Hamp, P. Honigschmid, A. Schafferhans, M. Roos, M. Bernhofer, L. Richter, H. Ashkenazy, M. Punta, A. Schlessinger, Y. Bromberg, R. Schneider, G. Vriend, C. Sander, N. Ben-Tal, and B. Rost. 2014. PredictProtein--an open resource for online prediction of protein structural and functional features. *Nucleic acids research*. 42:W337-343.

Yao, L., Y. Kawakami, and T. Kawakami. 1994. The pleckstrin homology domain of Bruton tyrosine kinase interacts with protein kinase C. *Proceedings of the National Academy of Sciences of the United States of America*. 91:9175-9179.

Yao, L., H. Suzuki, K. Ozawa, J. Deng, C. Lehel, H. Fukamachi, W.B. Anderson, Y. Kawakami, and T. Kawakami. 1997. Interactions between protein kinase C and pleckstrin homology domains. Inhibition by phosphatidylinositol 4,5-bisphosphate and phorbol 12-myristate 13-acetate. *The Journal of biological chemistry*. 272:13033-13039.

Yook, K. 2005. Complementation. *WormBook*:1-17.

Yoshina, S., K. Sakaki, A. Yonezumi-Hayashi, K. Gengyo-Ando, H. Inoue, Y. Iino, and S. Mitani. 2012. Identification of a novel ADAMTS9/GON-1 function for protein transport from the ER to the Golgi. *Molecular biology of the cell*. 23:1728-1741.

Yue, Z., S. Jin, C. Yang, A.J. Levine, and N. Heintz. 2003. Beclin 1, an autophagy gene essential for early embryonic development, is a haploinsufficient tumor suppressor. *Proceedings of the National Academy of Sciences of the United States of America*. 100:15077-15082.

Zerial, M., and H. McBride. 2001. Rab proteins as membrane organizers. *Nature reviews. Molecular cell biology*. 2:107-117.

Zheng, X., J. Zhang, and K. Liao. 2014. The basic amino acids in the coiled-coil domain of CIN85 regulate its interaction with c-Cbl and phosphatidic acid during epidermal growth factor receptor (EGFR) endocytosis. *BMC Biochem*. 15:13.

Zheng, Y. 2001. Dbl family guanine nucleotide exchange factors. *Trends in biochemical sciences*. 26:724-732.

Zhou, X., L. Sun, F. Bastos de Oliveira, X. Qi, W.J. Brown, M.B. Smolka, Y. Sun, and F. Hu. 2015. Prosaposin facilitates sortilin-independent lysosomal trafficking of progranulin. *The Journal of cell biology*. 210:991-1002.

Zhou, Y., M. Toth, M.S. Hamman, S.J. Monahan, P.A. Lodge, A.L. Boynton, and M.L. Salgaller. 2002. Serological cloning of PARIS-1: a new TBC domain-containing, immunogenic tumor antigen from a prostate cancer cell line. *Biochemical and biophysical research communications*. 290:830-838.

Zhu, B.Y., N.E. Zhou, C.M. Kay, and R.S. Hodges. 1993. Packing and hydrophobicity effects on protein folding and stability: effects of beta-branched amino acids, valine and isoleucine,

on the formation and stability of two-stranded alpha-helical coiled coils/leucine zippers. *Protein Sci*. 2:383-394.

Zhu, H., G. Zhu, J. Liu, Z. Liang, X.C. Zhang, and G. Li. 2007. Rabaptin-5-independent membrane targeting and Rab5 activation by Rabex-5 in the cell. *Molecular biology of the cell*. 18:4119-4128.

Zou, W., Q. Lu, D. Zhao, W. Li, J. Mapes, Y. Xie, and X. Wang. 2009. Caenorhabditis elegans myotubularin MTM-1 negatively regulates the engulfment of apoptotic cells. *PLoS genetics*. 5:e1000679.